RIGA TECHNICAL UNIVERSITY

Arturs ABOLTINS

SYNCHRONIZATION AND EQUALIZATION FOR MULTICARRIER SYSTEMS WITH PARAMETRIC GENERALIZED UNITARY ROTATION BASED MODULATION

Doctoral thesis

Riga 2013

RIGA TECHNICAL UNIVERSITY

Faculty of Electronics and Telecommunications

Institute of Radio Electronics

Arturs ABOLTINS

Student of the Doctoral study program "Electronics"

SYNCHRONIZATION AND EQUALIZATION FOR MULTICARRIER SYSTEMS WITH PARAMETRIC GENERALIZED UNITARY ROTATION BASED MODULATION

Doctoral thesis

Academic supervisor

Dr. sc. ing., professor

P. MISANS

RTU Press

Riga 2013

Aboltins A. Synchronization and equalization for multicarrier systems with parametric generalized unitary rotation based modulation. Doctoral thesis. R.:RTU Press, 2013. - 156 p.

Printed according to the decision of FET promotion council "RTU P-08" on June 27, 2013, protocol No. 16.

This work has been supported by the European Social Fund within the project "Support for the implementation of doctoral studies at Riga Technical University".

A DOCTORAL THESIS SUBMITTED TO RIGA TECHNICAL UNIVERSITY IN FULFILLMENT OF THE REQUIREMENTS FOR THE DEGREE OF DOCTOR OF SCIENCE IN ENGINEERING

The public defense of the doctoral thesis for promotion to the doctor's degree in engineering will take place on 10th of October, 2013, at 17:45 in Room 102, Faculty of Electronics and Telecommunications, Azenes 12.

OFFICIAL REVIEWERS

Professor, Dr.sc.ing. Guntars Balodis
Faculty of Electronics and Telecommunications, Riga Technical University, Latvia

Professor, Dr.habil.ing. Andreas Ahrens
Hochschule Wismar, University of Applied Sciences Technology, Business and Design, Faculty of Engineering, Department of Electrical Engineering and Computer Science, Germany

Senior Researcher Dr.habil.math. Aivars Lorencs
Institute of Electronics and Computer Science, Latvia

CONFIRMATION

I confirm that this doctoral thesis, submitted for a degree in engineering at the Riga Technical University, is my own work. The doctoral thesis has not been submitted for a degree in any other university.

Arturs Aboltins ..... (Signature)

Date: .....

The doctoral thesis is written in English, contains introduction, 8 chapters, conclusions, references, 2 appendices, index, 70 Figures and 9 Tables, 156 pages in total. The list of references consists of 107 titles.

Acknowledgements

I would like to thank everybody who inspired and helped me to write this thesis. A lot of efforts of different people have made it possible to finish this, to me, very important work.

Especially I would like to thank my advisor professor Peteris Misans, who inspired me to start working with unitary transforms. I have learned from him to maintain high standard of work and patience. We have had many hours of interesting discussions not only about signal processing but also about cars, traditional and non-traditional lifestyle.

This work would not be possible without professor Elmars Bekeris, who involved me into scientific research 15 years ago. He encouraged me to return to Riga Technical University and to continue my education. He gave me a unique possibility to learn signal processing by teaching this topic to students.

The first models of GUR-based parametric multicarrier (PMC) systems were based on the diploma work of M.Sc. Dainis Klavins. Thanks Dainis, who helped me a lot at the initial stages of the research.

I would like to thank my family, who patiently supported me during this long and sophisticated journey.

Arturs Aboltins,

Riga 2013

This work has been supported by the European Social Fund within the project "Support for the implementation of doctoral studies at Riga Technical University".

Abstract

Rotation-based unitary transformations have gained remarkable interest during last years due to the growing need for sophisticated signal transformations on one hand, and advances in signal processing hardware on the other hand. Such important properties as parametrization, fast algorithms and generalization of other transforms raised the question about the applicability of these transformations for multicarrier modulation and demodulation in communication systems. Utilization of this new class of transforms for multicarrier modulation allows to create parametric systems with dynamically adjustable subcarrier waveforms. However, the proposed parametric multicarrier systems requires the design of new and the adaptation of existing channel estimation, equalization and synchronization algorithms. Moreover, since equalization and synchronization are two most critical parts of any communication system, a large amount of work in reviewing the existing solutions is done. One of the major objectives of this doctoral thesis is the analysis and development of building blocks for generalized unitary rotation -based multicarrier systems, which will allow in the future to create rapidly innovative designs. The contributions of this work include both the development of new signal processing structures and the analysis of possible mutual configurations for these structures. Finally, a complete example of parametric multicarrier system, which includes a selection of the proposed methods, is discussed.

The doctoral thesis is written in English, contains introduction, 8 chapters, conclusions, references, 2 appendices, index, 70 Figures and 9 Tables, 156 pages in total. The list of references consists of 107 titles.

Anotācija

Pateicoties augošai nepieciešamībai pēc sarežģītiem signālu pārveidojumiem un sasniegumiem signālu apstrādes aparatūras nodrošinājumā, uz rotāciju balstītie unitārie pārveidojumi pēdējo gadu laikā ir guvuši ievērojamu uzmanību. Tādas svarīgas īpašības kā parametrizācija, ātrie algoritmi un citu transformāciju vispārinājums izvirzīja jautājumu par šo pārveidojumu izmantošanu modulācijai un demodulācijai sakaru sistēmās. Jaunās transformāciju klases pielietošana daudznesēju modulācijās dod iespēju radīt parametriskas sistēmas ar dinamiski pārskaņojamām apakšnesēju formām. Tomēr, piedāvātās parametriskās daudznesēju sistēmas prasa izstrādāt jaunus un adaptēt jau esošus kanāla novērtēšanas, izlīdzināšanas un sinhronizācijas algoritmus. Turklāt, ņemot vērā izlīdzināšanas un sinhronizācijas neaizvietojamo lomu jebkurā sakaru sistēmā, liels darbs ir veikts jau esošo risinājumu apskatā un izprašanā. Viens no galvenajiem šī promocijas darba mērķiem ir uz vispārināto unitāro rotāciju balstīto daudznesēju sistēmu sastāvdaļu analīze un izstrāde, kas nākotnē pavērs iespēju ātrai inovatīvu risinājumu radīšanai. Šī darba rezultāti aptver gan atsevišķu signālapstrādes struktūru izstrādi, gan arī iespējamo šo struktūru savstarpējo konfigurāciju analīzi. Darba beigās tiek apskatīts pilns parametriskās daudz-nesēju sistēmas piemērs, kas ietver izlasi no piedāvātajām metodēm.

Promocijas darbs ir uzrakstīts angļu valodā, satur ievadu, 8 nodaļas, nobeigumu, 2 pielikumus, literatūras sarakstu, terminu rādītāju, kopā 156 lappuses. Darbā ir 70 zīmējumi un ilustrācijas, 9 tabulas, literatūras sarakstā ir 107 nosaukumi.

Contents

List of figures

List of Tables

List of abbreviations

3GPP 3rd Generation Partnership Project.

AC autocorrelation.
ADC analog-to-digital converter.
AWGN additive white Gaussian noise.

BER bit error ratio.
BF basis function.
BTO block timing offset.

CAZAC constant amplitude zero autocorrelation.
CCDF complementary cumulative distribution function.
CCRAIMOT complex constant rotation angle in matrix OT.
CCRAOT complex constant rotation angle OT.
CDMA code division multiple access.
CFO carrier frequency offset.
CP cyclic prefix.
CPU central processing unit.
CRAOT constant rotation angle OT.
CRB Cramer-Rao bound.
CSI channel state information.

DA data-aided.
DAC digital-to-analog converter.
DD data-directed.
DFE decision-feedback equalizer.
DFT discrete Fourier transform.
DMX demultiplexer.
DPSK differential phase shift keying.
DQAM differential quadrature amplitude modulation.
DSL digital subscriber line.
DSP digital signal processor.

EGUR Elementary Generalized Unitary Rotation.

FBMC filter bank multicarrier.
FCFO fractional carrier frequency offset.
FD frequency domain.
FDE frequency domain equalizer.
FFT fast Fourier transform.
FIR finite impulse response.
FMT filtered multitone.
FPGA field-programmable gate array.
FrFT fractional Fourier transform.

GD GUR domain.
GI guard interval.
GUR Generalized Unitary Rotation.

IBI inter-block interference.
IC integrated circuit.
ICI inter-carrier interference.
IDFT inverse discrete Fourier transform.
IEEE Institute of Electrical and Electronics Engineers.
IF intermediate frequency.
IP intellectual property.
IQ in-phase quadrature.
ISI inter-symbol interference.

LAN local area network.
LMS least mean squares.
LPF low-pass filter.
LS least squares.
LTE Long Term Evolution.
LTI linear time-invariant.

MAC media access control.
MC multicarrier.
MF matched filter.
MIMO multiple-input multiple-output.
ML maximum likelihood.
MLS maximum length sequence.
MMSE minimum mean squared error.
MSE mean squared error.

MUX multiplexer.

NCO numerically controlled oscillator.
NDA non data-aided.

OFDM orthogonal frequency division multiplexing.
OSI Open System Interconnection.
OT orthogonal transform.

P/S parallel-to-serial.
PAPR peak-to-average power ratio.
PDF probability density function.
PI proportional integral.
PID proportional integral derivative.
PLL phase locked loop.
PN pseudo-noise.
PSAM pilot signal assisted modulation.

QAM quadrature amplitude modulation.
QPSK quadrature phase-shift keying.

RABOT Rotation Angle Based OT.
RF radio frequency.
RLS recursive least squares.
RRC root-raised-cosine.

S/P serial to parallel.
SC single carrier.
SC-FDE single carrier FDE.
SDR software-defined radio.
SFO sampling frequency offset.
SI super-imposed.
SINR signal-to-interference ratio.
SIS super-imposed sequence.
SNR signal-to-noise ratio.
SOGRM stairs-like orthogonal generalized rotation matrix.
SS spread spectrum.
SVD singular value decomposition.

TD time domain.

UW unique word.

WGN white Gaussian noise.
WHT Walsh-Hadamard transform.

XC cross-correlation.

ZC Zadoff-Chu.
ZP zero padding.

Nomenclature

$\boldsymbol{X}$	transform domain samples in transmitter
$\boldsymbol{x}$	transmitted time domain (TD) baseband samples
$\boldsymbol{s}$	transmitted time domain (TD) passband samples
$\boldsymbol{x_{cp}}$	transmitted time domain (TD) baseband samples with cyclic prefix (CP)
$\boldsymbol{x_{zp}}$	transmitted time domain (TD) baseband samples with zero padding (ZP)
$\boldsymbol{x_{uw}}$	transmitted time domain (TD) baseband samples with unique word (UW) prefix
$\boldsymbol{r}$	received time domain (TD) passband samples
$\boldsymbol{Y}$	received transform domain baseband samples
$\boldsymbol{y}$	received time domain (TD) baseband samples
L	length of padding
φ	basis function
$\boldsymbol{h}$	time domain impulse response
$\boldsymbol{\Lambda}$	frequency response
Λ	log-likelihood function
$\boldsymbol{u}$	synchronization unique word (UW) sequence
σ	standard deviation, square root of variance
ϵ	absolute carrier frequency offset (CFO)
ε	fractional carrier frequency offset (FCFO)
$\boldsymbol{w}$	white Gaussian noise (WGN)
τ	chip time
t	time
n	transform domain index
k	time domain index
j	imaginary unit $j^2 = -1$
ϕ, γ, ψ	real-valued angle
$\boldsymbol{\Phi}$	unitary transformation matrix
$\boldsymbol{H}$	time domain (TD) channel matrix
$\hat{\boldsymbol{H}}$	estimate of time domain (TD) channel matrix
$\boldsymbol{A}$	transform domain channel matrix
$\boldsymbol{A}^{-1}$	inverse of transform domain channel matrix
$\hat{\boldsymbol{A}}$	estimate of transform domain channel matrix
$\boldsymbol{I}$	identity matrix
$\boldsymbol{B_p}$	stairs-like orthogonal generalized rotation matrix (SOGRM)
$\boldsymbol{F}$	discrete Fourier transform (DFT) matrix

Table 1: List of main mathematical symbols used in this work

$\overline{\boldsymbol{z}}$	mean of vector $\boldsymbol{z}$
$\|\|\boldsymbol{x}\|\|$	ℓ^2 norm of the vector $\boldsymbol{x}$
$\|x\|$	modulus of variable x
$\angle(x)$	angle of complex variable x
$\Re(x)$	real part of variable x
$\Im(x)$	imaginary part of variable x
$\boldsymbol{M}^*$	transposed conjugate (Hermitian adjoint) of a matrix $\boldsymbol{M}$
$\boldsymbol{M}^{-1}$	inverse of a matrix $\boldsymbol{M}$
$\langle \boldsymbol{x}, \boldsymbol{y} \rangle$	inner product between vectors $\boldsymbol{x}$ and $\boldsymbol{y}$
$\otimes$	Kronecker product
$*$	convolution
$\circledast$	circular convolution

Table 2: Mathematical notation

1 General description of the work

1.1 Urgency of the subject matter

At the beginning of 21-th century we are witnessing a rapid growth of demand for high-speed data communications. Due to the limited frequency resources and the growing geographical density of the devices, more and more efficient, low power and secure modulation techniques are required. Multicarrier (MC) communications are one of the most attractive technologies for providing high speed digital transmission. Multiple subcarriers provide an additional dimension for the mitigation of distortions caused by the propagation media and multiple access interference.

MC systems with sinusoidal basis functions (BFs), such as orthogonal frequency division multiplexing (OFDM) [1], are the most widely used MC technologies. OFDM technology became popular just a few decades ago due to the achievements in digital signal processor (DSP) hardware design [2]. It has become the modulation technique of choice in many widely-used telecommunication standards due to high spectral efficiency, achieved by means of computationally simple and powerful frequency domain (FD) equalization technique. Many modern facilities like wireless computer networks, digital television and digital subscriber line modems are based on OFDM. This modulation technique provides improved (compared to single carrier (SC) systems) spectral efficiency and ease of equalization.

Along with many advantages, the OFDM-based modulation has several serious drawbacks:

- Reduction of communication system capacity and power efficiency due to the use of cyclic prefix (CP), which is necessary for elimination of inter-block interference (IBI) and for FD equalization;
- Large envelope fluctuations, i.e. the peak-to-average power ratio (PAPR) of the time domain (TD) signal requires radio frequency (RF) power amplifiers with high dynamic range;
- High sensitivity to timing and frequency synchronization errors due to large sidelobes of individual subcarriers;
- Susceptibility to the single frequency fading/jamming because each subcarrier occupies just a small portion of the frequency spectrum.

Attempts to eliminate the mentioned drawbacks have led to several MC communication system research directions:

- Filter bank multicarrier (FBMC) communication systems. Filter banks [3], [4] utilize advanced waveforms, for instance wavelets, for obtaining higher spectral density and

reduced inter-carrier interference (ICI). Good frequency localization of the mentioned systems makes them an attractive choice for cognitive radio. Problems of synchronization and equalization in these communication systems have been reviewed multiple times [5], [6]. Moreover, due to good time and frequency localization of individual subcarriers, FBMC-based systems are much more immune to synchronization errors than OFDM. However, the complexity of equalization and a large PAPR are the main show stoppers for a widespread adaptation of the mentioned modulation scheme.

- Utilization of non-sinusoidal subcarriers in order to improve immunity to the single frequency fading and narrowband jamming. In publication [7] it is shown that under certain conditions the Walsh-Hadamard transform (WHT) can outperform the discrete Fourier transform (DFT). Patent [8] describes equalization techniques for a WHT-based MC communication system. However, there are no known papers devoted to the timing and frequency synchronization in this kind of communication systems.

- Doctoral thesis [9] has provided very important results about eigenfunctions of non-stationary propagation environments. The fact that eigenfunctions of these environments are non-sinusoidal leads to ideas about the construction of more efficient modulation schemes than OFDM. Paper [10] proposes fractional Fourier transform (FrFT)-based modulation in order to improve OFDM in case of double-dispersive (time and frequency varying) communication channels. However, a much more complex decision-feedback equalizer (DFE)-based equalizer must be used in this case. Nothing on the part of timing and frequency synchronization is reviewed in [10].

- In paper [11] and in some other papers (see references in [12]) an alternative and very simple approach to performance improvement of an MC communication system, based on the transforms, which are described by a set of *rotation angles* , is proposed. It is shown that in non-Gaussian channels, the proposed communication system achieves a lower bit error ratio (BER) than the classic OFDM. The initial paper on Generalized Unitary Rotation (GUR)-based MC modulation [12] has also confirmed the possibility to use parametric unitary transformations for MC communication systems. However, no equalization and synchronization problems are discussed in these papers.

- Various hybrid schemes using spread spectrum (SS) concepts and OFDM, for instance [13], allow to improve the performance of MC communication systems. Synchronization and channel estimation in SS and code division multiple access (CDMA) communication systems have been addressed many times. However, no parametric *spreading codes* are considered in these communication systems.

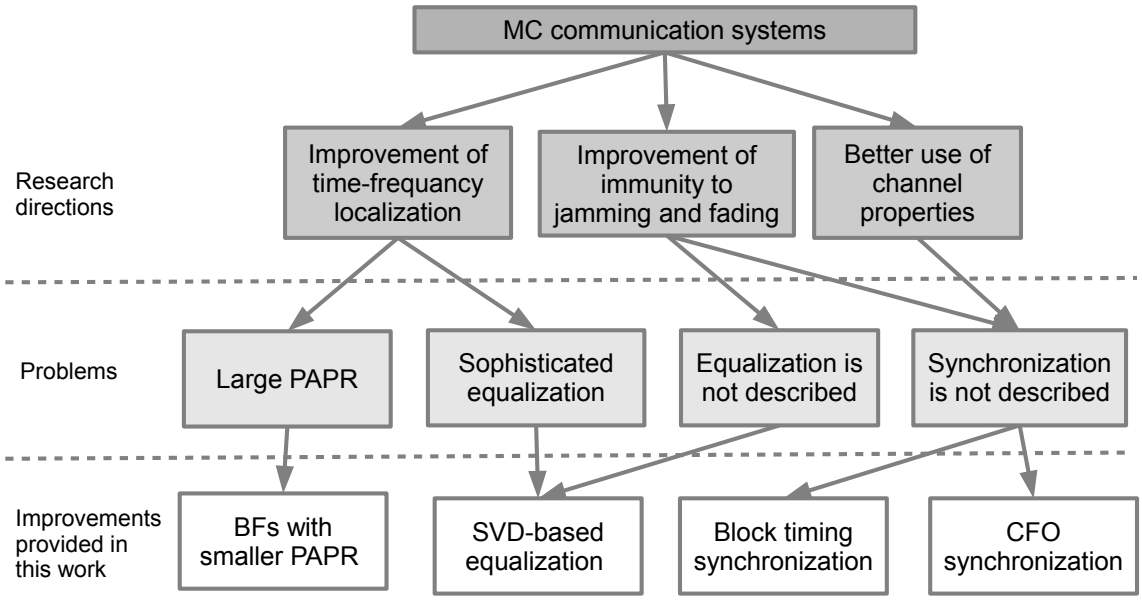

Figure 1.1: Development directions and improvements provided by this doctoral thesis

This doctoral thesis is addressed to improve existing MC systems, by introduction of GUR-based parametric multicarrier (PMC) modulation, which allows to create communication systems with dynamically adjustable subcarrier waveforms. The summary of the MC communication system development directions and improvements, provided by this doctoral thesis, is given in Figure 1.1.

1.2 Objective of the work

The purpose of this work is to explore baseband algorithms of an PMC system[1], where subcarriers are produced by means of GUR. Therefore, the work has to provide a theoretical basis for the implementation of GUR-based PMC systems.

To achieve the goal, the following objectives have to be fulfilled:

- Explore GUR-based MC modulation;
- Explore timing synchronization;
- Explore frequency synchronization;
- Explore GUR domain (GD) equalization of the communication channel. A new GD equalization algorithm has to be developed.

[1]description of PMC is given in Section 3.5.1

The compatibility of the existing synchronization algorithms for other MC modulations, like OFDM, with GUR-based PMC systems has to be verified. New algorithms, if necessary, must be developed. Additionally, the impact of the accuracy of synchronization and equalization on the performance of the PMC system has to be evaluated.

1.3 Scientific novelty and main results

The following list outlines the major contributions, that have been done during writing of this doctoral thesis:

- For the first time a concept of GUR-based PMC systems is presented (Section 3.5.1).
- For the first time a method of GD equalization has been developed (Section 6.6.3.1).
- For the first time a method of GD channel estimation has been proposed (Section 6.5.2).
- For the first time a method of application of TD channel estimate to the GD has been developed (Section 6.5.1.3).
- For the first time a real-valued Rotation Angle Based OT (RABOT) rotation algorithm for the creation of the transform with a desired first BF with length $N = \mathbb{Z}$ has been developed.
- An improved method for block timing offset (BTO) estimation, based on the combination of decision-directed (DD) and data-aided (DA) estimators, has been proposed (Section 4.3.2.2).
- Several *new methods* for fractional carrier frequency offset (FCFO) estimation have been proposed (Section 5.4.3).
- Two different TD signal structures, based on the unique word (UW) prefix and superimposed (SI) sequence, have been proposed (Sections 2.3.4.3 and 2.4.2.2).
- New configurations of unitary transformation unit - transmultiplexer and subband coder have been explored (Section 3.3.5).
- A large number of models for the simulation of communication systems and their counterparts have been created. These models can be used for teaching.

1.4 Theses to be defended

1. Using GUR it is possible to create practically usable multicarrier systems with parametric modulation.

2. Multicarrier system with parametric GUR-based modulation reduces the bit error ratio (BER) as compared to orthogonal frequency division multiplexing (OFDM) with frequency domain equalizer having the same number of subcarriers and training symbols.

3. Singular value decomposition (SVD)-based GUR domain equalizer completely mitigates inter-carrier interference, caused by the convolution in the communication channel and transmitter/receiver filters.

4. For the block timing synchronization in the multicarrier systems with parametric modulation, an estimator, which is based on the combination of proposed decision-directed cross-correlation algorithms and classic data-aided autocorrelation algorithms, must be used.

5. New, decision-directed cross-correlation based fractional carrier frequency offset (FCFO) estimation algorithms, proposed in the work, provide a maximum FCFO acquisition range, which is larger or equal to the range of classic, data-aided autocorrelation based methods.

1.5 Research technique

This research is based on the adoption of existing synchronization and channel estimation techniques for MC communication systems to GUR-based PMC systems. However, since various equalization and synchronization problems are highly related to each other, research must be done in several directions simultaneously. One of the largest challenges in this research is finding global solutions that are acceptable at all levels of communication system operation.[1]

Research included the use of both analytical and numerical approach. Most of the estimator algorithms (see, for example, Section 5.4.3) and their parameters are derived analytically. It allows to make general conclusions about the derived algorithms. However, inclusion of these algorithms into more complex systems, like synchronization loops (see, for example, Section 5.6) leads to a very complex analytical description. In these situations the numerical approach

[1] Synchronization and equalization are hot research topics due to the large demand for high-speed data communication solutions. The high commercial value of new synchronization and equalization algorithms leads to patenting of new inventions prior to any publications. Very frequently new algorithms do not get published at all due to intellectual property (IP) rights held by communication chip vendors.

is preferred. Moreover, the numerical approach allows to verify designs in real conditions, i.e. in software where they are intended to be used.

Development of all algorithms was carried out in several steps:

- Scientific literature was explored and most suitable for the new communication system existing solutions were theoretically understood and compared to others.
- Potentially suitable algorithms were implemented as computer simulation scenarios. This crucial step provides a stable basis for experimentation and further research.
- Drawbacks and incompatibilities of the existing algorithms with GUR-based PMC system were figured out.
- Existing algorithms were improved or new algorithms developed.
- New approaches were verified by modification of existing model scenarios.
- Most successful findings were implemented into simplified models of the communication systems. These models were focused on a specific problem, leaving the rest of the communication system at the basic level.
- Finally, achieved results were verified using a complete PMC system model in conjunction with other already developed methods. This step checked the compatibility of the developed algorithms, and the needs for modification of the previously developed methods could be outlined.

1.6 Research object

The research object of this doctoral thesis is the *baseband* of a PMC system, where transmission is carried out using many mutually orthogonal waveforms, created using GUR. Unlike traditional MC communication systems, where the set of subcarriers is fixed, in the explored PMC systems the set of waveforms can be adjusted dynamically.

The major tasks of the researched PMC system baseband are:

- MC modulation and demodulation;
- equalization;
- timing offset synchronization;
- frequency offset synchronization.

The PMC system baseband includes the following items, which can be divided into smaller parts responsible for various specific functions:

- transmitter baseband;
- baseband equivalent of communication channel;
- receiver baseband.

The most important components of the *transmitter* baseband are:

- MC modulator;
- synchronization and training signal generator;
- pulse shaping filter.

The most important components of the *receiver* baseband are:

- timing offset synchronizer;
- FCFO synchronizer;
- communication channel equalizer;
- MC demodulator.

1.7 Practical significance of the research

Implementation of any digital data communication system is not possible without synchronization and equalization. Therefore, this doctoral thesis is oriented on solving of issues related to the practical implementation of MC systems with GUR-based modulation. At the moment of preparation of this text (June, 2013) no working prototypes of GUR-based PMC systems are available yet. However, this work can be used as an ultimate guide for building such systems.

The results of this work can be used as a general guide for building and improving non-GUR-based MC communication systems. This work contains more than 30 block diagrams and several algorithm descriptions, which allow to start practical implementation of the described devices.

The largest practical contribution of this doctoral thesis is a complete ©Mathworks Simulink model of GUR-based PMC system baseband. Moreover, dozens of different models of communication systems and separate counterparts have been created during the preparation of this work. All these models will be used for teaching students and will provide a substantial support for future research (see Chapter 8).

1.8 Approbation

The following papers have been presented in scientific conferences:

[14] Misans P., Aboltins A., Terauds M., Valters G. MATLAB/SIMULINK Implementation of Phi Transforms – A New Toolbox Only or the Rival of Wavelet Toolbox for the Next Decade? // Nordic MATLAB User Conference 2008, Stockholm, Sweden, November 20-21, 2008, pp.1-8.

[15] Aboltins A. Comparison of Orthogonal Transforms for OFDM Communication System//15th International Conference of ELECTRONICS, Kaunas, Lithuania, May 17-19, 2011.

[16] Aboltins A., Misans P., Singular Value Decomposition Based Phi Domain Equalization For Multi-Carrier Communication System // 16th International Conference of ELECTRONICS, Kaunas, Lithuania, June 18-20, 2012.

[17] Aboltins A. Block Synchronization Using a UniqueWord for a Generalized Unitary Rotation Based Communication System // 13th Biennial Baltic Electronics Conference (BEC 2012), Tallinn, Estonia, October 4-5, 2012, pp 149-152.

[18] Aboltins, A. Carrier Frequency Offset Estimator Based on Unique Word Cross-Correlation. // 20th Telecommunications Forum (TELFOR 2012) , Belgrade, Serbia, November 20-22, 2012, pp.486-489.

[19] Aboltins, A., Misans, P. Removal of Super-Imposed Synchronization Sequence Using Matched Filter. // Radioelektronika 2013: 23th Microwave and Radio Electronics Week (MAREW 2013), Pardubice, Czech Republic, April 16-17, 2013, pp.84-88.

The following papers have been published in scientific journals:

[20] Aboltins A., Misans P., Terauds M., Valters G. Initial Implementation of Generalized Haar Like Orthonormal Transforms into FPGA-Based Devices - Part I: Signal Spectrum Analyzer Synthesizer Module // RTU, Telecommunications and electronics. Vol.8 (2008), pp. 16-21

[21] Aboltins A., Klavins D. Synchronization and Correction of Channel Parameters for an OFDM-Based Communication System // Automatic Control and Computer Sciences. - Vol.44, No.3. (2010), pp. 160-170.

[15] Aboltins A. Comparison of Orthogonal Transforms for OFDM Communication System // Electronics and Electrical Engineering. - Vol.5. (2011), pp. 77-80.

[16] Aboltins, A., Misans, P. Singular Value Decomposition Based Phi Domain Equalization For Multi-Carrier Communication System // Electronics and Electrical Engineering, Vol.18, No.9, (2012), pp.71-74.

All mentioned papers are referred by various citation databases. The summary of the paper and their citation availability in databases is given in Table 1.1.

1.9 Structure of the work

Since a considerable amount of background information is needed in order to explain the newly developed methods and other contributions, this doctoral thesis is supplemented with the description of known approaches and basic principles necessary for the completeness of the work.

Reference	International	Web of science	Scopus	IEEExplore
[20]	X			
[14]	X	X		
[21]	X	X	X	
[15]	X	X	X	
[16]	X	X	X	
[17]	X	X	X	X
[18]	X	X	X	X
[19]	X	X	X	X
total	8	7	6	3

Table 1.1: References of my publications, related to this work, in databases

It provides the possibility for a moderately prepared reader to understand the presented topics without substantial external reading. Therefore, this doctoral thesis is more similar to a book rather than a report on a research project or study.

The work is divided into 8 chapters:

Chapter 1 contains a formal part related to the scientific research methodology and this document as a doctoral thesis.

Chapter 2 describes the structure of a PMC system and its counterparts. The GD and TD signal constructions, their generation and allocation into the final signal structure are discussed.

In Chapter 3 the concept of MC modulation based on GUR is discussed. This chapter gives an introduction into other unitary transformations and their application into MC communication systems.This chapter describes and compares several configurations of MC modulator.

The problem of *timing offset synchronization* which is necessary for block and frame synchronization, is explored in Chapter 4.

Chapter 5 is devoted to the problem of *frequency synchronization* in GUR-based MC communication systems.

Chapter 6 contributes to *channel estimation* and *equalization* in GUR-based MC communication systems.

Chapter 7 describes how all previously described ideas can be connected together into a particular variant of GUR-based PMC system. The results of numerous simulations are given.

Chapter 8 is devoted to a variety of new perspectives which have opened up after completing this research.

2 Baseband components

2.1 Formulation of the problem

2.1.1 Objective

In this chapter major components of parametric Generalized Unitary Rotation (GUR)-based parametric multicarrier (PMC) system transmitter and receiver must be reviewed. Additionally, the requirements to constructions of the GUR domain (GD) and time domain (TD) signals, compatible with the proposed PMC system baseband structures, must be developed.

2.1.2 Tasks

In order to meet the objective the following tasks have to be fulfilled:

- Proposition of *transmitter* structure ;
- Proposition of *receiver* structure;
- Analysis of the compatibility of block *padding* methods with non-sinusoidal multicarrier (MC) modulation;
- Review of known synchronization and training *sequences*;
- Development of requirements for an MC *signal* at the output of transmitter baseband;
- Development of methods for adding and removal of synchronization sequences;
- Analysis of the impact of *upconversion* , *downconversion* and pulse *shaping* on non-sinusoidal MC modulation.

2.2 Structure of a parametric multicarrier modulation system

2.2.1 Introduction

Modern data communication systems contain units performing various operations in order to transmit information from a binary source to a destination. In accordance with Open System Interconnection (OSI) architecture, any data system can be divided into 7 layers. First four layers - physical, data link, network and transport are closely related to the communication systems.

Figure 2.1 depicts the major components located in the *physical layer* of a PMC communication system. The most important and complex parts of the physical layer are *baseband* units.

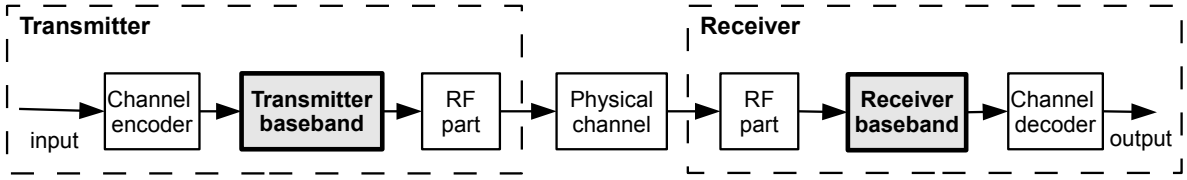

Figure 2.1: Physical layer of a PMC system

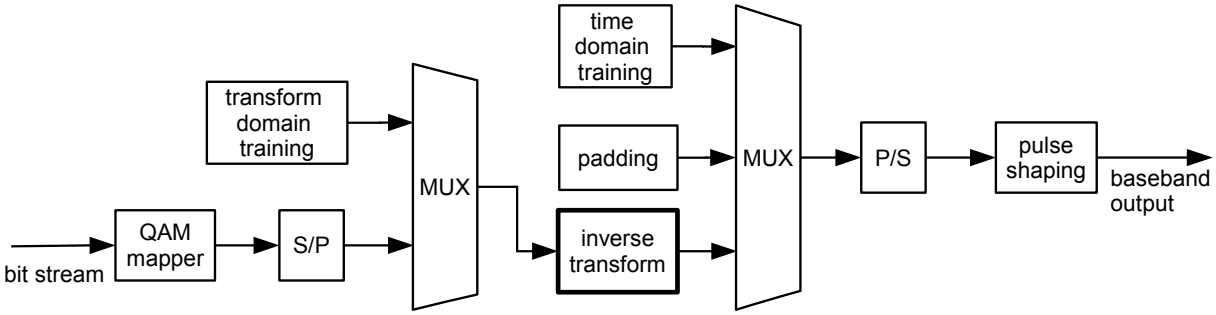

Figure 2.2: Baseband of proposed PMC system transmitter

The baseband of the PMC system transmitter produces a low-pass signal whose lowest frequency is 0. Then, by means of radio frequency (RF) modulator , a complex-valued baseband signal is up-converted to a real-valued passband signal. An RF signal propagates via the communication channel - air, cable, fiber etc. until reaches the receiver, which, in turn, by means of RF down-converter, provides conversion of a passband signal into a baseband signal.

Some communication systems, for example digital subscriber line (DSL) do not use upconversion, in this case the low-pass signal is transmitted into the propagation media, for example, cable. In this case complex signal is converted into real one by adding of additional subcarriers, which in conjunction with existing ones lead to a real-valued TD signal. This approach can be used in PMC systems as well.

This doctoral thesis addresses the baseband parts of GUR-based transmitter and receiver . Moreover, in further text we are dealing with baseband equivalent (see Section 7.3.3) of the communication channel, which includes all RF parts (quadrature modulator, physical communication channel and quadrature demodulator, see Figure 2.10).

2.2.2 Transmitter baseband

The bit stream from the data link (media access control (MAC)) layer enters the physical layer, consisting of channel encoder , baseband part and passband (RF) part. Structure of PMC system transmitter baseband is depicted in Figure 2.2.

The purpose of the first baseband unit - the mapper is converting binary symbol groups into symbols with higher dimensions and/or larger alphabets. For instance, the mapper will map the

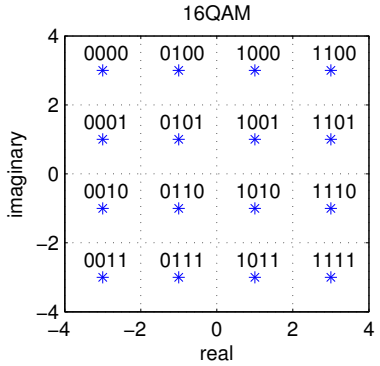

Figure 2.3: 16-QAM constellation

binary combination `0111` into the complex number `-1.0000 - 3.0000i`, which is one of the `4x4=16` possible values in the 16-QAM constellation, shown in Figure 2.3.

Before inverse unitary transform unit, which provides MC modulation, the output vector of the mapper is mixed with transform-domain training (pilot) samples, using multiplexer (MUX). The purpose of these special samples is to provide synchronization references to the receiver as well as to help detect the transform-domain response of the channel.

The unitary transform (see Section 3.2) unit is one of the key elements of a PMC system. The purpose of this unit is to create such set of orthogonal *subcarriers*, which is most appropriate for transmission via communication channel. In other words, the goal of the transform is to make the incoming vector space more resistant to channel effects, such as scattering, noise and attenuation. More information about the MC modulation is given in Chapter 3.

After MC modulation TD training blocks, containing training symbols, are usually added. These symbols act as timing references and can be used for TD channel estimation. Moreover, padding samples like cyclic prefix (CP) (see Section 2.3.4.1), unique word (UW) (see Section 2.3.4.3) or zero padding (ZP) (see Section 2.3.4.2) can be added to the block at the output of unitary transform.

Finally, after output samples are converted into serial form[1], they are filtered with the pulse shaping filter (see Section 2.5). The purpose of this filter is to maximize the in-band energy of the signal and minimize the out-of-band emission. A filter provides an additional facility for increasing the efficiency of PMC system by converting rectangular pulses into overlapping $sinc$ pulses.

[1] in some cases it is not necessary, see Section 3.3.3

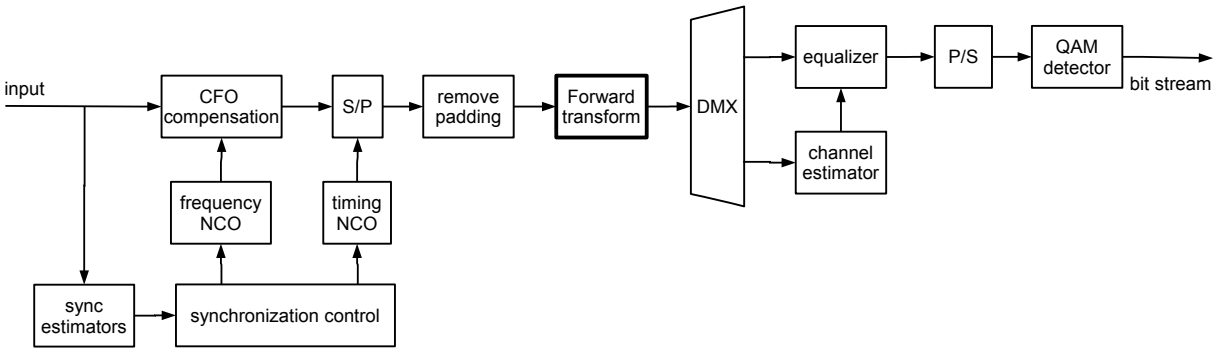

Figure 2.4: Baseband of proposed PMC system receiver

2.2.3 Receiver baseband

Structure of PMC system receiver baseband is depicted in Figure 2.4 and it resembles typical MC receiver architectures. Notice, that because of the necessity to perform synchronization and equalization, the receiver structure is much more sophisticated than that of the transmitter .

After down-conversion, a baseband signal enters the receiver baseband. A TD signal is being split here into two branches - main branch for useful information extraction and synchronization branch - for synchronization and TD channel estimation. Early synchronization extraction is necessary, because the receiver is unable to perform any operation in the main branch until at least coarse timing and frequency synchronization is established. Thus, the purpose of the ”sync estimators” unit is to obtain initial timing and frequency synchronization. Later, when the received signal will be equalized, more precise synchronization will be possible.

Timing and frequency synchronization is performed by means of two numerically controlled oscillators (NCOs). First, the frequency NCO, generates signal, which is being multiplied with the received signal in the unit ”carrier frequency offset (CFO) compensation” for CFO (see Section 5.2.2) correction. The second NCO generates pulses, which are directed to the serial to parallel (S/P) converter to create blocks of samples from the serial stream. It is necessary to obtain correct block synchronization (see Section 4.3) in order to separate blocks correctly.

Before forward transformation, the block padding, which is used for synchronization, estimation and inter-block interference (IBI) reduction can be removed [1]. The forward transform unit (see Section 3.2) performs one of the major operations - demodulation of the subcarriers.

After forward transformation into the transform domain, estimation (see Section 6.5) and equalization (see Section 6.6) take place. The purpose of the equalization is to eliminate inter-symbol interference (ISI) and inter-carrier interference (ICI), introduced by the communication channel. In order to perform GD equalization, it is necessary to estimate characteristics of the *GD* communication channel, which runs from the inverse transform unit in the transmitter to

[1] it is possible to build the transform unit, which utilizes padding as well

the forward transform unit in the receiver. For this purpose received training signals are separated from the useful signal by means of demultiplexer (DMX) and analyzed by the "channel estimator" unit.

The Quadrature amplitude modulation (QAM) detector performs inverse operation of the mapper - converts complex modulation symbols into binary digits. It has to be noticed, that QAM detection is a much more sophisticated operation than QAM mapping, since samples at the input of the detector can be strongly corrupted by the noise, ICI and ISI. Detection is based on selection of a constellation point with a minimum distance to the received sample.

2.3 Structures of baseband signals

2.3.1 Continuous transmission

It is possible to create continuous MC transmission using tree-like unitary transform structures, called transmultiplexers (see Section 3.3.3). However, creation of such a truly continuous stream, which reception can be started at any point, is possible if a linear time-invariant (LTI) transform, which is tolerant to time shifts, is used. Fourier transform (see Section 3.2.2), based on the trigonometric functions, does allow to build an LTI system. It is on of the largest advantages of Fourier transform. An LTI-based system can also be created using wavelets [22]. In the current state of art it is not possible to create a pure LTI system using GUR methods.

2.3.2 Block-wise transmission

Block transmission employs grouping of information symbols into blocks before sending them over the communication channel. Since grouping is performed before the unitary transformation i.e. in GD, samples remain grouped into blocks after the unitary transformation as well.

In the baseband part of the PMC system transmitter , complex-valued data symbols manipulate N discrete basis functions $\varphi(n,k)$ of unitary transformation $\mathbf{\Phi}$, where n is the subcarrier index (in the transform domain) and k is the sample index (in the TD).

2.3.2.1 Equation form

Subcarrier manipulation and transformation from the transform domain to the TD is given as:

$$x(k) = \frac{1}{\sqrt{N}} \sum_{n=0}^{N-1} X(n)\varphi^{-1}(n,k), \quad k = 0,1,...,N-1, \tag{2.1}$$

where $X(n)$ is the useful information samples and N is the size of the information block. These

transform domain samples are, in fact, spectrum coefficients. The respective continuous-time representation of (2.1) is:

$$x(t) = \frac{1}{\sqrt{N}} \sum_{n=0}^{N-1} X(n)\varphi^{-1}(n,t) \quad t \in [0,T], \tag{2.2}$$

where T is the length of the information block. The TD waveform $x(k)$ sent over the communication channel becomes corrupted and the received TD signal is given by:

$$y(k) = \sum_{m=0}^{M-1} h(m)x(k-m) + w(k), \tag{2.3}$$

where h is the impulse response of the channel with length M and w is an additive noise. Received transform domain samples are obtained using a forward transform of the received TD samples:

$$Y(n) = \frac{1}{\sqrt{N}} \sum_{k=0}^{N-1} y(k)\varphi(n,k), \quad n = 0,1,...,N-1. \tag{2.4}$$

2.3.2.2 Matrix form

In matrix form these equations can be written as follows:

An information block $\boldsymbol{X}$ originally is located in the transform domain. Before transmission, the inverse unitary transform brings it from the transform domain to the TD:

$$\boldsymbol{x} = \boldsymbol{\Phi}^{-1}\boldsymbol{X} \tag{2.5}$$

The communication channel distorts transmitted blocks $\boldsymbol{x}$ by various effects described by TD channel matrix $\boldsymbol{H}$ and additive noise $\boldsymbol{w}$:

$$\boldsymbol{y} = \boldsymbol{H}\boldsymbol{x} + \boldsymbol{w}, \tag{2.6}$$

If the channel is static and linear, then $\boldsymbol{y} = \boldsymbol{h} * \boldsymbol{x} + \boldsymbol{w}$ and $\boldsymbol{H}$ corresponds to the subset of Toeplitz matrices [23] called *convolution matrix* (6.3).

The receiver transforms received TD blocks back into the transform domain:

$$\boldsymbol{Y} = \boldsymbol{\Phi}\boldsymbol{y}, \tag{2.7}$$

Equalization restores the original GD samples:

$$\boldsymbol{X} = \boldsymbol{A}^{-1}\boldsymbol{Y}, \tag{2.8}$$

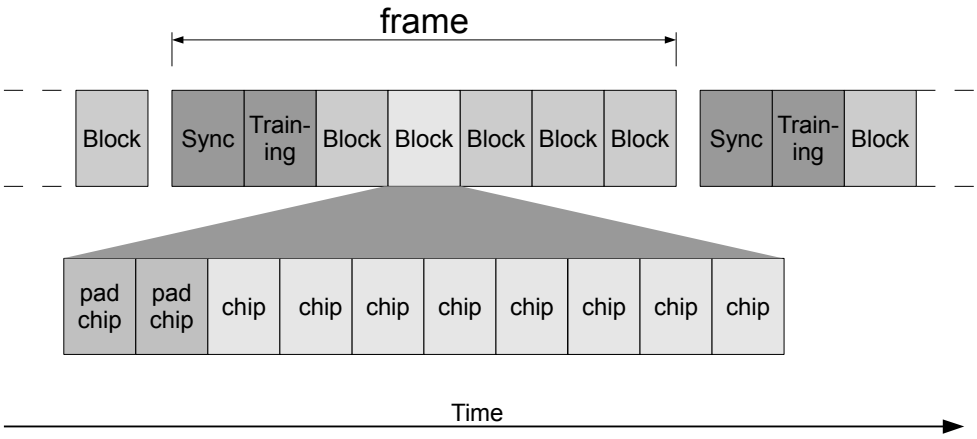

Figure 2.5: Proposed structure of a TD signal

where $\boldsymbol{A}^{-1}$ is the GD equalization matrix, which is obtained by inversion of GD channel matrix $\boldsymbol{A} = \boldsymbol{\Phi}\boldsymbol{H}\boldsymbol{\Phi}^{-1}$ and $\boldsymbol{H}$ is the TD channel matrix. See more about equalization in Section 6.6.

Basis functions $\varphi(n,k)$ in (2.1) and (2.4) are related to the transformation matrix $\boldsymbol{\Phi}$ in the following manner:

$$\boldsymbol{\Phi} = \begin{bmatrix} \varphi(1,1) & \varphi(1,2) & \dots & \varphi(1,k) \\ \varphi(2,1) & \varphi(2,2) & \dots & \varphi(2,k) \\ \dots & \dots & \ddots & \dots \\ \varphi(n,1) & \varphi(n,2) & \dots & \varphi(n,k) \end{bmatrix} \tag{2.9}$$

2.3.3 Block framing

In a digital MC communication system TD information blocks are being transmitted serially - one after another. For synchronization and signaling special synchronization blocks can be inserted. Moreover, transmission may be performed via asynchronous packets containing these blocks. In all these cases an additional TD level of aggregation arises - blocks are grouped into frames. In Figure 2.5 the proposed structure of a TD signal for block-wise transmission is shown.

2.3.4 Block padding

In order to mitigate IBI, TD blocks of the samples are padded by certain patterns. Moreover, padding patterns can be used also for synchronization and channel estimation. The most widely used padding patterns are:

- Cyclic prefix (Section 2.3.4.1)
- Zero padding (Section 2.3.4.2)

- Unique word (Section 2.3.4.1)

In the following sections the applicability of these padding patterns to the GUR-based PMC systems is discussed.

2.3.4.1 Cyclic prefix

When a signal (2.2) is transmitted along a channel with a timing dispersion, a partial superposition of adjacent blocks, i.e., ISI, can occur. Peled and Ruiz in [24] suggested using cyclic continuation of blocks - a CP - for solving this problem. The whole block $\boldsymbol{x_{cp}}$ with a CP of length L is obtained from the TD block $\boldsymbol{s}$:

$$\boldsymbol{x_{cp}} = \left[s_{K-L+1}, s_{K-L+2}, \ldots, s_K, s_1, s_2, \ldots, s_K\right]. \tag{2.10}$$

The cyclic continuation of a signal preserves its amplitude spectrum and just shifts the signal's phase spectrum. The CP plays crucial role in frequency domain (FD) equalization (see Section 6.6) for orthogonal frequency division multiplexing (OFDM) systems and CP-based SC systems [25]. The cyclic continuation of a signal makes the channel impulse response to appear cyclic and turns the TD channel matrix $\boldsymbol{H}$ into *circulant* [23], whereas the FD channel matrix $\boldsymbol{A_F} = \boldsymbol{FHF^{-1}}$, where $\boldsymbol{F}$ denotes the discrete Fourier transform (DFT) matrix, becomes *diagonal* . Since the channel matrix is diagonal, its inversion is straightforward and 1-tap FD equalization can be used. Thus we can say that the cyclic extension of TD signal eliminates ICI. If the length of CP is greater than the pulse response of the channel, then the ISI is completely resolved by a proper choice of the time for the beginning of the block, i.e., by block synchronization (see Section 4.3).

However, in accordance with simulation results, presented in Section 6.8, CP in a GUR-based PMC system does not provide those advantages available in OFDM. This is because unlike the FD, CP does not eliminate ICI in the GD, since the GD channel matrix $\boldsymbol{A_\Phi} = \boldsymbol{\Phi H \Phi^{-1}}$ is not diagonal, more details see Section 6.6.3.

2.3.4.2 Zero padding

ZP is the simplest padding method, based on padding of the transmitted vector $\boldsymbol{s}$ with zeroes:

$$\boldsymbol{x_{zp}} = \left[0, 0, \ldots, 0, s_1, s_2, \ldots, s_K\right]. \tag{2.11}$$

ZP provides a guard interval (GI), which prevents IBI. ZP is an energy-efficient kind of padding, since it does not require additional energy for the transmission. However, in OFDM systems ZP poses an additional source of noise, which is generated in case of block synchronization (see Section 4.3) imperfections [26]. Moreover, ZP provides too few facilities for

synchronization and channel estimation.

2.3.4.3 Unique word

UW is a padding method where each block of samples $\boldsymbol{s}$ is preceded by a constant combination of samples $\boldsymbol{u}$:

$$\boldsymbol{x_{uw}} = \big[u_1, u_2, \ldots, u_L, s_1, s_2, \ldots, s_K\big]. \tag{2.12}$$

UW is usually known to the receiver and can provide means for channel estimation (see Section 6.5) and synchronization (see Chapters 4 and 5). UW-based padding has several advantages compared to the CP-based padding. Many of them are analyzed in [27] in context of single carrier FDE (SC-FDE). Moreover, UW-based padding has gained significant interest during the last decade in OFDM communication systems [28]. Due to fact, that UW repeats itself in adjacent blocks, it is suitable for frequency domain equalizer (FDE) (see Section 6.6.2).

The possibility to choose between specialized sequences for synchronization and the possibility to use them for channel estimation [16], in many cases makes UW-based padding an optimal choice.

For GUR-based systems UW has the following advantages compared to CP:

- UW can provide better means for block timing (see Section 4.3) and frequency synchronization via the choice of specialized sequences.
- CP autocorrelation (AC)-based synchronization algorithms can be used in UW systems.

2.4 Synchronization sequences

2.4.1 Introduction

Synchronization is an essential part of any digital communication system. A digital communication receiver must perform sampling of the received analog signal, must detect the start and the end of transmission and must be able to extract various service-related information from the received signal. All synchronization methods can be classified by technique, domain and structure. Chapter 5 is devoted to the problem of frequency synchronization in GUR-based PMC systems, but Chapter 4 is dedicated to the timing synchronization.

The synchronization process is usually divided into several stages. At the very beginning the receiver is in *acquisition* mode. In this mode the receiver tries to establish timing and frequency synchronization and to start reception. Due to the instability of receiver parameters and channel

influence, the receiver needs to continuously update synchronization -related information. In this case it is said that the receiver is in *tracking* mode.

In order to provide data-aided (DA) or decision-directed (DD) timing and frequency synchronization, special sequences must be added to the payload signal. Additionally, for the non-blind *channel estimation* , training sequences must be added. Moreover, in an ideal case the same sequence can be used simultaneously for timing/frequency synchronization and channel estimation. In order to provide efficient synchronization and channel estimation, sequences must have certain properties which depend on estimation algorithms. In the following subsections two popular synchronization and training sequences will be reviewed.

2.4.2 Adding and removal of synchronization sequences

There are several ways how a synchronization sequence can be embedded into a transmitted signal. Two most popular ways of super-position between the payload signal and the synchronization signal are:

- inserted sequence;
- super-imposed (SI) sequence.

2.4.2.1 Inserted sequences

Synchronization and training sequences can be inserted into a signal, between the useful samples. This operation can be performed before transformation into the TD, in this case this sequence can be regarded as “transform domain sequence”. Otherwise, the training sequence can be inserted into a TD signal and called as “TD sequence”. The UW prefix (see Section 2.3.4.3) is a typical example of an inserted synchronization sequence.

Once correct timing offset synchronization (see Chapter 4) is established, inserted sequences can be easily removed by discarding respective samples of the received signal.

The major drawback of the inserted sequences is that they consume time and frequency resources, since during transmission of synchronization sequences no payload is being transmitted.

2.4.2.2 Super-imposed sequences

SI sequences are added to the useful signal. SI synchronization and training signals can provide a considerable bandwidth saving, since they consume just a small portion of the dynamic range of the signal rather than time or frequency resources. There are several main uses of super-imposed signals:

- timing offset estimation (see Chapter 4);

name	formula	$\langle \boldsymbol{U}, \boldsymbol{X} \rangle$
Zadoff-Chu	$e^{j\frac{3n^2}{N}}$	$0.89/\sqrt{N}$
m-sequence	see [31]	$0.88/\sqrt{N}$
random	$a + jb$	$0.88/\sqrt{N}$
complex exponent	$e^{j2\pi\frac{n}{N}}$	$1/\sqrt{N}$

Table 2.1: Comparison of UW sequences

- frequency offset estimation (see Chapter 5);
- channel estimation or equalization, using TD system identification techniques, like least mean squares (LMS)(see Section 6.5.1.3).

Unlike inserted sequences, SI sequences cannot be easily removed. One typical approach [29] is based on subtraction of the synchronization sequence from the received signal. Namely, if the transmitted signal $\boldsymbol{x_{si}}$ is a sum of useful signal $\boldsymbol{x}$ and UW sequence $\boldsymbol{u}$:

$$\boldsymbol{x_{si}} = \boldsymbol{x} + \beta \boldsymbol{u}, \tag{2.13}$$

where β is the magnitude of the SI unique word (UW) signal, then subtraction of UW sequence from the received baseband signal y_{si} allows to recover the useful signal:

$$\boldsymbol{y} = \boldsymbol{y_{si}} - \beta \boldsymbol{u} \tag{2.14}$$

However, this approach works only in case of good equalization (see Chapter 6), when $\boldsymbol{y_{si}} \approx \boldsymbol{x_{si}}$. Moreover, the magnitude β of SI signal must be known.

The randomness of the useful MC signal can be exploited in order to remove the SI sequence without the knowledge of its amplitude [19]. For example, in literature, OFDM is frequently treated as a complex random process having a circular symmetric complex normal (Gaussian) distribution [30]. Therefore, the correlation of OFDM signal with any other independent signals will be weak and the orthogonality will increase along with the number of subcarriers. The orthogonality between some pseudo-noise (PN) signals [1] and an OFDM signal has been analyzed. The third column of Table 2.1 shows the inner product between a UW sequence with $||\boldsymbol{u}|| = 1$ and an OFDM signal with $||\boldsymbol{x}|| = 1$. From the table it is seen, that the orthogonality between the UW sequence and the OFDM signal improves as the dimension of vectors (i.e the number of OFDM subcarriers) increases.

[1] the complex exponent is given for reference

In this case a special filter must be used for the removal of the SI sequence. The purpose of this filter is to remove a known UW sequence, scaled by an unknown factor β, from an equalized signal $\boldsymbol{x_{si}}$. In other words, the filter removes the vector $\boldsymbol{u}$ from the sum of vectors $\boldsymbol{x_{si}} = \boldsymbol{x} + \hat{\beta}\boldsymbol{u}$, where $\hat{\beta}$ is an unknown scaling coefficient.

The proposed filter utilizes the partial orthogonality between two random signals - a PN sequence of the UW and the useful MC signal. In case of full orthogonality, the following condition would hold:

$$\langle \boldsymbol{u}, \boldsymbol{x} \rangle = \boldsymbol{u}^* \boldsymbol{x} = 0 \tag{2.15}$$

Indeed, if the orthogonality condition (2.15) holds, then it is possible to find such orthogonal basis, where samples from the first signal do not overlap with the samples of the second signal.

Such basis can be found using GUR (see Section 3.2.4.1). Namely, it is possible to find the orthogonal basis $\boldsymbol{\Phi}$, which transforms the given vector into a new vector $\boldsymbol{u}' = \boldsymbol{\Phi u}$ consisting only from one non-zero sample. Noticeably, that the first basis function of the transform $\boldsymbol{\Phi}$ is equal to the normalized $\boldsymbol{u}$.

Since one signal coincides with one of the basis functions, signals orthogonal to it will not overlap with it in this basis. Thus, taking into account the orthogonality condition (2.15), removal of UW from the received signal reduces to the transformation of the mixture of signals $\boldsymbol{y_{si}}$ to the new domain:

$$\boldsymbol{y}^{\phi}_{\boldsymbol{si}} = \boldsymbol{\Phi} \boldsymbol{y_{si}}, \tag{2.16}$$

where $\boldsymbol{\Phi}$ can be constructed using the method described in Section 3.2.4.1. Filtering reduces to the zeroing of the (first) sample, which corresponds to the SI signal in the GUR domain:

$$\boldsymbol{y}^{\phi} = \boldsymbol{P} \boldsymbol{y}^{\phi}_{\boldsymbol{si}}, \text{ where } \boldsymbol{P} = \text{diag}(011 \ldots 1) \tag{2.17}$$

Finally, the signal must be reverted into the original domain using the inverse transformation:

$$\boldsymbol{y} = \boldsymbol{\Phi}^{-1} \boldsymbol{y}^{\phi} \tag{2.18}$$

Alternatively, the direct approach using a matched filter (MF) can be employed. Actually, in order to perform filtering, a complete orthogonal basis is not necessary, it is sufficient to find the first sample of the mixture $\boldsymbol{y_{si}}$ in the new (unknown) basis, and remove it from the signal. Since the first basis function coincides with the UW signal $\boldsymbol{u}$, the inner product between the mixture $\boldsymbol{x_{si}}$ and the UW signal $\boldsymbol{u}$ yields a scaled first sample in the new basis:

$$\boldsymbol{u}^{*}\boldsymbol{y_{si}} = \boldsymbol{u}^{*}\boldsymbol{y} + \beta\,\boldsymbol{u}^{*}\boldsymbol{u} = \beta\,||\boldsymbol{u}||^{2} \tag{2.19}$$

The first member of the sum (2.19) is equal to zero due to the orthogonality condition (2.15). Therefore, the calculation of the unknown scaling coefficient $\hat{\beta}$ is straight-forward:

$$\hat{\beta} = \frac{\boldsymbol{u}^{*}\boldsymbol{y_{si}}}{||\boldsymbol{u}||^{2}} \tag{2.20}$$

We have obtained an ordinary MF, which correlates a known template $\boldsymbol{u}$ with an unknown signal $\boldsymbol{y_{si}}$. The filtering process reduces to finding the inner product between the mixture and undesired signal and the extraction of a correctly scaled undesired signal. By inserting (2.20) into (2.14), the equation describing the whole direct filtering process is as follows:

$$\boldsymbol{y} = \boldsymbol{y_{si}} - \frac{\boldsymbol{u}^{*}\boldsymbol{y_{si}}}{||\boldsymbol{u}||^{2}}\boldsymbol{u} \tag{2.21}$$

Notice,that the full orthogonality condition (2.15) can be *fully* satisfied if the UW sequence is one of the orthogonal subcarriers of MC signal.

2.4.3 Review of the UW sequences

2.4.3.1 Zadoff-Chu sequence

In the article by Chu [32], based on an earlier paper by Frank and Zadoff [33], the approach of generating codes with good periodic correlation properties is described [1]. These sequences represent so -called constant amplitude zero autocorrelation (CAZAC) sequences. The codes are generated using the equations:

$$a_k = \begin{cases} e^{j\frac{M}{Q}\pi k^2}, & \text{if Q is odd} \\ e^{j\frac{M}{Q}\pi k(k+1)}, & \text{if Q is even} \end{cases} \tag{2.22}$$

where $k = 0, 1, \ldots, Q-1$ is the sample index, M is an integer *coprime* with Q. Zadoff-Chu (ZC) sequences can be used for timing synchronization (see Chapter 4), frequency synchronization (see Chapter 5) and channel estimation (see Section 6.5). In Figure 2.6 the properties of an example ZC sequence with $M = 16$ and $Q = 3$ and its probability density function (PDF) are presented. From the time series graph we can observe, that ZC is obtained by periodic sampling of chirp signal.

[1] These codes are widely used [34],[35] in the modern standard for broadband mobile communications, called Long Term Evolution (LTE), developed by 3rd Generation Partnership Project (3GPP) standardization group.

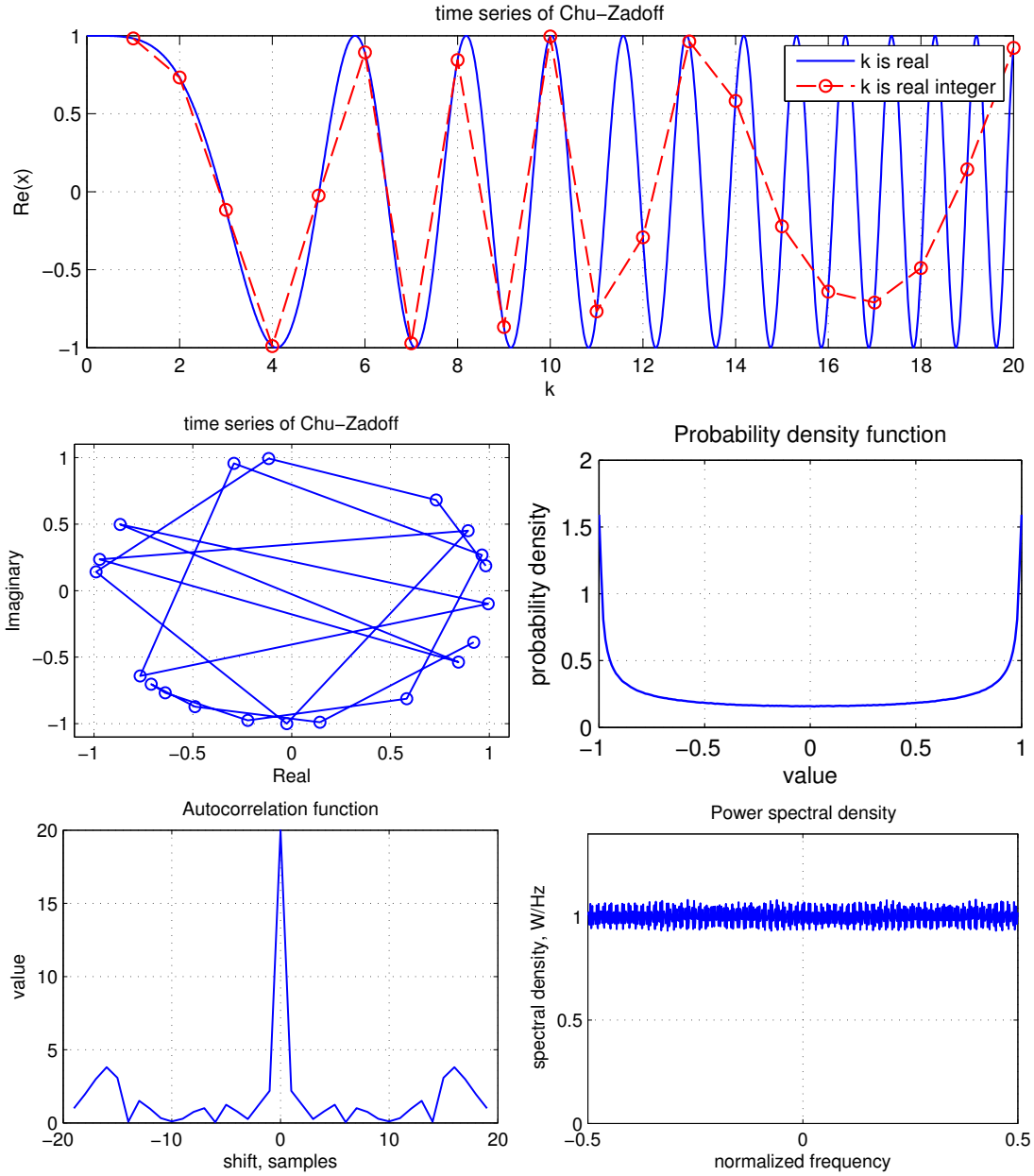

Figure 2.6: Properties of an example ZC sequence with $M = 16$ and $Q = 3$

2.4.3.2 Schmidl-Cox sequence

In the widely-cited paper [36] by Schmidl and Cox, the authors propose to use two special training blocks. The first block in the TD consists of two equal parts. It is generated by filling even subcarriers with a complex PN sequence and setting odd subcarriers to zero. The symmetry of the block makes it immune to carrier and sampling frequency offsets and makes possible fast detection of the block start. Moreover, the values on even OFDM subcarriers allow to make FD channel measurements. The second block consists of two another PN sequences. They will

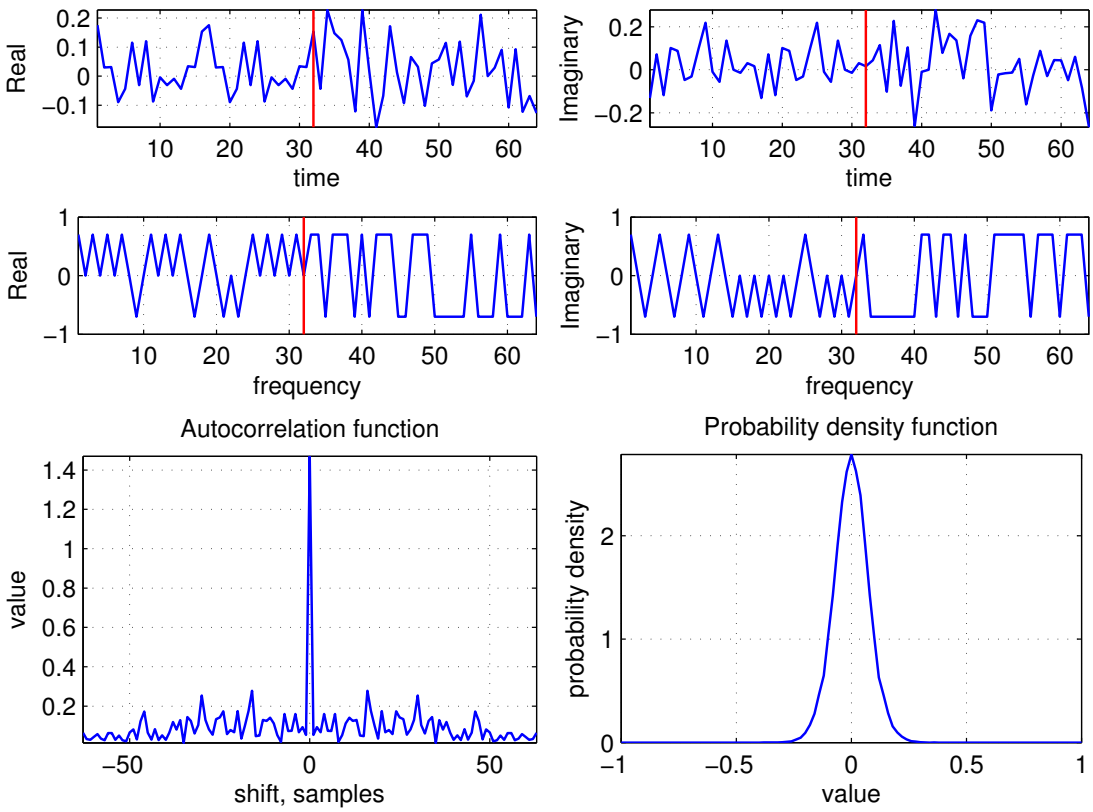

Figure 2.7: Properties of an example Schmidl-Cox sequence

help to measure the channel frequency response on the remaining (odd) OFDM subcarriers and to calculate the frequency offset.

In order to check the applicability of Schmidl-Cox sequence to a GUR-based PMC system, Schmidl-Cox sequences were generated using the original method, described in paper [36], and their properties were analyzed. Two PN sequences with possible values 0 and ± 0.7 for real and imaginary parts were created (Figure 2.7 left). Using the inverse discrete Fourier transform (IDFT) they have been transformed into the TD (Figure 2.7 right). The autocorrelation function and PDF of the given sequences are shown in Figure 2.7.

Schmidl-Cox sequences can be used for frame and block timing synchronization in GUR-based PMC systems (see Chapter 4). However, since FD equalization is not used in GUR-based PMC systems (see Section 6.6.2), part of the advantages remain unused.

2.4.4 Impact of communication channel on the training sequences

The dispersion in the communication channel and pulse shaping filters corrupts the training sequences designated for the time and frequency synchronization. It is of big importance to understand how channel effects, namely convolution, affect the amplitude and phase of AC and

cross-correlation (XC).

2.4.4.1 Cross-correlation

XC between two vectors x and y with length K is described by Equation (2.23):

$$v_{xc}(i) = \sum_{k=0}^{K-1} y(k)x(k-i), \quad i \in [-K; 2K] \tag{2.23}$$

If transmitted and received TD training signals are denoted respectively as x and y and the impact of the communication channel with the impulse response h with length M and the additive noise w is described by Equation (2.3), then inserting of (2.3) into (2.23) produces the following result:

$$v_{xc}(i) = \sum_{k=0}^{K-1} \left(x(k-i) \sum_{m=0}^{M-1} h(m)x(k-m) \right) + \sum_{k=0}^{K-1} x(k-i)w(k), \quad i \in [-K; 2K] \tag{2.24}$$

Convolution and XC are strongly related to each other, since convlution is XC with reversed one of the vectors. Moreover, XC from the convolution can be replaced by reversed convolution from AC, namely:

$$\langle \boldsymbol{x}, (\boldsymbol{x} * \boldsymbol{h}) \rangle = \langle \boldsymbol{x}, \boldsymbol{x} \rangle * \tilde{\boldsymbol{h}} \tag{2.25}$$

where $\tilde{\boldsymbol{h}}$ is reversed vector $\boldsymbol{h}$. *Therefore XC function of the received signal is equal to the convolution between AC function of the transmitted signal and reversed channel impulse reponse.*

Figure 2.8 depicts the results of XC of the ZC sequence after its convolution with one particular, randomly generated channel impulse response. It is perfectly visible from Figure 2.8, that the XC function mimics the channel impulse response. By comparing Figures 2.6 and 2.8 it can be concluded, that convolution in the communication channel significantly affects the XC properties of training sequences.

2.4.4.2 Autocorrelation

AC of vector y with length K is described by Equation (2.26):

$$v_{ac}(i) = \sum_{k=0}^{K-1} y(k)y(k-i), \quad i \in [-K; 2K] \tag{2.26}$$

If transmitted and received TD training signals are denoted respectively as x and y and the impact of the communication channel with the impulse response h with length M and the

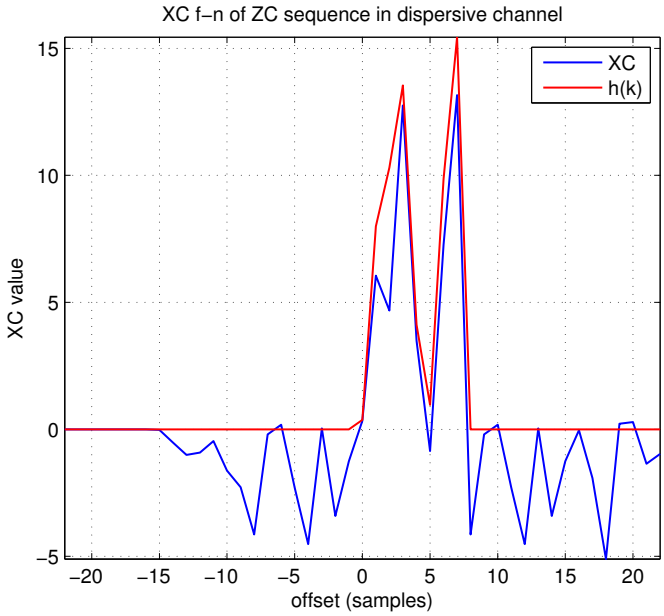

Figure 2.8: Impact of the channel impulse response on the cross -correlation function of the training sequence

additive noise w is described by Equation (2.3), then inserting of (2.3) into (2.26) produces the following result:

$$v_{xc}(i) = \sum_{k=0}^{K-1}\left(\sum_{m=0}^{M-1} h(m)x(k-m) + w(k)\right)\sum_{k=0}^{K-1}\left(\sum_{m=0}^{M-1} h(m)x(k-m-i) + w(k-i)\right), \quad i \in [-K; 2K] \tag{2.27}$$

Figure 2.9 depicts the results of AC of the ZC sequence after its convolution with one particular, randomly generated channel impulse response. By comparing Figures 2.6 and 2.8 it can be concluded, that static convolution of the shaping filters and time-dispersive communication channel does not have a strong impact on the AC properties of training sequences.

2.5 Transmit filtering and upconversion

Serialized complex signal at the output of parallel-to-serial (P/S) converter has the sampling rate $f_{chip} = 1/\tau$, is N times higher than speed of unitary transform unit. Before transmission over the communication channel digital complex samples must be converted to an analog signal and upconverted to the carrier frequency (in case of *passband transmission*) or converted into a real-valued signal (if *baseband transmission* is used).

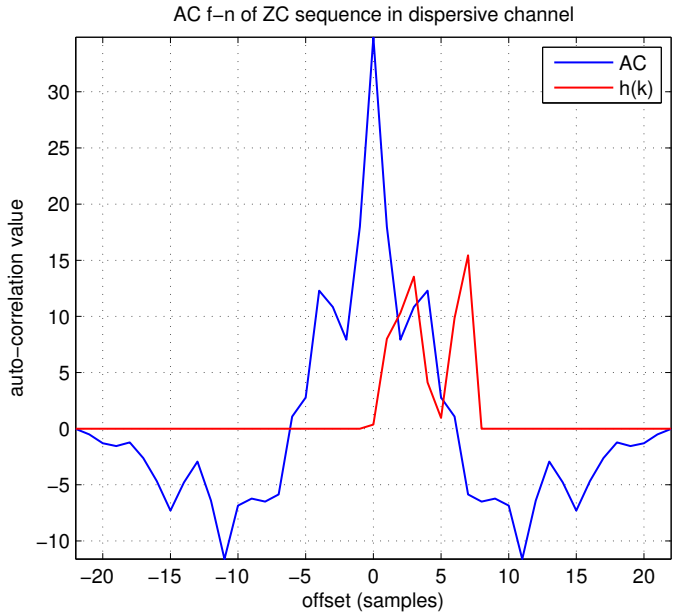

Figure 2.9: Autocorrelation function of the ZC training sequence after convolution with the impulse response $h(k)$

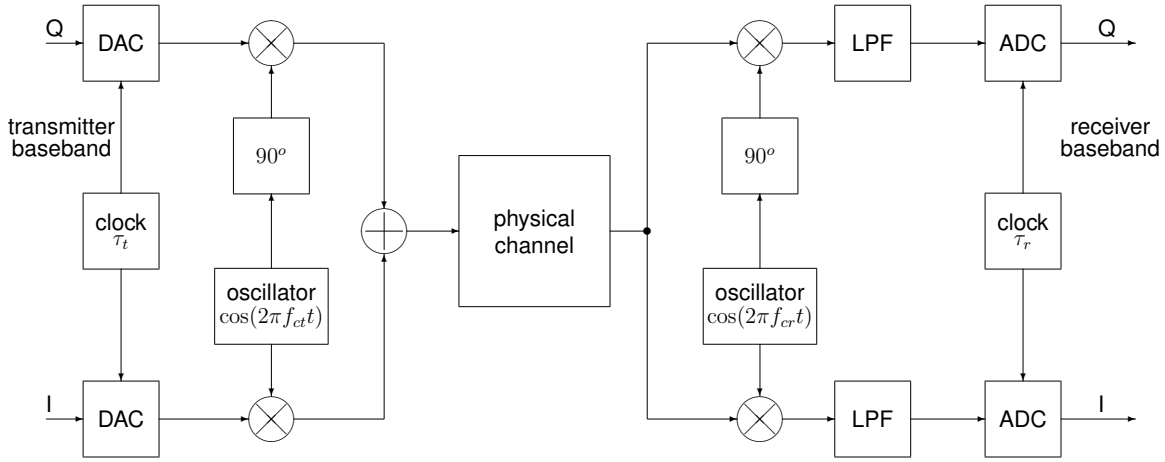

Figure 2.10: RF part of a PMC system

Additionally, before *upconversion* a signal must be filtered in order to eliminate harmonics created by the transitions between the samples, i.e. sample rate conversion of the signal is necessary. Signal must be upsampled to the highest possible frequency $f_{sampling}$, since at a higher sampling frequency the filter with a larger delay and, thus, a better stopband attenuation can be used. Unfortunately convolution of the TD signal leads to the ICI between subcarriers produced using GUR.

Since the pulse shaping filter performs filtering in the FD by means of *convolution* in the TD, the zero ICI condition (6.12) is not fulfilled (see Section 6.4.3). Therefore, any FD filtering, including transmit pulse shaping, leads to the ICI between GD subcarriers. Turns out that a filter

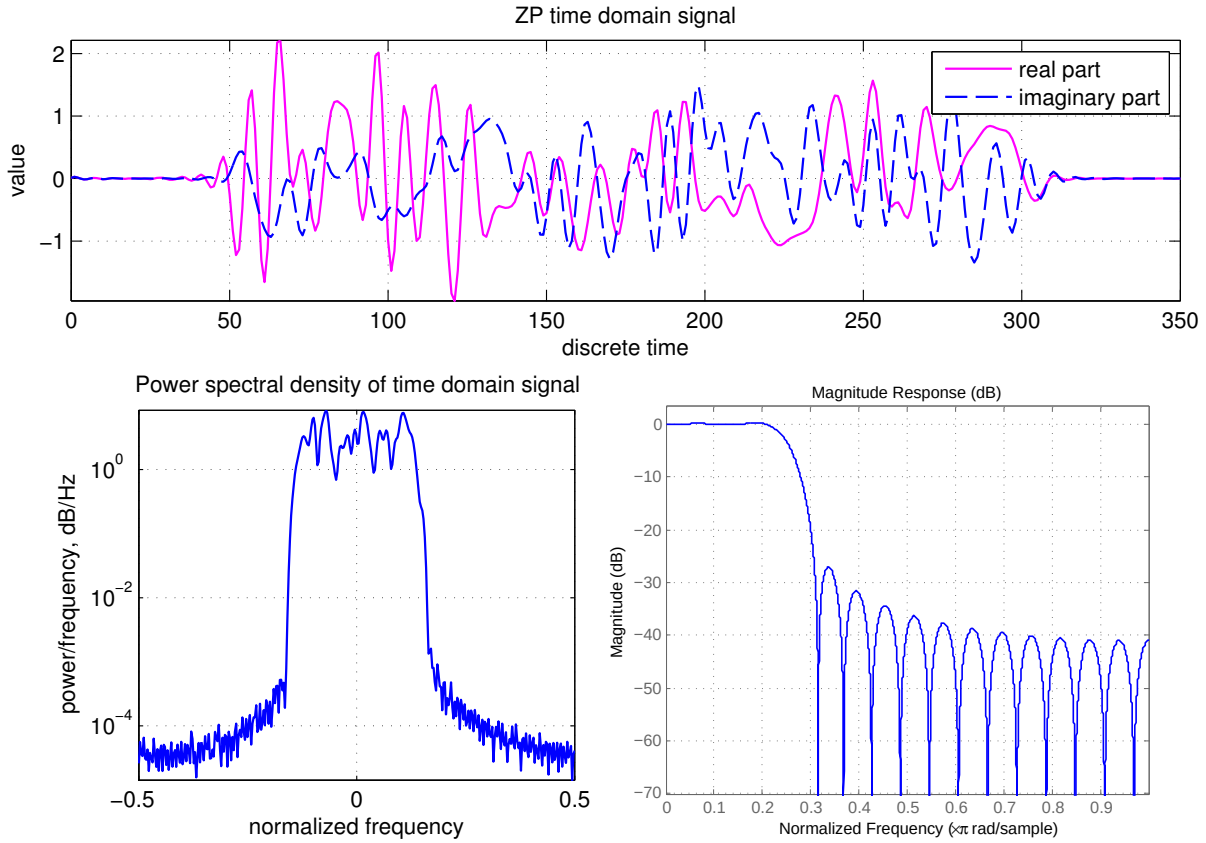

Figure 2.11: Example of GUR-based PMC system's TD signal, power spectrum after upsampling and filtering, and frequency response of the raised cosine FIR filter with 65 coefficients. ($\phi = 30^o$, 4x upsampling, filter delay is 8, excess bandwidth is 0.25)

with a larger delay increases the interference between GD subcarriers and more equalization at the receiver side will be required. An example of the signal after filtering in a GUR-based PMC system is given in Figure 2.11. From this figure it is visible that the filter with order 8 provides a 40 dB stopband attenuation, which is enough in many practical cases.

Upconversion can be performed by standard means of quadrature modulation - the real part of the signal is modulated by $cos(2\pi f_{ct}t)$, whereas the imaginary part by $sin(2\pi f_{ct}t)$. By f_{ct} in this formula the transmitter carrier frequency is denoted. In practical implementations it is important to choose a carrier frequency generator with low phase noise and high frequency stability, since MC systems are very sensitive to frequency offsets (see Chapter 5). The RF part of a PMC system with upconversion is depicted in Figure 2.10.

2.6 Conclusions

- CP cannot be used within GUR-based PMC systems, because it do not mitigate ICI.

- UW prefix is suitable for use in GUR-based PMC systems.
- Super-imposed sequence (SIS) is an alternative method for the transmission of training and synchronization sequences in PMC systems.
- Convolution in the communication channel seriously affects XC properties of the received signal.
- Pulse shaping filter at the transmitter baseband output causes ICI.

2.7 Summary of contributions

- TD signal structure, which compatible with GUR transform is proposed (see Section 2.3.3).
- Impact of the convolution on the correlation properties of the signal is analyzed (see Section 2.4.4).
- Impact of the transmitter pulse shaping filter is analyzed (see Section 2.5).
- Two methods of removal of SI UW sequence using GUR domain filter and MF are proposed (see Section 2.4.2.2).

3 Multicarrier modulation

3.1 Formulation of the problem

3.1.1 Objective

This chapter is devoted to the exploration of multicarrier (MC) *modulation* and *demodulation* based on Generalized Unitary Rotation (GUR).

3.1.2 Tasks

In order to meet the objective the following tasks have to be fulfilled:

- Review of known unitary transforms used for MC data transmission;
- Review of known GUR algorithms;
- Impact of the transformation direction (forward for modulation, inverse for demodulation or vice versa) must be explored;
- Research of tree-like configurations of MC modulation and demodulation;
- Exploration of basic mechanisms for the selection of a unitary transform;
- Measurement of peak-to-average power ratio (PAPR) of an MC signal, created using GUR.

3.2 Unitary transforms for digital modulation

In order to provide a MC modulation, unitary transforms can be used (see Section 2.3.2). Although there is a large variety of known unitary transforms, only few of them are widely used for the creation of the subcarriers in MC modulation.

3.2.1 Identity transform

Transformation matrix of the identity transform is represented by the identity matrix and it is shown in the Equation 3.2.1. Since there is no any signal transformation, plain quadrature amplitude modulation (QAM) signal is transmitted between the transmitter and the receiver.

$$\boldsymbol{I} = \begin{bmatrix} 1 & 0 & \cdots & 0 \\ 0 & 1 & \cdots & 0 \\ \vdots & \vdots & \ddots & \vdots \\ 0 & 0 & \cdots & 1 \end{bmatrix} \tag{3.1}$$

3.2.2 Fourier transform

A typical example of block transmission technique employing Fourier transform is orthogonal frequency division multiplexing (OFDM). In this case the forward transform φ in (2.4) is given by:

$$\varphi(k,n) = e^{-j2\pi k\frac{n}{N}} \tag{3.2}$$

And the inverse transform φ^{-1} in (2.1) is defined as:

$$\varphi^{-1}(k,n) = e^{j2\pi k\frac{n}{N}} \tag{3.3}$$

The lowest *arithmetical complexity* equal to $\frac{34}{9}N\log_2 N$ for the fast variant of discrete Fourier transform (DFT), called fast Fourier transform (FFT), was achieved by algorithm ,described in [37].

3.2.3 Complex Hadamard transform

Basis functions $\varphi(n,k)$ of complex Hadamard transform are columns of Hadamard matrix [38]. Inverse basis functions can be obtained from the rows of the same matrix. A variant of complex Hadamard transform is given in Equations (3.4) and (3.5). The symbol $\otimes$ denotes Kronecker product and $\otimes^n$ denotes n-time multiple Kronecker products. The Hadamard transform, which consists only of *real* values, is also known as Walsh-Hadamard transform (WHT).

$$\mathbf{\Phi_1} = \begin{bmatrix} 1 & -j \\ 1 & j \end{bmatrix} \tag{3.4}$$

$$\mathbf{\Phi_n} = \mathbf{\Phi_1} \otimes \mathbf{\Phi_{n-1}} = \mathbf{\Phi_1}\otimes^n \tag{3.5}$$

In accordance with [39], Fast Hadamard transform requires $N\log_2 N$ additions or subtractions.

3.2.4 Generalized Unitary Rotation transform

GUR[1] is a technique, which allows to factorize unitary matrices using fast elementary rotations in real or complex signal space [41]. Unitary matrices can be factorized using also another algorithms, see, for example [42] .

[1]Term "GUR" has been introduced by Misans and Valters [40], and in earlier publications [41] it was called "Phi transform".

Moreover, GUR provides a fast mechanism for the creation of arbitrary unitary bases by means of a factorization of N-dimensional (currently, 2-dimensional) rotation. Another N-dimensional rotation algorithm in real space has been described in [43], however, this algorithm performs considerably slower than [41], since it does only one rotation per iteration. The unitary transform matrix $\mathbf{\Phi}$ of GUR transform is defined as follows:

$$\mathbf{\Phi} = \prod_{p=\log_2(N)}^{1} \boldsymbol{B_p}(\phi, \gamma, \psi) \tag{3.6}$$

In this equation ϕ, γ and ψ are real angles which could take any value $\in [0; 2\pi]$, and stairs-like orthogonal generalized rotation matrix (SOGRM) $\boldsymbol{B_p}$ is defined as:

$$\boldsymbol{B_p} = \begin{bmatrix} \tau^1_{1,p} & 0 \;\; 0 & \dots & 0 \;\; 0 \\ 0 \;\; 0 & \tau^1_{2,p} & \dots & 0 \;\; 0 \\ \dots & \dots & \ddots & \dots \\ 0 \;\; 0 & 0 \;\; 0 & \dots & \tau^1_{N/2,p} \\ \tau^2_{1,p} & 0 \;\; 0 & \dots & 0 \;\; 0 \\ 0 \;\; 0 & \tau^2_{1,p} & \dots & 0 \;\; 0 \\ \dots & \dots & \ddots & \dots \\ 0 \;\; 0 & 0 \;\; 0 & \dots & \tau^2_{N/2,p} \end{bmatrix} \tag{3.7}$$

This matrix contains only mutually independent plane rotations. However, it contains just a fraction of the total number of rotations, therefore it is necessary to factorize $\log_2(N)$ such matrices in (3.6). The elements of each SOGRM are obtained from unitary four-element single-plane rotation matrices. There are possible 64 variants (sine, cosine, + and - combinations) of a single-plane rotation matrix. One variant of a single-plane rotation matrix could be:

$$\Upsilon = \begin{bmatrix} \tau^1_{q,p} \\ \tau^2_{q,p} \end{bmatrix} = \begin{bmatrix} \mp sin\phi_{q,p} e^{-j\psi_{q,p}} & cos\phi_{q,p} e^{j\gamma_{q,p}} \\ cos\phi_{q,p} e^{-j\gamma_{q,p}} & \pm sin\phi_{q,p} e^{j\psi_{q,p}} \end{bmatrix} \tag{3.8}$$

3.2.4.1 Fast creation of unitary bases with a desired first basis function

One of the most important applications of GUR is creating of such unitary basis, where one of the basis functions coincides with the required waveform $\boldsymbol{U_d}$. If the vector to be transformed is equal to $\boldsymbol{U_d}$, then the output of the transformation contains only one non-zero sample. Therefore, this algorithm provides an excellent facility for the compression of signals similar to $\boldsymbol{U_d}$. On the other hand, it is possible, using this operation, to super-impose a signal $\boldsymbol{U_d}$ into output sequence.

Algorithm 1: Algorithm *rgur*(), which produces an orthonormal matrix.

Data: required real waveform
Result: orthonormal matrix
set the number of samples equal to the length of waveform;
set factorized matrix ϕ as identity matrix;
while *number of samples* $\geqslant$ *2* **do**
    divide signal into pairs;
    find angles α_i between vectors, which are described by pairs, and first axes;
    rotate all vectors by respective angles α_i;
    factorize all rotation matrices into ϕ;
    divide the number of samples by 2;
end

3.2.4.1.1 Algorithm for vectors with length $N = 2^{\mathbb{Z}}$

If it is a complex waveform, a rotation in complex space is required. This task can be fulfilled using two real rotations [41] and the transformation of a complex vector $\boldsymbol{X_d}$ can be performed in the following manner:

$$\boldsymbol{\Phi X_d} = \boldsymbol{\phi_R}\Re(\boldsymbol{X_d}) + j\ \boldsymbol{\phi_I}\Im(\boldsymbol{X_d}), \tag{3.9}$$

where $\Re$ and $\Im$ denote respectively real and imaginary parts of the vector.

$$\boldsymbol{\phi_R} = rgur(\Re(\boldsymbol{U_d})) \tag{3.10}$$

$$\boldsymbol{\phi_I} = rgur(\Im(\boldsymbol{U_d})) \tag{3.11}$$

Notice that $\Phi_R \neq \Re(\boldsymbol{\Phi})$ and $\Phi_I \neq \Im(\boldsymbol{\Phi})$. The function *rgur*() represents a real rotation algorithm, which takes the required real waveform as an argument and produces a real orthonormal matrix. Algorithm 1 shows the main operations in the original algorithm, developed by Misans [41]. This algorithm is capable to create such orthonormal matrix, where the first basis function coincides with the requested waveform $\boldsymbol{U_d}$.

3.2.4.1.2 Algorithm for vectors with length $N = \mathbb{Z}$

The limitation of the algorithm, described in Section 3.2.4.1.1, is that it can process incoming vectors with the number of samples, which is the power of two. In some cases, for example, if just a part of block should be transformed, it is necessary to process blocks, whose length is not the power of two. Algorithm 1 was extended in order to produce orthonormal bases, whose dimensions are any real integer. Algorithm 2 shows the main operations, which have

Algorithm 2: Algorithm *rgur*(), which produces an orthonormal matrix.

Data: required real waveform
Result: orthonormal matrix
set the number of samples equal to the length of waveform;
set factorized matrix ϕ as identity matrix;
while *number of samples* $\geqslant 2$ **do**
  if *number of samples is odd* **then**
    find angle α between vector, which is described by first and last sample, and first axis;
    rotate this vector by α;
    factorize rotation matrix into ϕ;
  else
    divide signal into pairs;
    find angles α_i between vectors, which are described by pairs, and first axes;
    rotate all vectors by respective angles α_i;
    factorize all rotation matrices into ϕ;
    divide the number of samples by 2;
  end
end

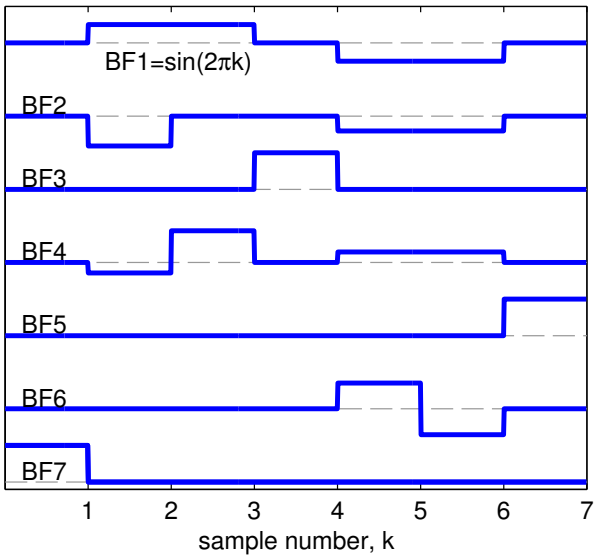

Figure 3.1: Basis function set produced by $\mathrm{rgur}()$ from a 7-sample sine wave

to be performed in order to produce a required orthonormal matrix. It must be noticed, that the placement of operation "find angle α between vector, which is described by first and last sample, and first axis" affects the structure of the final matrix. Therefore, there are possible $N/2$ variations of this algorithm, which create different unitary matrices. Figure 3.1 shows an example basis function set produced by processing a 7-sample sine wave.

Acronym	Explanation
RABOT	Rotation Angle Based OT
CCRAOT	Constant Rotation Angle OT
CRAIMOT	Constant Rotation Angle Inside Matrix OT
CRMOT	Constant Rotation Matrix OT
RA-HT	Rotation Angles Based Haar Transform
CRA-HT	Constant Rotation Angle HT
CRAIM-HT	Constant Rotation Angle Inside Matrix HT
RSA-HT	HT with Reduced Sequences of Rotation Angles

Table 3.1: GUR classification

3.2.4.2 Classification of GUR transforms

In this subsection the major families of GUR basis functions (BFs) are briefly described. Table 3.1, which is reprinted from [14], summarizes information about GUR-based transform subclasses. More information can be found in [14].

Basic GUR transformations like complex constant rotation angle OT (CCRAOT) are sensitive to shifts, i.e. shifting the input vector by one sample produces completely different set of coefficients. In contrast, linear time-invariant (LTI) systems like complex exponent-based transforms and undecimated wavelets are tolerant to (cyclic) shifts and impact of the shift can be easily eliminated. MC communication systems, based on such transforms, do not require very precise time synchronization (see Chapter 4). The utilization of GUR methods for the creation of LTI transforms would allow to create advanced parametric multicarrier (PMC) systems (see Chapter 8).

3.2.4.2.1 CCRAOT

This complex transform has all angles ϕ, γ and ψ constant throughout all SOGRMs as well as inside each SOGRM. For instance, the angle values $\phi = \pi/6$, $\gamma = \pi/2$ and $\psi = 0$ was used in most simulations of PMC systems[1]. At current state of art the utilization of CCRAOT in PMC systems is very well explored. Figure 3.2 shows an example of modulation of 16 samples `1000 0100 0010 0001` using a 4-carrier inverse CCRAOT using different values of ϕ.

The computational complexity of the *fast transformation* algorithm for CCRAOT, in accordance with [44] is $2N^2 - N$, using direct matrix multiplication, and $3N^2$ using Kronecker product.

[1] In the thesis angle ϕ in equation 3.8 usually is written besides transform name. Default values of the other angles are $\gamma = \pi/2, \psi = 0$.

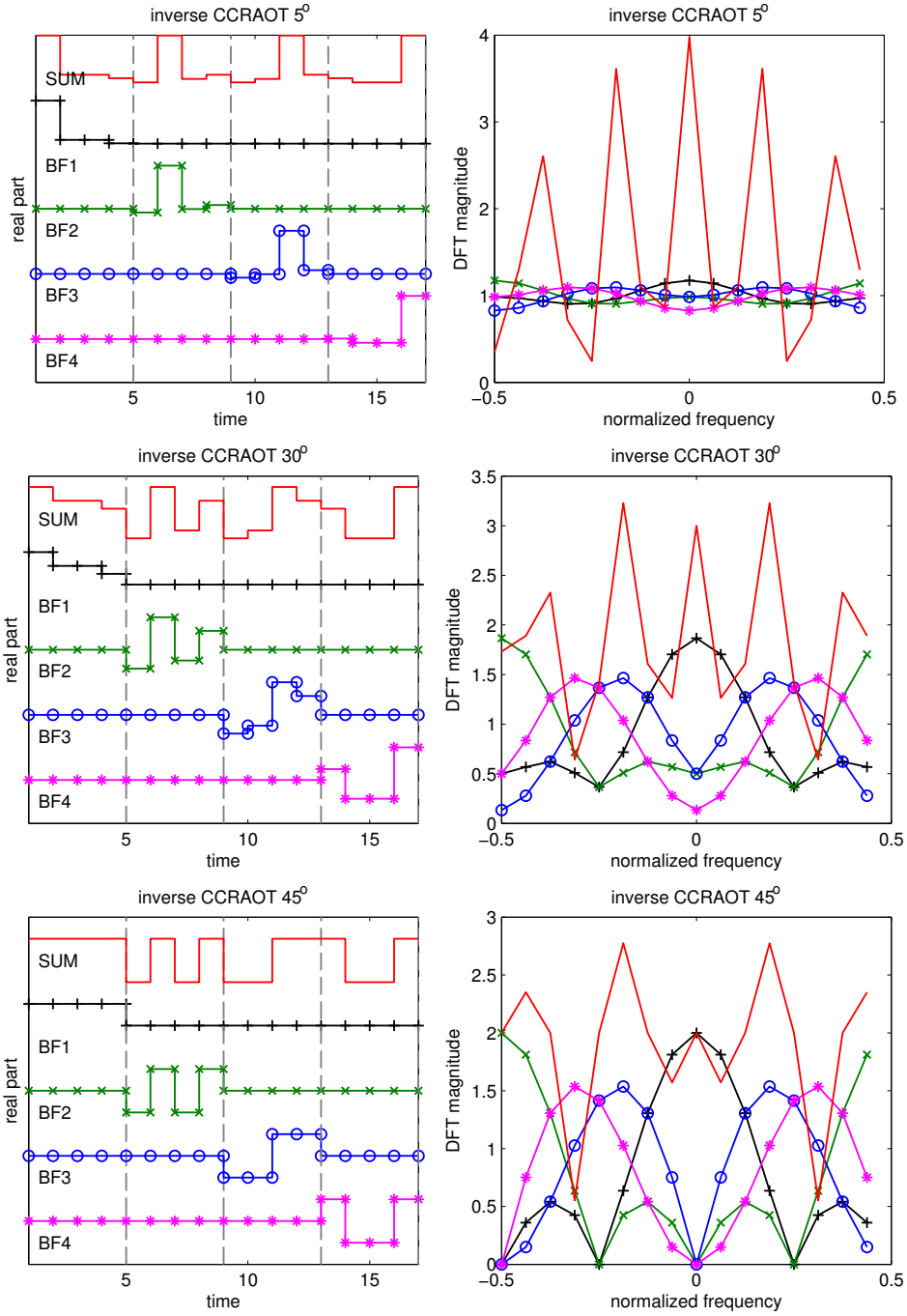

Figure 3.2: Example of transmission of 16 QAM samples 1000 0100 0010 0001 using a 4-carrier MC modulation, based on inverse CRAOT with different ϕ values

3.2.4.2.2 CCRAIMOT

Unlike CCRAOT, each SOGRM of complex constant rotation angle in matrix OT (CCRAIMOT) is different. However, inside SOGRM the angles remain constant. For instance, in $\boldsymbol{B_1}$ the angles are $\phi_{q,1} = \pi/6$, $\gamma_{q,1} = \pi/2$, $\psi_{q,1} = 0$, and in $\boldsymbol{B_2}$ the angles are $\phi_{q,2} = \pi/3$, $\gamma_{q,2} = \pi/2$,

$\psi_{q,2} = 0$, etc.

3.2.4.2.3 RABOT

This is the most general transformation, where all parameters are variable.

3.3 Configurations of multicarrier modulator and demodulator

There are sevaral ways how to perform unitary transformation and MC modulation. This section is devoted to description of possible solutions for performing this task.

3.3.1 Parametric multicarrier modulation system with matrix-based transform algorithm

It is possible to perform a GUR transformation of a vector in a variety of ways. The most simple and most obvious way to perform a unitary transformation is to build a unit, which directly mimics the unitary transformation matrix (3.6). However, in order to build the transformation matrix $\mathbf{\Phi}$ several steps must be performed:

1. For chosen ϕ, γ and ψ single plane rotation matrices (3.8) must be calculated. In one plane rotation matrix there is one ϕ, γ and one ψ.

2. SOGRM (3.7) must be built. This matrix will contain only mutually independent plane rotations. It is worth to note, that it is possible to build 64 different SOGRMs with given ϕ, γ and ψ.

3. Final factorization of $\log_2(N)$ SOGRMs into the final unitary transformation matrix must be performed.

In non-PMC systems, where the set of angles ϕ, γ and ψ is constant, the matrices $\boldsymbol{B_p}$ and $\mathbf{\Phi}$ can be calculated offline and the unitary transformation matrix $\mathbf{\Phi}$ can be stored in a table. On one hand, this solution will consume more memory than needed for some parameters and factorization algorithm, on the other hand, no computational resources for the factorization of matrix (3.6) will be necessary. Partial offline calculation, for example of matrices (3.7) can also be used.

3.3.1.1 Example of generalized unitary rotation transformation

The following example from [12] demonstrates how to build a fast transformation matrix where all angles inside one SOGRM are constant (CCRAIMOT) for $N = 4$, $\gamma = 0$, $\psi = \pi/2$ and some set of angles ϕ.

1. First of all, we define elementary single-plane rotation matrices for the chosen angles:

$$\Upsilon_1\left(\frac{\pi}{3}, \frac{\pi}{2}, 0\right) = \begin{bmatrix} 1/2 & j\sqrt{3}/2 \\ j\sqrt{3}/2 & 1/2 \end{bmatrix} \tag{3.12}$$

$$\Upsilon_2\left(\frac{\pi}{4}, \frac{\pi}{2}, 0\right) = \begin{bmatrix} \sqrt{2}/2 & j\sqrt{2}/2 \\ j\sqrt{2}/2 & \sqrt{2}/2 \end{bmatrix} \tag{3.13}$$

2. Next we construct appropriate SOGRMs from these matrices:

$$B_1\left(\frac{\pi}{4}, \frac{\pi}{2}, 0\right) = \begin{bmatrix} 1/2 & j\sqrt{3}/2 & 0 & 0 \\ 0 & 0 & 1/2 & j\sqrt{3}/2 \\ j\sqrt{3}/2 & 1/2 & 0 & 0 \\ 0 & 0 & j\sqrt{3}/2 & 1/2 \end{bmatrix} \tag{3.14}$$

$$B_2\left(\frac{\pi}{4}, \frac{\pi}{2}, 0\right) = \begin{bmatrix} \sqrt{2}/2 & j\sqrt{2}/2 & 0 & 0 \\ 0 & 0 & \sqrt{2}/2 & j\sqrt{2}/2 \\ j\sqrt{2}/2 & \sqrt{2}/2 & 0 & 0 \\ 0 & 0 & j\sqrt{2}/2 & \sqrt{2}/2 \end{bmatrix} \tag{3.15}$$

3. The final forward transformation matrix is obtained by factorization of SOGRMs:

$$\Phi = B_1 B_2 = \begin{bmatrix} \sqrt{2} & j\sqrt{6} & j\sqrt{2} & -\sqrt{6} \\ j\sqrt{6} & \sqrt{2} & -\sqrt{6} & j\sqrt{2} \\ j\sqrt{2} & -\sqrt{6} & \sqrt{2} & j\sqrt{6} \\ -j\sqrt{6} & j\sqrt{2} & j\sqrt{6} & \sqrt{2} \end{bmatrix} \tag{3.16}$$

Inverse transform matrix can be obtained by transposition and conjugation of forward transform matrix:

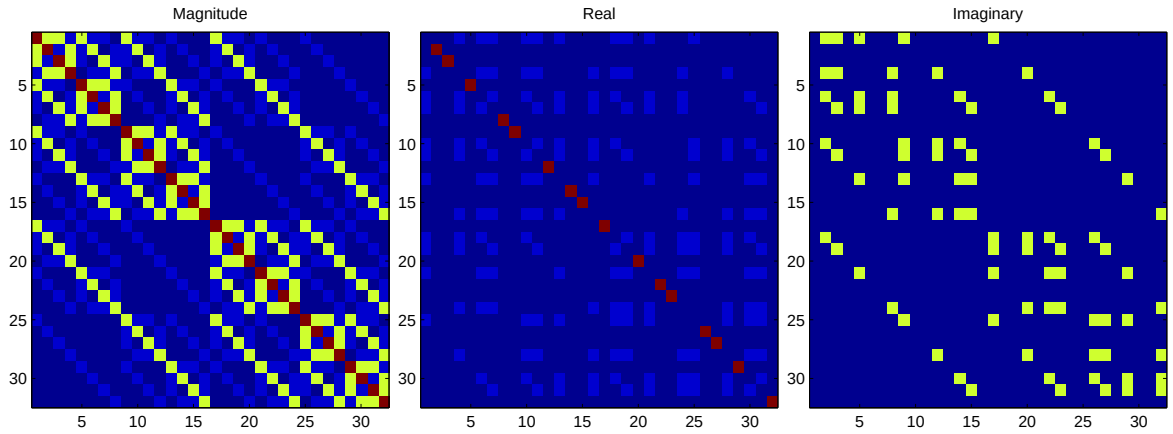

Figure 3.3: Example of the set of CCRAOT basis functions ($N = 32$, all $\phi = \pi/6$, all $\gamma = \pi/2$ and all $\psi = 0$). Darker values in the image map represent lower values, lighter - higher values.

$$\Phi^{-1} = \begin{bmatrix} \sqrt{2} & -j\sqrt{6} & -j\sqrt{2} & j\sqrt{6} \\ -j\sqrt{6} & \sqrt{2} & -\sqrt{6} & -j\sqrt{2} \\ -j\sqrt{2} & -\sqrt{6} & \sqrt{2} & -j\sqrt{6} \\ -j\sqrt{6} & -j\sqrt{2} & -j\sqrt{6} & \sqrt{2} \end{bmatrix} \tag{3.17}$$

It is possible to generate an infinite number of transforms even if all angles remain the same in all matrices $\boldsymbol{B_p}$. In Figure 3.3 an example of CCRAOT basis functions is shown as various image maps.

3.3.2 Parametric multicarrier modulation system with a tree-like transform algorithm

In order to transform a vector by means of a unitary matrix, internal products between the rows of the transformation matrix and the original vector are calculated. This operation can be viewed as correlation or filtering of the input signal by a bank of finite impulse response (FIR) filters. Each row of the orthogonal transform (OT) thus represents a different filter.

This concept has led to many interesting theories and highly efficient designs [4], especially in the area related to frequency division systems, such as filtered multitone (FMT) and filter bank multicarrier (FBMC) .

The main difference between FMT and OFDM is in amount of overlapping between *frequency* responses of basis functions. One of the largest drawbacks of OFDM is large inter-carrier interference (ICI) in case of synchronization errors. This is because basis functions - fragments of complex exponents, have rectangular windows and thus large (-13dB for first) sidelobes. In an ideal case, sidelobes of different subcarriers cancel each other. However, even

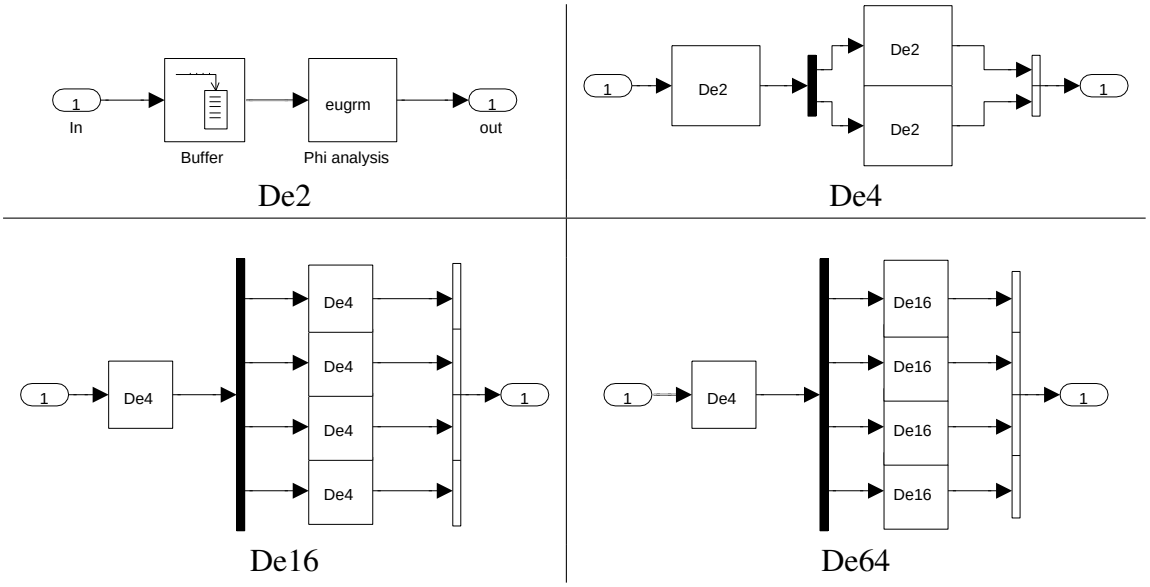

Figure 3.4: EGUR-based *decomposition* module hierarchy. The black bar represents vector conversion into scalars, but the white bar represents vector concatenation.

small synchronization errors cause sampling at time instants, where canceling is incomplete. Moreover, a perfect orthogonality between subcarriers is possible if there is no inter-block interference (IBI). This, in turn, implies padding (see Section 2.3.4) of transmitted chip blocks.

3.3.2.1 Factorization of GUR using tree-like structures

Implementation of Equation (3.6) can be carried out using classic block type structures (see Section 3.3.1). It is also possible to use tree-like structures for obtaining factorization (3.6). The resulting tree-like structure resembles wavelet Decomposition/Reconstruction (De/Re) trees. The following derivation of tree-like structures is based on paper by Misans and Valters [40].

As a basic building block an Elementary Generalized Unitary Rotation (EGUR) is used. The EGUR function is described by Equation (3.8). The EGUR module can bee steered by two parameters:

1. Forward/inverse transform (boolean);
2. Rotation angle (double).

The EGUR module can be exploited as part of:

- 2D reconstruction module (2Re);
- 2D decomposition module (2De);

Figure 3.4 explains how to build a 64-dimensional decomposition tree. `De2` is a very simple decomposition unit, which provides a two-dimensional decomposition in accordance with Equation (3.8). The input of this block is two serial samples, but the output - two parallel samples. A four-dimensional decomposition can be achieved by using three two-dimensional

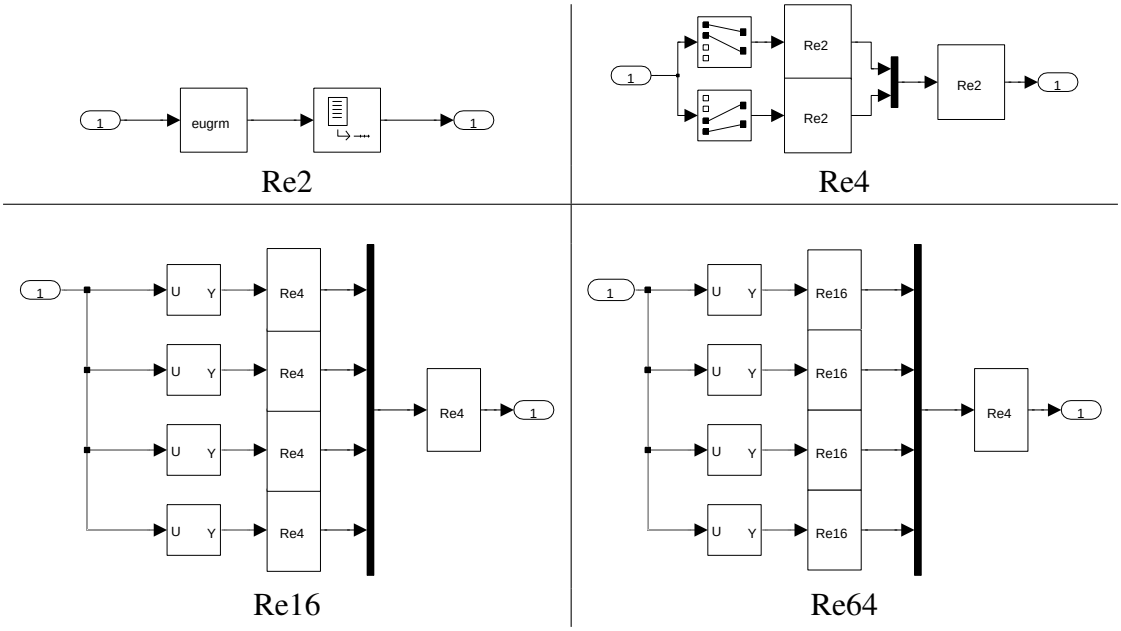

Figure 3.5: EGUR-based *reconstruction* module hierarchy. The black bars represent scalar concatenation into a vector. Modules 'UY' are selectors, which select some part of the vector.

`Re2` units. The black bar represents vector conversion into separate scalars, but the white bar represents vector concatenation.

The hierarchy of reconstruction filters is shown in Figure 3.5. The final filter `Re64` consists of four `Re16` and one `Re4` filter. The filter `Re16`, in turn, consists of four `Re4` filters. The most basic module is `Re2`, which contains an EGUR matrix. The input of `Re64` is a parallel vector of 64 samples, whereas the output of this unit is a serial sequence of 64 samples.

3.3.3 Transmultiplexer

3.3.3.1 Introduction

The FMT technology [45] is a typical example of transmultiplexer. In FMT each subcarrier is produced by an individual digital bandpass filter. Usually bandpass filters are created by combining the inverse discrete Fourier transform (IDFT) and low pass filters with different phase responses. The whole transmitter filter system is called *synthesis filter bank*. At the receiver reverse processing takes place.

In order to avoid ICI, the orthogonality condition (6.12) must be fulfilled. The device referred to as *analysis filter bank* consists of filters whose responses h_r are matched to the responses of filters in the transmitter h_t and the response of communication channel h_c so that disturbance from neighboring subcarriers must be eliminated (see Section 6.4.3).

It is important to mention that fine frequency localization comes at the cost of overlapping

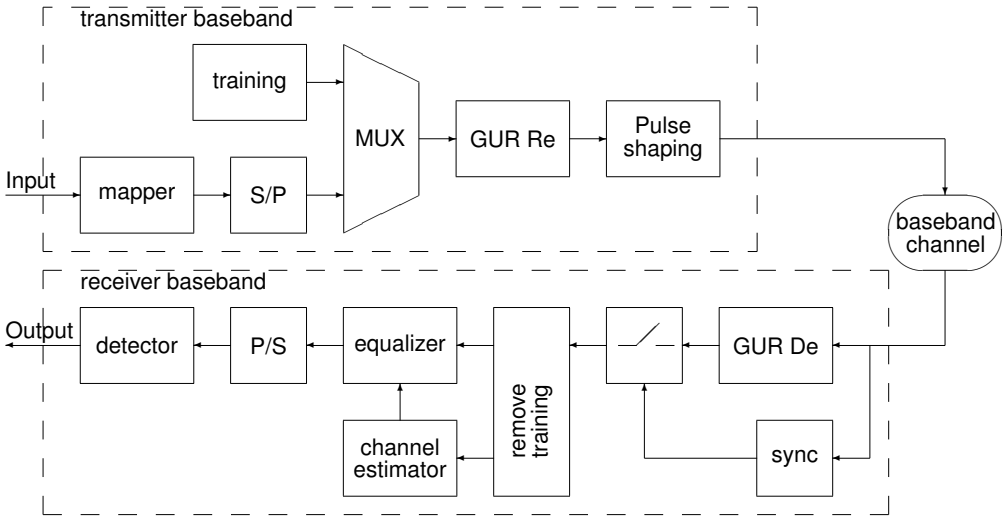

Figure 3.6: PMC system, based on a GUR-based transmultiplexer

of individual BF pulses in the time domain (TD). On one hand, this overlapping makes the communication system more resistant to synchronization issues, on the other hand, equalization of these sophisticated BFs requires much more effort than in OFDM. In literature, systems with synthesis filter banks in the transmitter and an analysis filter bank in the receiver are referred to as *transmultiplexer* .

3.3.3.2 GUR-based transmultiplexer

The transmitter of a transmultiplexer-based PMC system (see Figure 3.6) contains the reconstruction unit, whereas the receiver contains a unit responsible for the decomposition of a serial signal. Such configuration produces a serial stream of samples at the output of the unitary transform unit of the transmitter. The insertion of additional information, such as TD training and/or synchronization samples, in the transmitter must be done in the transform domain and any manipulations with TD signals are costly and inefficient.

Timing synchronization in the receiver is performed by reading the output of the decomposition unit at correct time instants. Since a unitary transform in the receiver cannot be performed correctly without time and frequency synchronization (see Chapters 4 and 5), estimators for synchronization must be located as close as possible to the input of the receiver. The largest challenge with the transmultiplexer configuration is that all synchronization samples must be generated and added to the data in the transform domain, whereas the estimation of synchronization can be performed in any domain. Moreover, GUR domain (GD) frequency and time synchronization schemes are not available yet, whereas plenty of TD methods are available (that's why Figure 3.6 shows a TD block timing offset (BTO) estimator).

Channel estimation (see Section 6.5) in a transmultiplexer-based PMC system must be per-

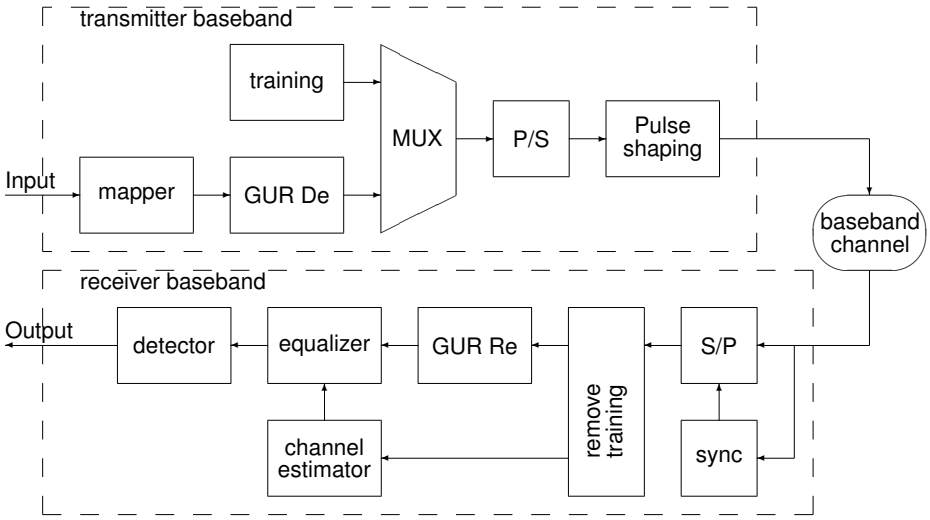

Figure 3.7: PMC system using a GUR-based subband coder

formed strictly in the GD, since TD samples are available only in serial form and the extraction of the training samples is problematic. In the current state of art only a very simple and inefficient GD channel estimator is available (see Section 6.5.2.1).

3.3.4 Subband coder

3.3.4.1 Introduction

It is possible to interchange decomposition and reconstruction stages, i.e. place decomposition (analysis) in the transmitter of communication system and reconstruction (synthesis) - in the receiver. Such solutions are called *subband coders*.

In a subband coder-based communication system it is not necessary to make serial-to-parallel conversion before the orthogonal transform unit. In this case block synchronization (Section 4.3) must be performed in a different way.

The equivalence between subband coders and transmultiplexers was analyzed by Vatterli in [46].

3.3.4.2 GUR-based subband coder

The first concept of a GUR-based subband coder was proposed by Misans and Valters in [12]. The transmitter included a decomposition filter, whereas the receiver used the reconstruction stage. A simplified model of a subband coder-based GUR-based PMC system is shown in Figure 3.7.

The transmitter utilizes `De64` module from Figure 3.4. While most of the design resembles the classic transmitter structure shown in Figure 2.2, there is a difference related to the

parallel-to-serial (P/S) conversion before the unitary transform. Since a tree-like decomposition structure `De64` accepts a serial stream of samples, the P/S converter before the unitary transform becomes redundant. However, this advantage quickly can turn into a significant drawback if there is a need to insert something (for example, transform domain training) into the signal before unitary transformation. Therefore, a PMC system, based on a subband coder, must exploit TD training structures in order to avoid serial to parallel (S/P)-P/S conversion, which will increase the latency of the PMC system.

The receiver side processing has also to be adjusted for utilization of reconstruction unit. The main challenge in this case is equalization (see Chapter 6), since it has to be performed on a serial sample stream. Since TD training structures are recommended for an efficient transmission, channel estimation in the TD is recommended.

3.3.5 Performance comparison of multicarrier modulators: simulation results

There are at least three different ways how to implement the unitary transform unit:

- Matrix-type transformation (see Section 3.3.1)
- Filter bank (transmultiplexer) (see Section 3.3.3.2)
- Subband coder (see Section 3.3.4.2)

Using numerical simulations, all three types of transform units have been compared. Communication systems with ideal timing and frequency synchronization and an additive white Gaussian noise (AWGN) communication channel have been simulated.

In accordance with the simulation results shown in Figure 3.8, the subband coder shows better results. However, differences are insignificant and this result well matches with the results obtained by Vatterli [46].

Please notice, that an AWGN channel has been used in the simulations. In case of a dispersive channel, the differences would be more significant. However, since a dispersive channel requires equalization, which is not yet available for tree like structures, this question remains open.

3.4 Peak-to-average power ratio of a multicarrier signal

Since an MC signal consists of several waveforms added together, it can have noticeable envelope variations. The ratio between the peak power and average power of a signal is called PAPR. PAPR (in dB) of a continuous signal $s(t)$ is defined as follows:

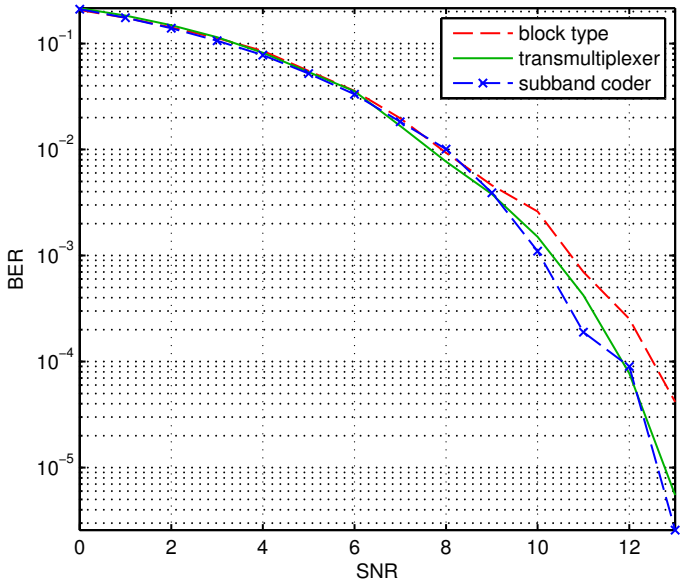

Figure 3.8: Performance of PMC systems with different transform unit configurations. A CCRAOT transform with the block size of 64 samples is used

$$\beta = 10log_{10}\frac{\max[s^2(t)]}{E[s^2(t)]} \tag{3.18}$$

System performance degradation due to nonlinearities of communication equipment have a larger effect on a signal with a larger PAPR. The problem of a high PAPR of an MC signals has been analyzed in the scientific literature many times (see, for example, [47]). The complementary cumulative distribution function (CCDF) of a signal can be used to explore variations of the instantaneous power of the signal. In Figure 3.9 CCDFs of the instantaneous power of several MC signals, created by various transforms and 4QAM constellation, are compared. From this plot we can observe a long tail of CCDF of an OFDM signal, created by the DFT. Moreover, CCDF of complex Hadamard (see Section 3.2.3) and CCRAOT with angles $> 20^o$ are very similar to CCDF of an OFDM signal, based on DFT. This observation allows to conclude, that PAPR of those signals is similar to PAPR of OFDM. From the same figure it can be observed that PAPR of a small angle CCRAOT is significantly lower. Finally, CCRAOT 0^o has a constant power of the 4QAM signal, since the transformation matrix of CCRAOT 0^o is equal to the identity matrix.

3.4.1 PAPR reduction using super-imposed sequences

In accordance with numerous researches, for example [48], the utilization of super-imposed (SI) training signals can lead to a reduced PAPR of the transmitted signal.

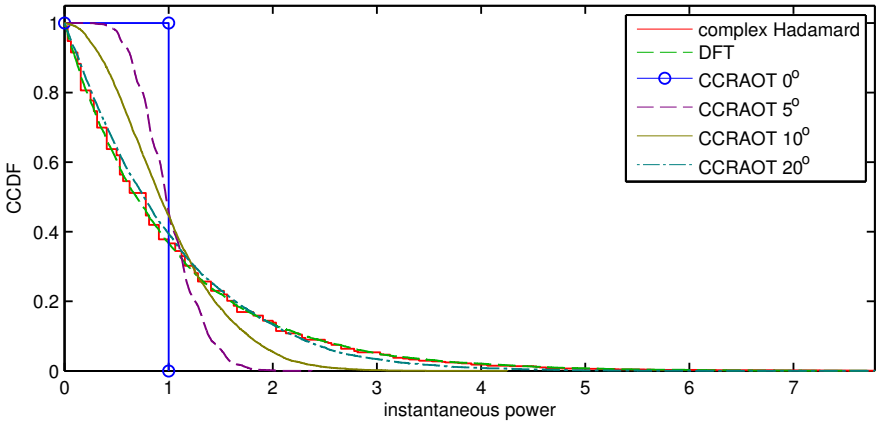

Figure 3.9: Comparison of CCDFs of MC signals, created by various transforms and 4QAM constellation

Adding of super-imposed sequence (SIS) to the useful signal also affects PAPR of the resulting signal. Due to the partial orthogonality between SIS and useful MC signal the power of SIS is added to the power of the useful signal and the resulting power CCDF is the sum of CCDF of SIS and CCDF of the useful signal over the power axis. Therefore, selecting of SIS with a low PAPR leads to a reduction of PAPR in the summary signal. Good candidates for PAPR reduction are a maximum length sequence (MLS) (m-sequence [31], Kasami sequence [49]) and constant amplitude zero autocorrelation (CAZAC) sequences, for example a Zadoff-Chu (ZC) sequence (see Chapter 2.4.3.1). The problem of PAPR reduction using pseudo-noise (PN) sequences is deeper investigated in papers [48] and [47].

3.5 Transform selection for a parametric multicarrier modulation system

Using GUR mechanism it is possible to construct an infinite number of unitary transformations. By looking at all the variety, a natural question arises "How to construct an optimal transform?".

Since the ultimate goal of any data communication system is to provide maximum data rate in a given frequency band and consume as less power as possible, the selection of basis function set must lead to the satisfaction of those conditions. There are several factors, which affect the throughput and power consumption and, therefore, the selection of a transform:

- Transform can be selected in accordance with channel state information (CSI)(see Section 6.5). Oka and Fossorier [11] used an angular matrix similar to (3.7), to construct an orthogonal transform family. They experimentally proved, that the performance of the communication system with a non-Gaussian communication channel depends on angles – some combinations of angles performed noticeably better. However, they did not propose

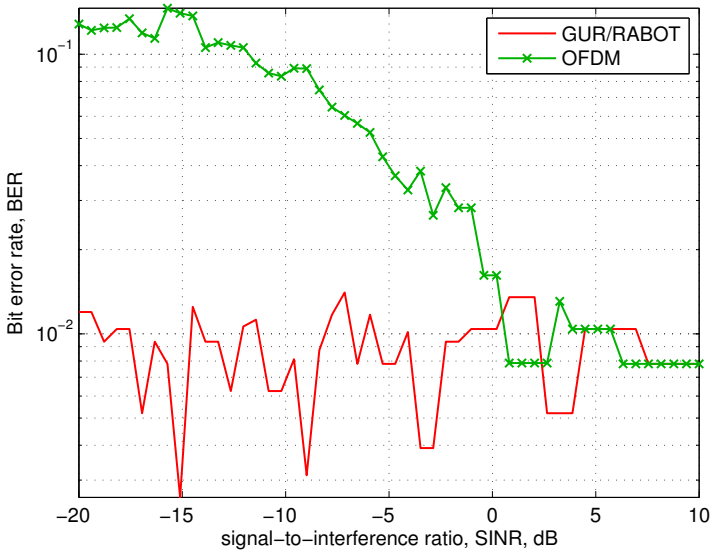

Figure 3.10: Impact of a random periodic 64-sample signal to an OFDM and a specially tuned GUR-based PMC system, both having 64 subcarriers.

an algorithm how to select a transform that is most appropriate to given communication channel conditions.

The doctoral thesis [9] is devoted to the time-frequency representation of non-stationary (i.e. changing in time) environments, like communication channels, using Weyl-Heisenberg expansions. In fact, the work provides a background for building filter banks, which perform optimally in these non-stationary environments. This approach can be adopted to GUR basis function family, thus providing an elegant way for the construction of optimal basis functions for non-stationary environments.

- Transform can be selected so that to minimize the impact of interference. For example, if one of the basis functions will coincide with a periodic interfering signal, then the impact of external interference will be limited to just one subcarrier and PMC system will continue to work even if signal-to-interference ratio (SINR), i.e. ratio between useful signal power and interference power, will be -20dB. Since other subcarriers will be orthogonal to the interference, they will not be affected at all and the throughput of the PMC system will not degrade significantly. It must be noticed, that in this case the length of the block as well as the phase of transmitted signal must be adjusted in order to obtain a perfect removal of the interference. Figure 3.10 shows the impact of random periodic broadband noise in the communication channel on the performance of OFDM and GUR-based systems, where the latter uses a basis function set, where one of the basis functions coincides with the undesired periodic signal (see Section 3.2.4.1).

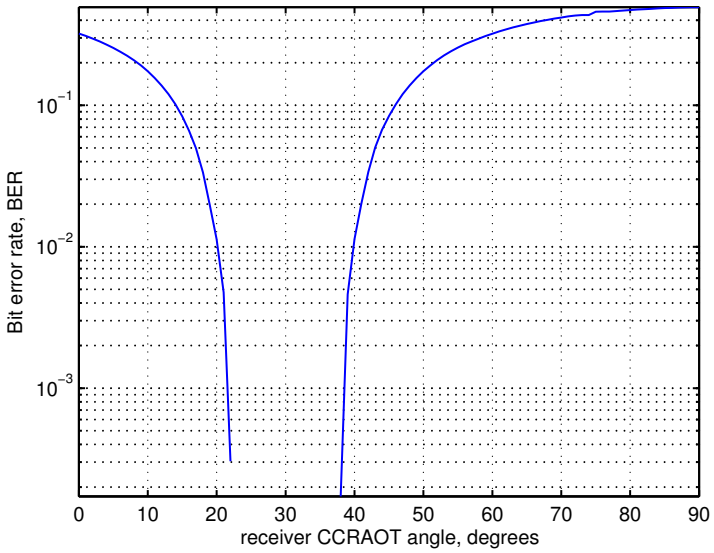

Figure 3.11: Angle resonance in a PMC system with the transmitter using CCRAOT 30^o

- Synchronization accuracy can affect the selection of a transform. Basis functions with compact time and frequency supports, like wavelets [50] in FBMC systems [51], can reduce ICI and sensitivity to carrier frequency offset (CFO).

- As it was said, using GUR, it is possible to obtain a large variety of transforms. If the receiving side does not know the parameters of the transform, it is unable to decode the received information. This feature can be used for the creation of secure and even masked PMC systems. Figure 3.11 shows the results of an experimental examination of *angle resonance* in a PMC system with the transmitter using CCRAOT 30^o. It can be seen, that the receiver is able to work if the angle error does not exceed approximately 8^o.

- Signals with a large PAPR require a large radio frequency (RF) amplifier backoff, which leads to an increased power consumption. Using parameters of GUR, it is possible to change the PAPR of a signal in a wide range. More details about this feature is given in Section 3.4.

However, there is still a lot of work to be done in this area. This doctoral thesis assumes the use of general GUR BF set, without focusing on a particular GUR BF family.

3.5.1 Parametric multicarrier modulation systems

One of the key advantages of GUR transforms is that they can be completely described, i.e. parametrized, by a set of angles, which in many cases is smaller than number of coefficients in the unitary matrix. This feature allows to create communication systems, where transforms

are changed dynamically, in accordance with a current situation. **Since, the transform in the transmitter and the receiver must be changed simultaneously, along with other information, parameters of the transform must be continuously transferred**. For signaling of the new transform, special block prefixes of frames (in case of a slower changes) must be used. Since, in many cases a *feedback* from the receiver to the transmitter is required, the proposed communication systems can be regarded as *communication systems with a limited feedback* [52].

Some of the criteria mentioned in Section 3.5 can be changing and a continuous adjustment of the transform would improve the performance of the communication system.

- Signal propagation conditions and interference tend to change over time. Fast channel variations, with a coherence time less than the block size, must be compensated within the unitary transform [9]. In turn, slow changes can require to change the structure of the transformation matrix. In all these cases a feedback from the receiver is necessary.
- Transform can be changing periodically, thus providing extra diversity and security for data transmission. In this case feedback is not necessary.

3.6 Conclusions

- In a PMC system with a AWGN communication channel performance of block type and tree-like GUR transform units is almost equal (see Section 3.3.5);
- Tree-like configurations require special synchronization and equalization methods working with a serial stream of samples.
- In the range of angles between 0^o and 45^o PAPR of a CCRAOT-based MC TD signal is proportional to the angle.
- Particular GUR-based transform can be selected in accordance with CSI, minimum interference, synchronization accuracy, security requirements, channel non-linearity.

3.7 Summary of the contributions

- New GUR algorithm for factorization of matrices with dimensions $N = \mathbb{Z}$ has been proposed (Section 3.2.4.1.2).
- New method of factorization of GUR transform using tree-like structures, based on buffers and selectors has been proposed (Section 3.3.2.1).
- Structure of GUR-based transmultiplexer has been presented for the first time (Section 3.3.3.2).

- Performance of block type GUR transform unit and tree-like structures has been compared (Section 3.3.5).
- The paradigm of parametric multicarrier (PMC) modulation has been explained (Section 3.5.1).
- Instantaneous power CCDFs of MC signals, created using CCRAOT-based modulation, has been compared to OFDM and WHT-based modulation (see Section 3.4).

4 Timing offset synchronization

4.1 Formulation of the problem

4.1.1 Objective

The purpose of this chapter is to review existing timing offset synchronization methods and verify their applicability and limitations to Generalized Unitary Rotation (GUR)-based parametric multicarrier (PMC) systems. If necessary, new timing offset estimation algorithms must be developed.

4.1.2 Tasks

In order to meet the objective the following tasks have to be fulfilled:

- Review of known timing offset estimation approaches;
- Examination of the *impact* of the block timing offset (BTO) to performance of a GUR-based PMC system;
- Review of known BTO estimation methods for multicarrier (MC) communication systems;
- Improvement of existing or development of new BTO estimation algorithms;
- Development of BTO synchronizer and its verification in a PMC system model;
- Review of known frame timing offset estimation methods.

4.2 Overview

The oversampled serial stream of samples at the receiver input must be divided into information units - chips, blocks and frames. In order to divide the stream at correct positions, it is necessary to estimate relative time instants, where various information units begin. Moreover, if the current timing position is known, it is possible to predict future time instants, when the separation must be done. The task, which is responsible for the estimation of current timing position is called *timing offset estimation*. There are several well-known timing offset estimation techniques:

- data-aided (DA) estimation , based on the correlation between repetitive parts, i.e. auto-correlation (AC),
- decision-directed (DD) estimation , based on a matched filter (MF) or cross-correlation (XC),
- non data-aided (NDA) estimation , based on deducting timing offset from disturbances of the received signal.

The detection of unit positions usually requires advanced estimation methods, such as maximum likelihood (ML) estimation [53], [54].

Most of the existing timing estimators for orthogonal frequency division multiplexing (OFDM) [30] are based on AC of cyclic prefix (CP). Unfortunately, CP is inefficient (see [15] and Sections 2.3.4.1 and 6.6.2) in systems based on non-sinusoidal basis functions. Since CP is not used in GUR-based PMC systems, CP-based methods are not directly applicable.

Another widely used method for timing synchronization is based on XC in conjunction with unique word (UW) prefix. In single carrier (SC) systems UWs traditionally have been used for frame synchronization [55]. On the other hand, in many recent publications there are proposals to use UW instead of CP in OFDM communication systems [27]. However, UW synchronizers are usually used in conjunction with other – fine synchronization methods. Many of fine synchronization methods rely on frequency domain (FD) information, which is not available in GUR-based PMC systems.

In subsequent sections a time synchronization method, which works in GUR-based PMC systems is derived. Timing estimation and synchronization methods are based on known principles and, therefore, are not unique. However, the given combination of elements is applied to GUR-based PMC systems for the first time.

4.3 Block synchronization

A received serial stream of chips must undergo serial to parallel (S/P) conversion before forward transformation. The dividing of the stream must be done at correct positions, otherwise the demodulation of data symbols (2.7) by means of the unitary transform unit based on a factorized matrix (3.6) will be impossible.

4.3.1 Impact of block timing offset

The BTO is severe issue in MC communication systems. In case of block padding (see Section 2.3.4), incorrectly detected block boundaries can lead to two different situations. If we denote BTO as θ and the length of the padding as L, then the following issues are possible:

1. if $\theta > L$ ("offset" 1 in Figure 4.1) – transformation of two incomplete sample blocks separated by the padding;
2. if $\theta < L$ ("offset 2" in Figure 4.1) – transformation of an incomplete block with a part of the padding.

In OFDM the second type of BTO is efficiently mitigated, because CP is used as padding. Due to properties of discrete Fourier transform (DFT), cyclic shift of the input vector does not

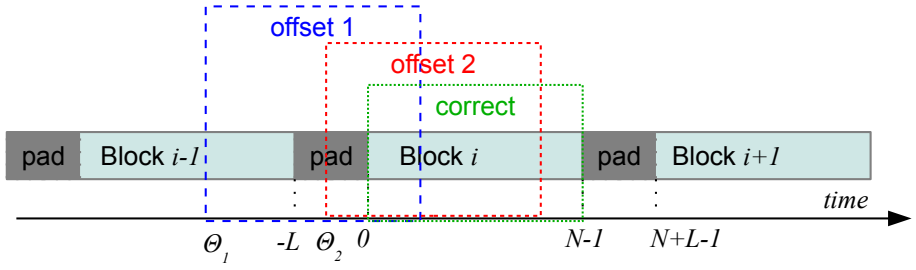

Figure 4.1: Types of BTO

lead to inter-carrier interference (ICI) (See Section 6.4.3) and, therefore, can be efficiently corrected by the frequency domain equalizer (FDE), which is able to estimate the communication channel *irrespective to the BTO of second type*.

Since GUR-based PMC systems use the UW padding rather than CP (see Section 2.3.4.1 for the explanation of reasons), they are sensitive to both types of BTO.

4.3.2 Block timing offset estimation

4.3.2.1 Data-aided block timig offset estimation

4.3.2.1.1 Overview

DA estimators rely on the signal structure in order to obtain necessary information. Autocorrelation between repeating parts is a typical example of DA estimation.

In OFDM literature several simple DA methods for BTO estimation are described. If the communication system uses CP (see Section 2.3.4.1), there are several ways of using a CP for determining the bounds of blocks. In study [56], the authors suggest using the absolute value of the difference between the signal and its copy delayed by N samples:

$$v_s(k) = \sum_{m=k}^{k+L-1} |y(m) - y(m+N)|, \; k \in \{0, ..., \theta, ...N + L - 1\} \tag{4.1}$$

Then the estimated BTO can be found using:

$$\hat{\theta}_s = \arg\min_{\theta} \{v_s(\theta)\} \tag{4.2}$$

Other authors in a more recent study [57] have suggested using of AC:

$$v_{ac}(k) = \sum_{m=k}^{k+L-1} y(m)y^*(m+N), \; k \in \{0, ..., \theta, ...N + L - 1\} \tag{4.3}$$

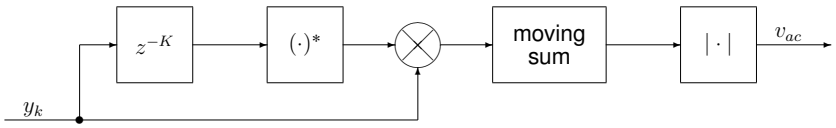

Figure 4.2: Classic AC-based BTO estimator

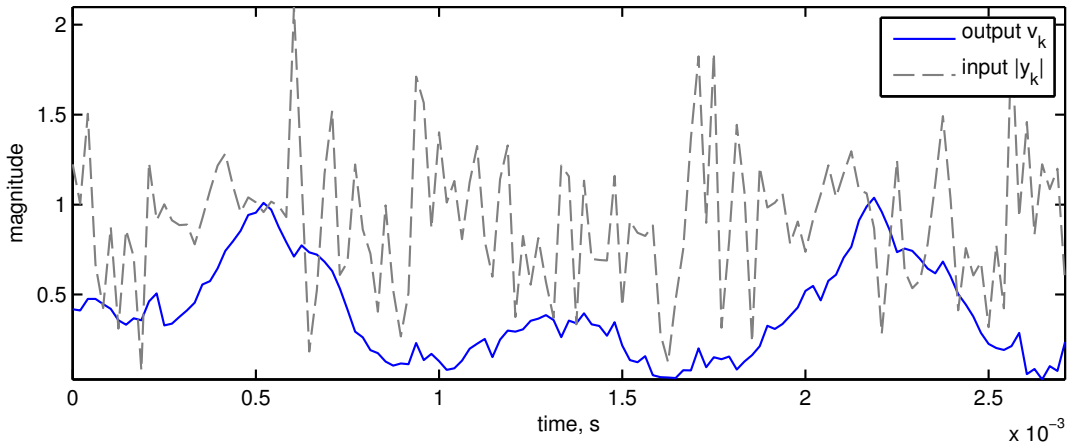

Figure 4.3: Signals in the UW AC-based estimator.

In this case the estimate of the block delay can be found using:

$$\hat{\theta}_{ac} = \arg\max_{\theta}\{v_{ac}(\theta)\} \tag{4.4}$$

4.3.2.1.2 Data-aided BTO estimation in GUR -based parametric multicarrier systems

The experimental results published in [15] have confirmed, that CP does not provide those advantages available in OFDM. As mentioned in Section 2.3.4.3, the UW-based padding is much more appropriate for GUR-based PMC systems. Since UW is repeated in each block, many AC-based methods for CP (see Section 2.3.4.1) can be adopted for UW.

The block diagram of a block synchronization estimator based on AC is depicted in Figure 4.2. Its operation is based on Formula (4.3). Although such synchronization estimator itself is relatively simple, unlike an XC-based estimator (see Section 4.3.2.2), its output is not suitable for direct keying of S/P conversion block, since (4.3) outputs slowly varying AC result (see Figure 4.3). Maximums of v_k (see Figure 4.3) must be tracked in order to obtain correct block synchronization metrics. Moreover, the search must be performed over the whole block time interval to ensure obtaining of the global maximum (v_k can have several local maximums). The result of this tracking operation is BTO, which can be used for the control of timing numerically controlled oscillator (NCO) (see Section 4.3.3).

4.3.2.1.3 Maximum likelihood AC-based block timig offset estimator

The simple timing estimator described in Section 4.3.2.1.2 is sub-optimal, since it does not take into account the statistical properties of synchronization sequence. Moreover, an optimal estimator for frequency-selective channels would take into account the impact of neighboring samples on the training sequence. The ML estimation technique is widely adopted in many BTO estimators for OFDM.

A well known method of deriving an optimal ML estimator for timing and frequency synchronization in OFDM systems using CP is presented in [57], [58]. In this section it will be adopted to systems with a complex normally distributed UW.

In a non-scattering medium, the samples of the transmitted signal $x(k)$ from (2.1) and the samples of the received signal $y(k)$ from (2.4) are related by the expression:

$$y(k) = [x(k-\theta) + w(k-\theta)]e^{j2\pi\varepsilon k/N} \tag{4.5}$$

where θ is the sought integer delay, ε is the difference in the carrier frequencies of the receiver and transmitter , and w is the additive Gaussian noise. To mark the beginning of the next block, a special UW sequence is transmitted at the beginning of each block. The purpose of the estimator is to estimate the parameters θ and ε.

In order to obtain all possible interactions between samples within a signal, we have to observe intervals, each consisting of $2N + 2L$ samples (see Figure 4.4). Index sets for k in the UW part of the block is defined as follows:

$$\begin{aligned} &I \triangleq \theta, \ldots, \theta + L - 1 \quad \text{and} \\ &I' \triangleq \theta + N + L, \ldots, \theta + N + 2L - 1 \end{aligned} \tag{4.6}$$

If the number of subcarriers in the transmitted signal is sufficiently large and data $X(k)$ constitute a white random process, then $x(k)$ is approximately a complex Gaussian process, whose real and imaginary parts are independent. However, the UW part of the block may have different from useful signal statistical properties. Let's assume that we are using circular symmetric complex normal random UW sequences with the following AC properties:

$$\forall k \in I: \quad E\{y(k)y^*(k+m)\} = \begin{cases} \sigma_u^2 + \sigma_w^2 & \text{if } m = 0 \\ \sigma_u^2 e^{-j2\pi\varepsilon} & \text{if } m = N + L \\ 0 & \text{otherwise} \end{cases} \tag{4.7}$$

where $\sigma_u^2 \triangleq E\{|u(k)|^2\}$ is the power of UW and $\sigma_w^2 \triangleq E\{|w(k)|^2\}$ is the power of noise, N is

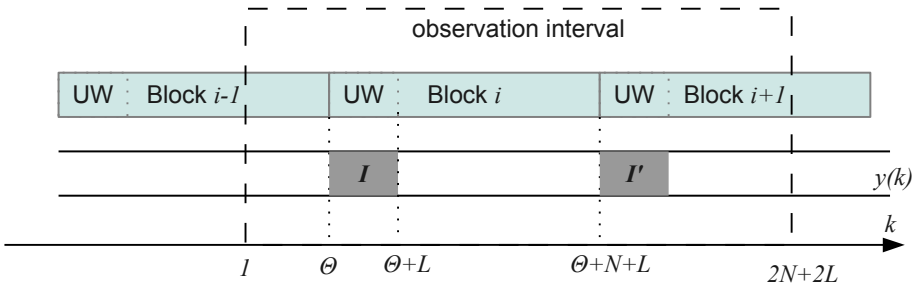

Figure 4.4: Structure of the signal with UW padding. Intervals I and I' contain the same UW.

the number of subcarriers and L is the length of UW prefix.

The probability density function (PDF) W of the reception vector of observations $\boldsymbol{y}$ with $2N + 2L$ samples at a given arrival time θ with a carrier frequency offset (CFO) ε:

$$\begin{aligned} W(\boldsymbol{y}) &= \prod_{k\in I} W(y(k), y(k+N+L)) \prod_{k\notin I\cup I'} W(y(k)) = \\ &= \prod_{k\in I} \frac{W(y(k), y(k+N+L))}{W(y(k))W(y(k+N+L))} \prod_{k} W(y(k) \end{aligned} \tag{4.8}$$

The second product does not depend on θ (since it is factorized over all k) and can be omitted:

$$W(\boldsymbol{y}) = \prod_{k\in I} \frac{W(y(k), y(k+N+L))}{W(y(k))W(y(k+N+L))} \tag{4.9}$$

The log-likelihood function Λ for unknown parameters θ and ε is the logarithm of PDF of the reception vector of observations with unknown parameters θ and ε:

$$\Lambda(\theta, \varepsilon) = \log W(\boldsymbol{y}|\theta, \varepsilon) = \sum_{k=0}^{\theta+L-1} \log \frac{W(y(k), y(k+N+L))}{W(y(k))W(y(k+N+L))}, \tag{4.10}$$

where ε is fractional carrier frequency offset (FCFO) (see Section 5.4) Using the correlation properties 4.7, the numerator of 4.10 can be written as:

$$W(y(k), y(k+N+L)) = \frac{\exp\left(\frac{|y(k)|^2 - 2\rho\Re\{\exp(j2\pi\varepsilon)y(k)y(k+N+L)\} + |y(k+N+L)|^2}{(\sigma_s^2+\sigma_w^2)(1-\rho^2)}\right)}{\pi^2(\sigma_s^2+\sigma_w^2)(1-\rho^2)} \tag{4.11}$$

where ρ is the signal-to-noise ratio (SNR) defined as follows:

$$\rho \triangleq \left| \frac{Ey(k)y^*(k+N+L)}{\sqrt{E|y(k)|^2 E|y(k+N+L)|^2}} \right| = \frac{\sigma_s^2}{\sigma_s^2+\sigma_w^2} = \frac{SNR}{SNR+1} \tag{4.12}$$

In turn, the denominator of 4.10 contains two complex Gaussian distributions:

$$W(y(k)) = \frac{\exp\left(-\frac{|y(k)|^2}{(\sigma_s^2+\sigma_w^2)}\right)}{\pi(\sigma_s^2+\sigma_w^2)} \tag{4.13}$$

Under the assumption that $\boldsymbol{y}$ is a jointly Gaussian vector, after some algebraic manipulations (see details in [30]) Equation (4.10) becomes:

$$\Lambda(\theta,\varepsilon) = |\gamma(\theta)|\cos(2\pi\varepsilon + \angle\gamma(\theta)) - \rho a(\theta) \tag{4.14}$$

Therefore, statistic (4.3) in conjunction with an additional statistic:

$$a(m) = \frac{1}{2}\sum_{k=m}^{m+L-1} |y(k)|^2 + |y(k+N)|^2 \tag{4.15}$$

leads to the combined estimate for the delay of the blocks is represented in the form:

$$\hat{\theta}_{ML} = \arg\max_{\theta}\{|v_{ac}(\theta)| - \rho a(\theta)\} \tag{4.16}$$

where $v_{ac}(\theta)$ is plain AC-based estimate (4.3).

Similarly like in case of the simple method (see 4.3.2.1.2), the output of ML autocorrelator is not suitable for direct control of S/P conversion.

4.3.2.2 Decision-directed block timing offset estimation

XC-based estimators are typical examples of DD estimators, i.e. such estimators, where the content of the synchronization sequence plays a crucial role. XC-based estimators have been very popular in the previous generation of communication systems [59], [60], [61], [62], [63], [64] based on plain quadrature phase-shift keying (QPSK) modulation. In these communication systems XC has been used for frame (see Section 4.4) and start-of-packet detection.

4.3.2.2.1 Cross-correlation -based BTO estimation for GUR-based parametric multicarrier systems

If the same UW sequences are placed in each block, a direct low -complexity XC-based BTO estimator can be designed. If we denote received samples as y and known UW samples as u,

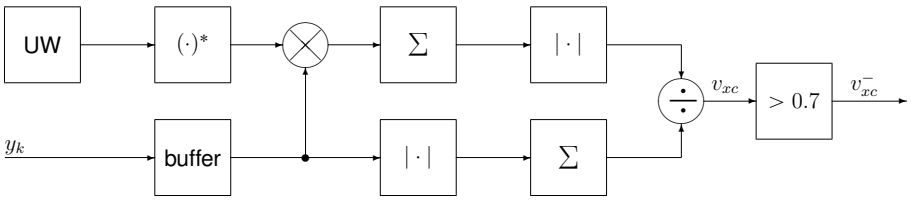

Figure 4.5: XC-based BTO estimator

then the correlation window operation will be described by the following equation:

$$c_{xc}(k) = \sum_{m=1}^{L} y(k+m)u(m)^* \,, \tag{4.17}$$

where L is the total length of UW padding and $(\cdot)^*$ denotes the complex conjugation. In order to provide normalization, it is necessary to divide the obtained result by the average magnitude of incoming signals:

$$v_{xc}(k) = \frac{c_{ac}(k)}{\overline{y(k)}} = \frac{\left|\sum_{m=1}^{L} y(k+m)u(m)^*\right|}{\sum_{m=1}^{L} |y(k+m)|} \tag{4.18}$$

A time delay estimate can be found by taking the argument of cross correlator output samples v_{xc} with the magnitude larger than a certain threshold v_{xc0}:

$$\hat{\theta}_{xc} = \arg_{\theta}\{v_{xc}(\theta)\}\Big|_{v_{xc}>v_{xc0}} \tag{4.19}$$

The diagram of the unit providing XC-based timing estimation is given in Figure 4.5. If sequences with good correlation properties are used (for instance, Zadoff-Chu (ZC) sequences, see Section 2.4.3.1), the XC algorithm -based estimator (4.18) outputs a sharp, one sample long peak at the end of each UW (see Figure 4.6). This pulse can be used directly for keying S/P converter in the receiver front-end. On other hand, these pulses can be used for the control of block timing NCO in feedback synchronizer (see Section 4.3.3).

Unfortunately Formula (4.18) is sub-optimal, since it does not take into account the distribution of UW sequence. For more precise estimation, a maximum likelihood estimator can be used.

If the medium in which a signal propagates is scattering, i.e., if multipath propagation takes place, then signals at the outputs of the correlators are badly distorted (see Section 2.4.4). Moreover, the part with a UW will be distorted by the end previous block. As a rule, this results in a wrong estimate for the beginning of a block. The simplest solution of this problem is to use

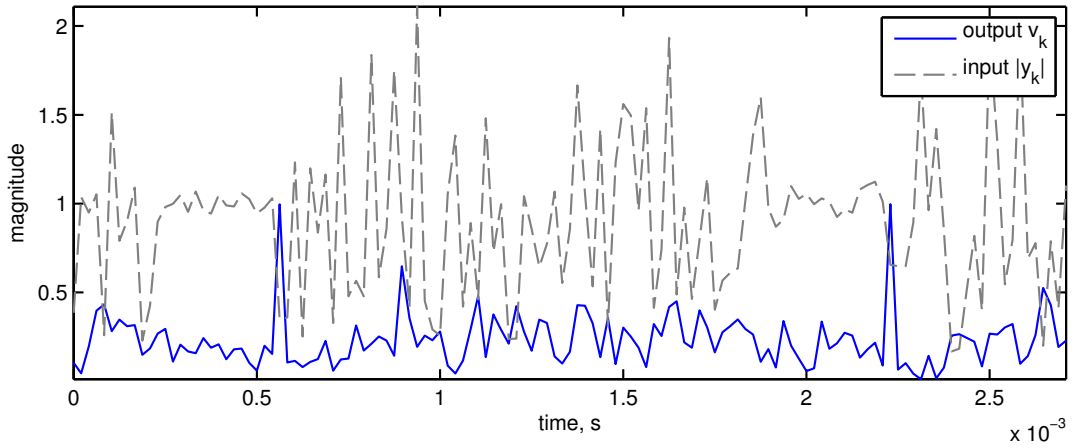

Figure 4.6: Signals in the UW XC-based BTO estimator.

continuous averaging of θ.

4.3.2.3 Combined block timing offset synchronizer

An AC-based estimator provides just approximate boundaries of blocks, whereas an XC-based estimator outputs a peak at the end of the UW sequence very precisely. On the other hand, an XC-based estimator is more sensitive to additive noise and convolution in the communication channel and pulse shaping filters (see Section 2.4.4.1). In contrast, a less precise AC-based estimator is more robust against channel noise and dispersion in a frequency-selective channel (see Section 2.4.4.2).

Since outputs of the estimators can significantly differ, a smart combining is necessary. After some testing, it turned out, that a combiner, which selects the *estimate with the minimum magnitude*, improves the performance of the synchronizer (see the simulation results in Figure 4.9).

The proposed solution provides an efficient low-complexity block synchronization solution for PMC systems with block-wise transmission. A more intelligent combining of estimator outputs would lead to decreasing the number of false detections and to a lower bit error ratio (BER) at the cost of increased computational complexity. For example, the utilization of ML estimation [30] in both XC and AC timing estimators would increase their accuracy. In the same time, even more advanced and computationally complex estimator combining methods are available in literature. For example, in [65] it is proposed to use AC for the coarse *frame* timing offset estimation, whereas XC is used for the fine tuning.

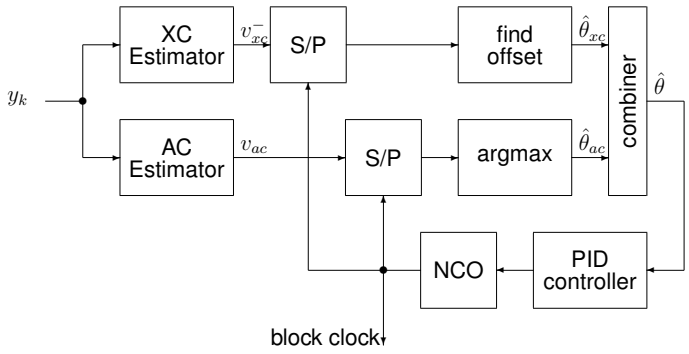

Figure 4.7: Block synchronizer

4.3.3 Block timing offset correction

4.3.3.1 Overview

A timing offset synchronizer can be implemented using two different approaches:

- Feedback (closed -loop) synchronizer: the estimator is located after the S/P converter and detects the *residual* timing offset. The detected offset via the control unit adjusts NCO, which, eventually affects the residual timing offset. The system operates in loop mode and adjusting can take several cycles.

- Open -loop synchronizer: the estimator is located before the main S/P converter. It inserts or deletes the required number of samples in order to achieve the breaking of the serial stream at correct positions and to obtain *immediate* synchronization.

4.3.3.2 PID controller-based feedback synchronizer

For adjusting NCO, which produces clock signal for S/P converter at the input of the receiver, proportional integral derivative (PID) controller can be used. Figure 4.7 depicts the structure of the synchronization unit.

4.3.3.2.1 Simulation results of the synchronizer

The performance of the feedback BTO synchronizer has been evaluated using simulations. For this purpose a model of baseband PMC system without equalization was created (see Figure 4.8). The BTO synchronizer was implemented in accordance with the design depicted in Figure 4.7. 10^6 bits were transmitted using 64 subcarriers produced by complex constant rotation angle OT (CCRAOT) with $\phi = 30^\circ$ (see Section 3.2.4.2) through an additive white Gaussian noise (AWGN) channel.

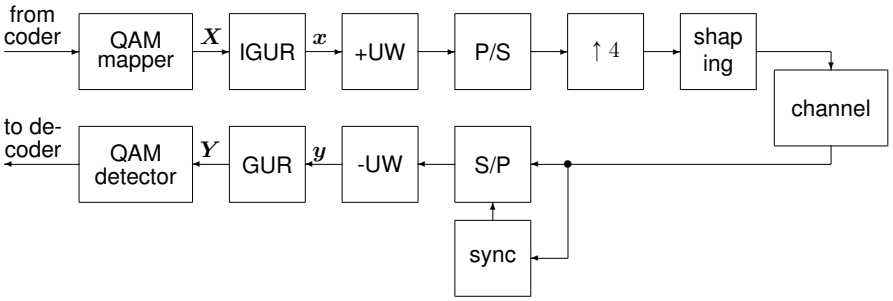

Figure 4.8: Communication system baseband model for BTO estimator testing

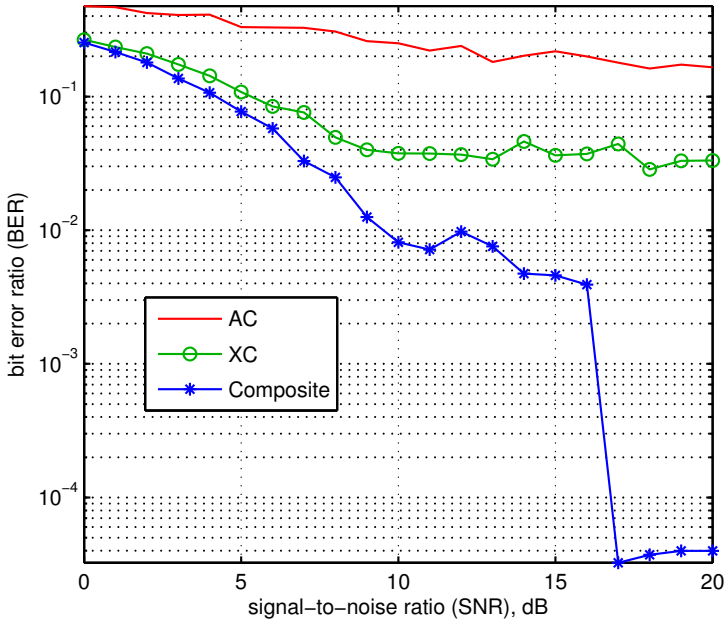

Figure 4.9: Performance of the PMC system using various estimators

After careful tuning of the PID controller, the system demonstrated a stable convergence to synchronized state within approximately 20 blocks. The achieved BER in synchronized state is shown in Figure 4.9.

4.4 Frame synchronization

Most of the modern block transmission oriented systems employ framing of the block flow. Signaling information and pilot blocks for a quick estimation of the channel parameters are commonly located at the beginning of a frame. Frame synchronization is required in order that the receiver can be able to determine the beginning of next frame. Moreover, if the transmission is carried out in relatively short frames, frame synchronization can be used as the only timing synchronization method. In this case block boundaries (see Section 4.3) can be calculated using

relative block positions in the frame.

4.4.1 Frame timing offset estimation

The most obvious way to provide frame timing synchronization is to insert special framing signals (synchronization sequences - see Section 2.4) into the transmitted signal. Then, similar methods as for BTO estimation (see Section 4.3.2) can be used.

In the literature problem of frame synchronization is discussed many times, since this kind of the synchronization has been used since first data transmission systems have been created. For example, in publication [66] comparison of various frame synchronization sequences is provided. It is concluded, that Kasami sequences [49] provide better results than ZC (see Section 2.4.3.1).

In article [67], an extended scheme for the frame and block synchronization is proposed. The authors of the article suggest using an additional burst frame containing a distinctive guard interval (GI) and pilot symbols to provide quick and accurate frame timing offset estimation during the course of one OFDM block. According to the results of the simulations performed by the authors of the article, in channels with Rayleigh fading and multipath propagation, the scheme in question is far superior to classical methods of synchronization.

In IEEE Standard 802.11a for wireless local area networks (LANs) [68], training blocks, called “short symbols”, with good correlation properties and a limited spectrum are used for frame and frequency synchronization [69]. A MF at the input of the receiver continuously correlates the incoming signal with a sample short symbol. When a pair of short symbols occurs at the input, ten peaks spaced 16 samples apart appear at the output of the matched filter. These peaks, in conjunction with a plateau of 80 samples in length at the output of the autocorrelator (4.16), are used to signal the beginning of the next OFDM frame.

Several advanced frame synchronization solutions are discussed in papers of Coulson [70], [71]. Similar synchronization sequences can be used in GUR-based PMC systems.

4.4.2 Frame timing offset correction

For the frame offset correction the same methods as for BTO correction (see Section 4.3.3) can be used. However, since frames are much longer than blocks, the loss of the synchronization frame has a much larger impact. Therefore, open -loop synchronization methods, which provide instant synchronization, are preferred.

4.5 Conclusions

- BTO in a PMC system can be successfully estimated, if the received signal contains a repeating UW sequence at the beginning of each sample block.
- CCRAOT-based PMC system demonstrates high sensitivity to the BTO, delay in one chip leads to an unrecoverable loss of data. Development of shift-invariant transforms using GUR would lead to much better immunity to timing synchronization errors.
- AC-based BTO estimator provides robustness against false detections, however, its accuracy is insufficient for synchronization within one chip range.
- XC-based BTO estimator provides sufficient accuracy for synchronization within one chip range. However, its performance noticeably degrades in PMC systems with frequency-selective channels.
- Combination between AC-based and XC-based BTO estimators provides high accuracy and is immune to the dispersion in the communication channel.

4.6 Summary of the contributions

The following contributions in the area of time synchronization for GUR-based PMC systems have been done:

- Data-aided (DA) AC-based BTO estimator has been implemented and evaluated (Section 4.3.2.1.2).
- Maximum likelihood (ML) AC-based BTO estimator for a complex Gaussian UW prefix has been derived (Section 4.3.2.1.3).
- Decision-directed (DD) XC-based BTO estimator has been proposed and evaluated (Section 4.3.2.2).
- Combiner of BTO estimators has been proposed and evaluated (Section 4.3.2.3).
- Feedback-type BTO synchronizer has been implemented and evaluated (Section 4.3.3.2).

5 Frequency synchronization

5.1 Formulation of the problem

5.1.1 Objective

The purpose of this chapter is to explore the problem of frequency synchronization in parametric multicarrier (PMC) systems, where subcarriers are created using Generalized Unitary Rotation (GUR).

5.1.2 Tasks

In order to meet the objective the following tasks have to be fulfilled:

- Review of frequency synchronization problems in known multicarrier (MC) communication systems;
- Measurement of the impact of frequency offsets on the performance of a GUR-based PMC system;
- Exploration of the compatibility between known fractional carrier frequency offset (FCFO) estimation methods and GUR-based MC modulation;
- Development of new FCFO estimation methods;
- Development of residual phase offset estimation method;
- Development of an FCFO and phase offset synchronizer.

5.2 Types of frequency offset

5.2.1 Introduction

In order to perform all required signal processing tasks, data communication systems have to use oscillators. As a rule, these oscillators are local and, since communication entities use different oscillators, synchronization across different entities of the communication network is necessary. Moreover, the stability of these oscillators is limited, therefore frequency synchronization must be maintained continuously. In *mobile* communication systems the situation becomes even worse, since the movement of a communicating entity leads to a deformation of the transmitted and received waves, regarded as Doppler effect.

5.2.2 Carrier frequency offset

Actual communication systems include intermediate frequency (IF) and radio frequency (RF) sections for the translation of a signal to the required frequency (up-conversion) and back.

A typical RF circuitry of the transmitter and receiver is shown in Figure 2.10. At the transmitter side, in-phase (I) and quadrature (Q) digital samples are converted into an analog signal by means of two digital-to-analog converters (DACs). Translation is performed by two mixers and carrier frequency oscillator . At the receiver side, RF demodulation is performed by means of a similar circuitry, consisting of two mixers and oscillator. Finally, after rejection of the image by means of two low-pass filters (LPFs), analog samples are converted back into digital domain by means of two analog-to-digital converters (ADCs).

The discrepancy between carrier frequency oscillator frequencies in the transmitter and receiver causes translation of the frequency spectrum on the frequency axis. This effect is called carrier frequency offset (CFO).

If at the output of the transmitter baseband we have a signal $x(t)$, then the translation of this signal to the carrier frequency f_{ct} (up-conversion) by means of quadrature modulation can be described as:

$$s(t) = \Re\{x(t)\}\cos(2\pi f_{ct}t) + \Im\{x(t)\}\sin(2\pi f_{ct}t) = \Re\left\{x(t)e^{j2\pi f_{ct}t}\right\} \tag{5.1}$$

If the stream of up-converted blocks is transmitted through an ideal propagation media, then the received passband signal $r(t)$ is equal to the transmitted passband signal $s(t)$. The down-conversion process can be described as the multiplication of the received passband signal by a complex exponent having the opposite argument sign:

$$y(t) = r(t)e^{-j2\pi f_{cr}t}\,, \tag{5.2}$$

where $r(t)$ is the received passband signal and f_{cr} is the carrier frequency of the receiver. If transmitter and receiver carrier frequencies are equal, the received baseband signal is equal to the transmitted baseband signal. However, as a rule, these carrier frequencies are generated by different oscillators and they are not exactly equal, therefore causing the CFO:

$$y(t) = x(t)e^{j2\pi(f_{ct}-f_{cr})t} \tag{5.3}$$

A CFO projection to the *baseband* can be described as the multiplication of the transmitted baseband signal by a complex exponent with the frequency equal to the CFO:

$$y(k) = x(k)e^{j2\pi\epsilon k\tau} = x(k)e^{j2\pi\varepsilon k} \tag{5.4}$$

where τ is the sample time, $\epsilon = (f_{ct} - f_{cr})$ is the absolute CFO and $\varepsilon = \epsilon\tau$ is relative CFO, which in literature, for example in [72], is referred as fractional carrier frequency offset (FCFO). From Equation 5.4 it can be noticed, that the complex exponent multiplier $e^{j2\pi\varepsilon k\tau}$ is a periodic

function with a period $\frac{1}{\epsilon\tau}$. Therefore, the maximum absolute CFO, which can be corrected at the baseband level, is limited to the value $\epsilon_{max} = \frac{1}{2\tau}$ and the FCFO $\varepsilon_{max} = 0.5$.

5.2.3 Sampling frequency offset

In accordance with Figure 2.10, before upconversion, a baseband signal is converted into analog form by means of two DACs. Later, at the receiver side, it is converted to periodic discrete samples by means of two ADCs. Translation from digital to analog signal must be performed at the sampling frequency $f_d = 1/\tau_t$. Inconsistency between transmitter and receiver sampling frequencies causes a scaling of the received time domain (TD) signal, moreover, it causes a scaling of the received signal spectrum on the frequency axis. This effect is called sampling frequency offset (SFO).

A DAC in the baseband of communication system transmitter creates a continuous signal $x_c(t)$ from the discrete $x(k)$ in accordance with the equation:

$$x_c(t) = \sum_{k=0}^{D} x(k) sinc\left[\left(\frac{t}{\tau_t} - k\right)\pi\right] \tag{5.5}$$

In case of no RF impact and other issues, the received baseband signal is equal to the transmitted baseband signal:

$$y_c(t) = x_c(t) \tag{5.6}$$

The ADC in the receiver baseband performs sampling of a continuous signal in accordance with the equation:

$$y(n) = y_c(n\tau_r) \tag{5.7}$$

By substituting Equations 5.5-5.6 into 5.7, we obtain:

$$y(n) = \sum_{k=0}^{D} x(k) sinc\left[\left(\frac{n\tau_r}{\tau_t} - k\right)\pi\right] \tag{5.8}$$

If $\tau_r = \tau_t$, then the received discrete samples are equal to the transmitted discrete samples. However, if sampling frequencies differ, it causes distortion of the received signal, and eventually leads to inter-carrier interference (ICI).

In mobile communication systems, due to the mobility of transmitter or receiver, or both, the time scale of the received signal changes. If the distance between the transmitter and the receiver changes non-uniformly, the frequency shift becomes also non-uniform. The shift of frequencies, known as *Doppler effect* , can be modeled as the varying SFO.

5.3 Impact of frequency offset in GUR-based PMC systems

5.3.1 Overview

An overall effect of frequency offset in orthogonal frequency division multiplexing (OFDM) was analyzed by Pollet etal. in [73]. For small frequency errors the signal-to-noise ratio (SNR) $\frac{E_s}{N_0}$ degradation in decibels can be described approximately by:

$$\Delta_{SNR} = \frac{10}{3ln10}(\pi\varepsilon)^2\frac{E_s}{N_0} \tag{5.9}$$

where ε is the normalized CFO. Speth and Meyr in [74] give the frequency offset limit which corresponds to the tolerable SNR degradation $\Delta_{SNR\max}$ in OFDM systems:

$$\varepsilon < \frac{\sqrt{3}}{\pi}\sqrt{\frac{N_0}{E_s}\left(1 - \frac{1}{\Delta_{SNR\max}}\right)} \tag{5.10}$$

5.3.2 Impact of carrier frequency offset

The effect of CFO can be described as the multiplication of the received baseband signal $y(k)$ by a complex exponent with the frequency equal to the carrier frequency offset:

$$y(k) = x(k)e^{j2\pi\varepsilon k} \tag{5.11}$$

where y are received samples, x are transmitted samples, ε is FCFO. Therefore, the carrier frequency offset causes rotation of the received TD samples in in-phase quadrature (IQ) plane.

5.3.3 Impact of sampling frequency offset

Discrepancies between the sampling frequencies lead to the situation when the receiver does resampling of the received signal by a non-integer number of original samples. This leads to the loss of the mutual orthogonality between subcarriers and, thus, ICI.

5.3.4 Experimental evaluation of the impact caused by CFO and SFO

In order to determine the impact of frequency offsets in GUR-based PMC systems, a series of simulations have been made. The simulated PMC system was based on complex constant rotation angle OT (CCRAOT) transform (see 3.2.4.2) having $\phi = 30^\circ$ with 64 subcarriers and 16-chip padding. The bit error ratio (BER) was calculated in a simulation of sending 64+16 chips (1 block) via resampling (for SFO) or mixing with a complex exponent signal (for CFO).

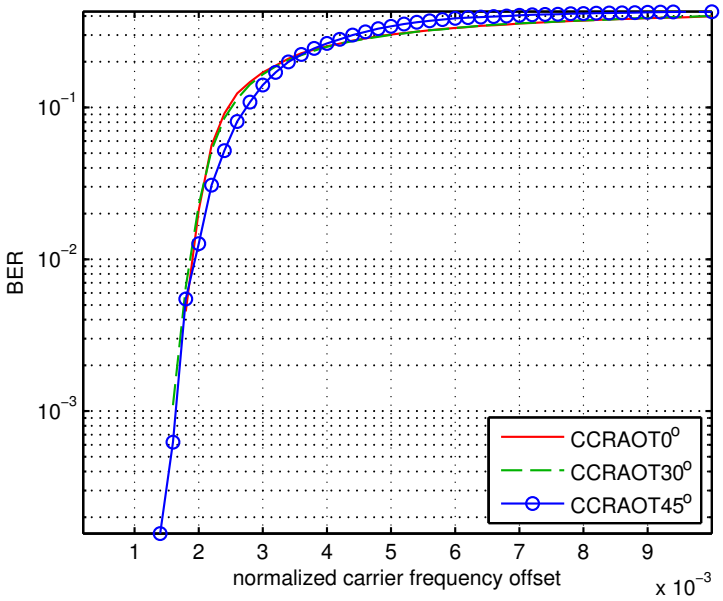

Figure 5.1: Dependence of BER on CFO in a 64-subcarrier GUR-based PMC system

Sending of just one block (80 chips) assumes a perfect timing synchronization (see Chapter 4), because without timing synchronization the impact of sampling frequency offset will be much larger. As it was mentioned in Section 4.3.3.2.1, generally, GUR-based PMC systems are very sensitive to timing offset. Both SFO and CFO create a gradually increasing timing offset, which must be corrected.

The graphs 5.1 and 5.2 were obtained by averaging the BER over 50 simulations of one block transmission. The graph 5.1 shows extremely high sensitivity to CFO and emphasizes the importance of good frequency synchronization. Moreover, the impact of CFO is much larger than the impact of SFO (see the comparison in Figure 5.2). This is because CFO has an immediate impact on the received TD samples, whereas the impact of SFO grows with time and in case of good timing synchronization the first samples always remain correct.

5.4 Carrier frequency offset estimation

5.4.1 Overview

In order to perform carrier frequency synchronization, it is necessary to estimate FCFO. An overview of FCFO estimation methods most suitable for GUR-based PMC systems are given in Figure 5.3. FCFO estimation methods can be classified using several criteria.

In accordance with [54] by Meyr et al., generally there are three types of estimators. Decision-directed (DD) estimators explicitly employ training samples for synchronization recovery. For

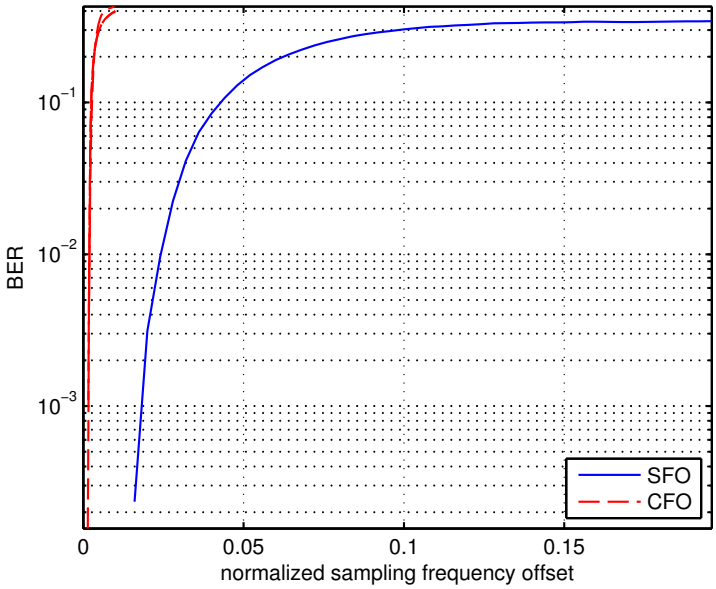

Figure 5.2: Dependence of BER on SFO in a 64-subcarrier CCRAOT $\phi = 30°$-based PMC system. For comparison , BER dependence on CFO is shown.

instance, matched filter (MF)-based estimators are DD estimators. If the estimator at the receiver side employs the structure of the signal created from the training samples transmitted by the transmitter , then it is called data-aided (DA) estimator . Autocorrelation (AC)-based estimators are typical DA estimators. The third type of estimators are so -called non data-aided (NDA) or blind estimators . These estimators do not employ any training samples, but extract synchronization information from data samples, see, for example [75].

Signals in modern, and especially, MC communication systems can be transformed between the TD and other domains, such as GUR domain (GD) or frequency domain (FD). Since the impact of CFO (multiplication with a complex exponent) is linear, it 'survives' during any unitary transformation and always shows itself as a linearly increasing phase shift of the received signal. Therefore, CFO can be estimated and corrected after the unitary transform unit (unit 'Forward transform' in Figure 2.4) of the receiver.

An especially convenient situation is in OFDM, where CFO is readily available via channel estimation. Small CFOs (phase shift $\zeta < \pi/2$) can be corrected by means of *FD equalizer* (see Section 6.6). Unfortunately, FD methods are barely applicable to GUR-based PMC systems, since equalization there is performed in the GD (see Chapter 6) and FD information is not available.

In this doctoral thesis the following two DA FCFO estimation methods will be considered in context of GUR-based PMC systems:

- Phase of repeating block AC;

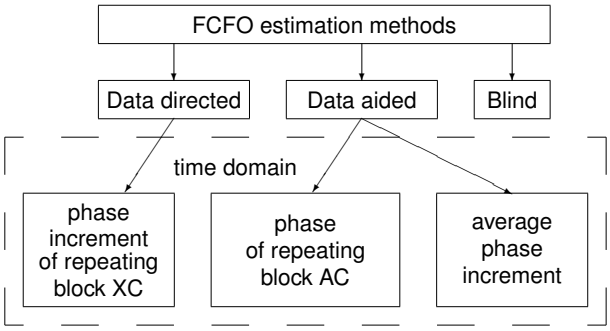

Figure 5.3: Overview of carrier frequency offset estimation methods reviewed in this thesis

- Phase increment of repeating block cross-correlation (XC);
- Average phase increment (reviewed only);

5.4.2 Data-aided fractional carrier frequency offset estimators

The described TD FCFO estimators employ repeating parts of TD signal. Repeating parts are usually located at the beginning of the frames or blocks (see TD signal structure in Figure 2.5).

If we have an ideal communication channel with no dispersion and noise, then the received TD baseband signal is described by (5.4). Multiplication of two equal samples $x(k) = x(k+D)$, having the temporal distance of D samples between each other, gives:

$$y(k)y^*(k+D) = |x(k)|^2 e^{j2\pi\varepsilon D} \tag{5.12}$$

FCFO can be expressed directly from (5.12) as follows:

$$\varepsilon = \frac{\arg(y(k)y^*(k+D))}{2\pi D} \tag{5.13}$$

5.4.2.1 Repeating block autocorrelation

For higher estimation accuracy, series of multiplications can be averaged over the block with length M and it leads to an AC-based FCFO estimator. Since all phase increments are expected to be the same, the complex exponent can be brought out of the sum:

$$J = \sum_{k=0}^{M-1} y(k)y^*(k+D) = e^{-j2\pi D\varepsilon} \sum_{k=0}^{M-1} |y(k)|^2 \tag{5.14}$$

from where FCFO can be expressed as:

$$\varepsilon = \frac{1}{2\pi D} \angle \left(\sum_{k=0}^{M-1} y(k)y^*(k+D) \right) \tag{5.15}$$

In accordance with [54] (page 488), this is a so -called D-spaced DA FCFO estimator. Since the argument of (5.15) cannot exceed π, the detection range of the mentioned estimator is limited by the condition:

$$\varepsilon_{max} = \frac{1}{2D} \tag{5.16}$$

Estimator based on repeating block AC can employ any repeating parts of the TD signal. For example, the frequency offset can be estimated by the correlation of the cyclic prefix (CP) and the end of any block. The frequency shift can be determined from the argument of the complex output signal of the AC-based block timing offset (BTO) estimator (see Section 4.3.2.1) at the instants when the absolute value of this signal reaches its maximum. Notice, that repeating unique word (UW) can be used in a similar fashion.

Scheme of frequency synchronization for an OFDM-based wireless local area network (LAN) [76] is based on the correlation of the timing functions of two adjacent identical pilot blocks for the estimation of the channel parameters. A pilot block (a block with all its subcarriers $y(k)$ occupied by pilot signals) is transformed into the TD with the aid of the inverse discrete Fourier transform (DFT) presented in Expression (2.2). Denote the period of the pilot blocks recurrence (correlation window) in samples by D, the length of the pilot part of the block [1] by M and the period of the pilot blocks recurrence in seconds by $T = \tau D$, where τ is the sample time. If the absolute shift of the carrier frequency is denoted by ϵ, then the total phase shift ζ over the time of one block is:

$$\zeta = \epsilon T = \epsilon D\tau = \varepsilon D, \tag{5.17}$$

where ε is FCFO. If there is no frequency shift, then the correlation between the equal samples of two repeating blocks is found from the formula:

$$J_0 = \sum_{k=0}^{M-1} y(k)y^*(k+D) = \sum_{k=0}^{M-1} |y(k)|^2, \tag{5.18}$$

where $y(k)$ are the received samples of the pilot blocks. If there is a frequency shift, then, at the output of the correlator, then equation (5.14) can be rewritten as:

$$J = J_0 e^{-j2\pi\zeta} \tag{5.19}$$

where the phase shift is determined by Expression 5.17.

[1] in this particular case blocks consist of pilot samples only, therefore $M = D$

This phase shift can be obtained from J using the following approach:

$$\zeta = \frac{1}{2\pi}\angle\left(\frac{J^*}{|J|}\right) \tag{5.20}$$

where $\angle()$ signifies the argument of a complex number. The frequency offset can be found using the expression:

$$\epsilon = \frac{\zeta}{T} \tag{5.21}$$

Since the capabilities of the described method are restricted by the condition $\zeta < 1$, the maximal frequency offset which can be unambiguously detected using this algorithm is:

$$\epsilon_{max} = \frac{1}{T} = \frac{1}{\tau D} \tag{5.22}$$

Notice, that the detection range depends on two factors: the chip frequency $1/\tau$, which can not be changed, and the length of the correlation window D. If the correlation window size is equal to the size of information block, the maximal detectable frequency offset is equal to the distance between samples of DFT spectrum from TD signal with padding.

For the extension of FCFO estimation range two approaches can be used:

- oversampling of received chips [77];
- shortening of correlation window.

It is possible to increase the detection range by shortening the correlation window at the cost of accuracy loss. The authors of [76] suggest correlating shorter training blocks of the frame synchronization for the rough estimation of the frequency shift:

$$G = \sum_{k=0}^{\frac{D}{4}-1} y(k)y^*(k+\frac{D}{4}) = e^{-j2\pi\frac{\zeta}{4}} \sum_{k=0}^{\frac{D}{4}-1} |y(k)|^2 \tag{5.23}$$

$$\frac{\zeta}{4} = \frac{1}{2\pi}\angle\left(\frac{G^*}{|G|}\right) \tag{5.24}$$

Since the correlator uses signals that are four times shorter than information blocks, no uncertainty occurs in finding ζ even for large discrepancies between the frequencies. For the same reason, the method in question is less accurate.

The required range and accuracy of the frequency synchronization are attained by combining the rough and the exact estimates:

$$\zeta = \frac{4}{2\pi}\angle\left(\frac{G^*}{|G|}\right) + \frac{1}{2\pi}\angle\left(\frac{J^*}{|J|}\right) \tag{5.25}$$

In a widely cited article by Schmidl and Cox [36], the authors suggest using two special adjacent training blocks (see Section 2.4.3.2). The symmetry of the first block renders it tolerant to the detuning of the carrier frequency. The second block consists of two other pseudo-noise (PN) sequences, which make it possible to perform the estimation of the channels parameters, as well as to compute the FCFO.

5.4.2.2 Maximum likelihood AC-based estimator

A maximum likelihood (ML) FCFO estimator based on AC of CP was proposed by the authors of [57]. ML FCFO estimator is obtained along with ML BTO estimator (see Section 4.3.2.1.3).

The maximization of the log-likelihood function with respect to FCFO can be obtained when the cosine term in Equation (4.14) approaches one:

$$\cos(2\pi\varepsilon + \angle\gamma(\theta)) = 1 \tag{5.26}$$

By substituting condition (5.26) into (4.14) we obtain:

$$\Lambda(\theta, \epsilon_{ML}) = |\gamma(\theta)| - \rho a(\theta) \tag{5.27}$$

Therefore the ML estimate of FCFO is:

$$\hat{\varepsilon}_{ML} = -\frac{1}{2\pi}\angle(\hat{\theta}_{ML}) \tag{5.28}$$

The given set of equations is suitable for systems where all received samples have Gaussian PDFs. In the meantime, many pilot sequences like Zadoff-Chu (ZC) (see Section 2.4.3.1) have other probability distributions and the described ML estimator does not fit to such systems.

5.4.2.3 Improved autocorrelation-based estimator

Morelli and Mengali in [78] have shown that correlation between more than two repeating blocks increases the accuracy of the FCFO estimator and attains Cramer-Rao bound (CRB). However, in this case the synchronization time will increase. On the other hand, selection of shorter synchronization blocks in accordance with (5.22) will lead to the extension of the estimation range at the cost of reduced accuracy.

5.4.2.4 AC-based fractional CFO estimator for GUR-based PMC systems

Frequency offset in GUR-based PMC systems has large negative impact (see Section 5.3). Therefore, the CFO estimation and correction circuitry must be placed as close as possible to the input of PMC system receiver.

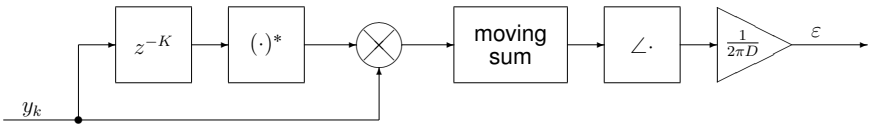

Figure 5.4: AC-based FCFO estimator

Signal processing in the baseband of the GUR-based PMC system receiver begins in the TD (see Figure 2.4). Therefore, CFO estimation and correction in the TD of GUR-based communication system is a natural approach.

UW (see Section 2.3.4.3) appended to the beginnings of sample blocks can be used for time offset synchronization (see Section 4.3.2.2). Since UW is repeated at the beginning of each block, it is possible to use the pilot block AC algorithm (5.21) described in Section 5.4.2.1. The diagram of the resulting FCFO estimator is shown in Figure 5.4

The algorithm (5.21) has been adopted to a GUR-based PMC system using blocks with a UW prefix. The adopted solution has been implemented as a part of PMC system model. This GUR-based PMC system has $N = 64$ subcarriers. The resulting TD block consists of 64 data samples and 64 UW samples generated using ZC algorithm (see Section 2.4.3.1). In accordance with Formula (4.3) the timing offset estimator based on AC (see Section 4.3.2.1) performs AC of chips $D = 128$ samples apart of each other. The maximum absolute FCFO, which can be detected, is $\varepsilon_{max} = \frac{1}{2D} = 0.0039$. The accuracy of this AC-based FCFO estimator has been verified using numerical simulation. Transmitter and receiver FCFOs were 0, 0.0005 and 0.001. FCFO determined by the AC-based estimator has been averaged over 10 blocks and compared to the original CFO. From the simulation results (shown in Figure 5.5), it can be concluded that the accuracy of AC-based FCFO estimator depends on CFO. Namely, small frequency offsets are estimated more precisely than larger ones. This feature makes AC-based FCFO estimators perfectly suitable for fine CFO estimation, whereas other FCFO estimators can be used for the coarse tuning.

5.4.2.5 Average phase increment method

Cvetkovic etal. in [79] proposed another interesting method of FCFO estimation, also based on periodic samples. Let's assume that the transmitted block of N samples consists of n equal sub-blocks by D samples. Transmitted baseband TD samples are defined as follows:

$$x_{nD+k} = x_k \quad \text{where} \quad n \in [0, \frac{N}{D} - 1], k \in [0, D-1] \tag{5.29}$$

If we denote the signal at the receiver input as y, then in case of ideal channel, the received signal is:

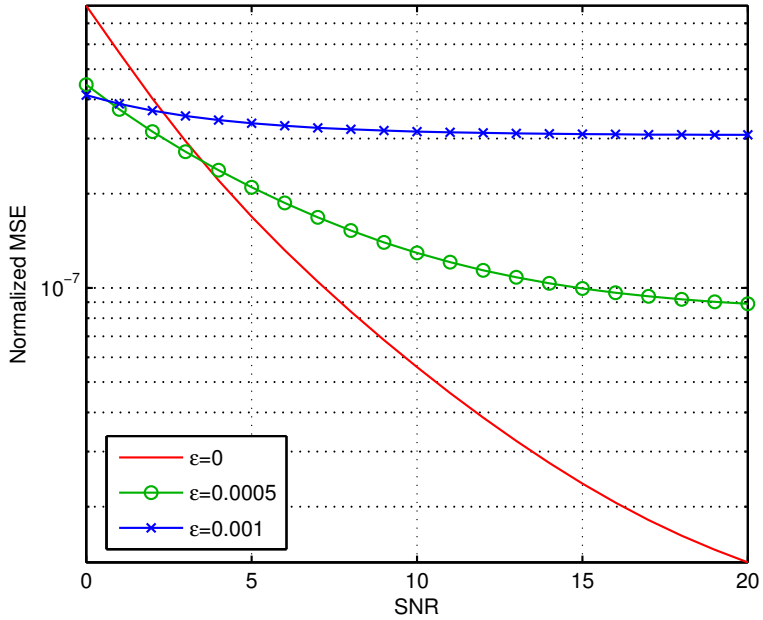

Figure 5.5: Accuracy of AC-based FCFO estimator

$$y_{nD+k} = x_k e^{j[\zeta_k + 2\pi\varepsilon(nD+k)]}, \tag{5.30}$$

where ε is FCFO and $\zeta_k = arg(x_k)$ are phases of transmitted samples. Now let's assume that we have measured phases of the received samples $\alpha_{nD+k} = arg(y_{nD+k})$. The authors define the error function between the measured samples α_{nD+k} and the phase part of Equation (5.30) as follows:

$$v = \sum_{k=0}^{D-1} \sum_{n=0}^{N/D-1} [\alpha_{nD+k} - \zeta_k - 2\pi\varepsilon(nD+k)]^2 \tag{5.31}$$

Minimization of (5.31) with respect to ε and ζ_k yields the following FCFO estimator:

$$\hat{\varepsilon} = \frac{3}{\pi} N(N-D)(N+D) \sum_{k=0}^{D-1} \sum_{n=0}^{N/D-1} (D - N + 2Dn)\alpha_{nD+k} \tag{5.32}$$

The given estimator performs an averaging (over k) of individual CFOs, obtained as slopes of straight lines, which approximate angle increments within individual sub-blocks $[0, D-1], [D, 2D-1], \ldots, [D(N-1), DN-1]$.

The authors compared their estimators with [36] and [78] and concluded that the given estimator attains an accuracy comparable with [78], which reaches the CRB at high SNR. Moreover, it has a much lower computational complexity (see Table 5.1) than AC-based methods including [78]. Compared to [36], the given estimator provides a 9 dB performance gain and

has a similar computational complexity.

5.4.3 Decision-directed fractional carrier frequency offset estimators

The proposed DD FCFO estimation algorithms are based on the XC between a known training sequence stored in the receiver and received samples. In other words, the proposed FCFO estimator is based on a matched filter. The proposed FCFO estimators are derived from decision-directed algorithms proposed by Meyr et al. in [54].

5.4.3.1 Method with increment averaging

If there are no channel impairments, except CFO, the received baseband signal is described by (5.4). Multiplication of respective transmitted and received samples yields the following result:

$$y(k)x(k)^* = |x(k)|^2 e^{j2\pi\varepsilon k} \tag{5.33}$$

From Equation (5.33) could be seen that the phase of $y(k)x(k)^*$ grows linearly in time with a speed which is proportional to the CFO. Using this observation, we can derive an XC-based FCFO estimator. Let's take two sample pairs with indexes k and $k + D$, where D is an integer offset. If multiplication of the second sample pair is described by a similar to (5.33) expression:

$$y(k + D)x(k + D)^* = |x(k + D)|^2 e^{j2\pi\varepsilon(k+D)}, \tag{5.34}$$

then subtracting the arguments of Equations (5.33) and (5.34) results in

$$\angle[y(k + D)x(k + D)^*] - \angle[y(k)x(k)^*] = 2\pi\varepsilon D \ , \tag{5.35}$$

Now CFO can be expressed from (5.35) as follows:

$$\varepsilon = \frac{\angle[y(k + D)x(k + D)^*] - \angle[y(k)x(k)^*]}{2\pi D} \tag{5.36}$$

Averaging offsets within a block of adjacent samples ($D = 1$) allows to obtain expression, which can be used in real FCFO estimator:

$$\varepsilon = \frac{1}{2(M-1)\pi} \sum_{k=0}^{M-2} (\alpha(k + 1) - \alpha(k)) \tag{5.37}$$

where

$$\alpha(k) = \angle[y(k)x(k)^*] \tag{5.38}$$

The structure of the resulting FCFO estimator is shown in Figure 5.6

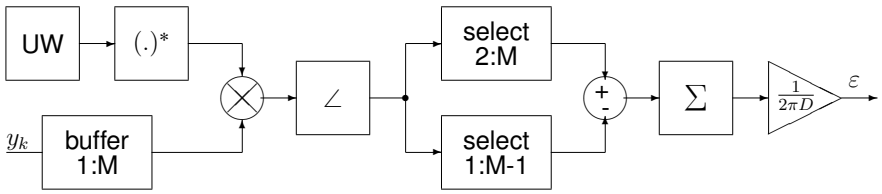

Figure 5.6: FCFO estimator based on the averaging of cross -correlation phase increments

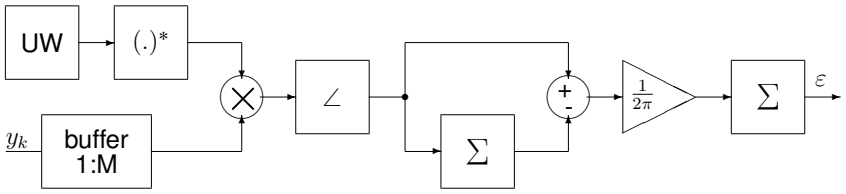

Figure 5.7: FCFO estimator based on a linear regression of correlation phase increments

Noticeably, that the detection range of the proposed estimator is still limited by the condition (5.16). However, due to the fact that $D = 1$ in this estimator, $\varepsilon_{AVGmax} = 1/2$. Similarly as in the case with the AC-based estimator (5.15), the accuracy of the given estimator can be increased at the cost of the detection range by taking $D > 1$. However, collecting the block of M phase increments will require D times more time.

5.4.3.2 Least squares -based method

Expression (5.37) performs an averaging-based line fit within a block of samples. However, simple averaging of phase increments is not optimal in the sense of mean squared error (MSE). A least squares (LS) estimator based on a simple linear regression [80], might improve the performance of the device. Similar method [81] is proposed for estimating the frequency of a noisy sinusoid. Replacing the averaging with an LS estimator yields the expression:

$$\varepsilon = \frac{1}{2\pi} \sum_{k=0}^{M-1} \frac{(\alpha(k) - \overline{\alpha})(k - \overline{k})}{\sum_{m=0}^{M-1}(k - \overline{k})^2} \tag{5.39}$$

Due to the symmetry of the multiplier $(k - \overline{k})$ in Equation (5.39), the mean of angles $\overline{\alpha}$ can be replaced by the sum, therefore saving one division by M:

$$\varepsilon = \frac{1}{2\pi} \sum_{k=0}^{M-1} \frac{(\alpha(k) - \sum_{m=0}^{M-1}\alpha(m))(k - \overline{k})}{\sum_{m=0}^{M-1}(k - \overline{k})^2} \tag{5.40}$$

The block diagram of the obtained FCFO estimator is depicted in Figure 5.7. Since $D_{LS} = 1$, the frequency acquisition range of the proposed estimator (5.40) remains $\varepsilon_{LSmax} = 1/2$.

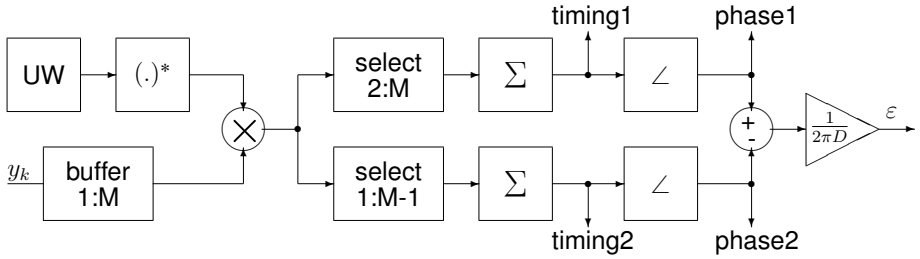

Figure 5.8: XC-based FCFO estimator optimized to CAZAC sequences

5.4.3.3 Method for CAZAC sequences

Equation (5.37) can be changed if we use training samples from constant amplitude zero auto-correlation (CAZAC) sequences. Such training samples can be obtained, for example, using ZC algorithm [32]. Using this method, (non-linear) complex argument operation can be exchanged with the sum. In this case Equation (5.37) can be rewritten as:

$$\varepsilon = \frac{1}{2(M-1)\pi}\left(\angle \sum_{k=0}^{M-2} z(k+1) - \angle \sum_{k=0}^{M-2} z(k)\right) \tag{5.41}$$

where

$$z(k) = y(k)x(k)^* \tag{5.42}$$

In this variant of XC-based FCFO estimator, the argument is taken from the averaged XC between the training block pattern and the received samples. The largest advantage of the estimator (5.41) is that it can be used in conjunction with the XC-based timing offset estimator described in Section 4.3.2.2. The resulting FCFO estimation scheme is shown in Figure 5.8.

If sequences with good correlation properties are used in the role of UW, the magnitude of either "timing" signal can be used for BTO estimation.

The FCFO acquisition range of the estimator (5.41) is also $\varepsilon_{CZmax} = 1/2$.

5.4.3.4 Simulation results of fractional carrier frequency offset estimators

The accuracy of the proposed XC-based FCFO estimators has been verified using computer simulations. The transmitted sequence contained 100 blocks, each consisting of $N = 64$ random data chips and a UW with three different lengths produced using ZC algorithm (see Section 2.4.3.1). The purpose of the first set of the simulations was to determine the dependency of MSE on SNR at various block lengths.

The simulation results of AC-based FCFO estimator (5.15) are shown in Figure 5.9. We see that by increasing the UW length we can increase the accuracy of the estimator.

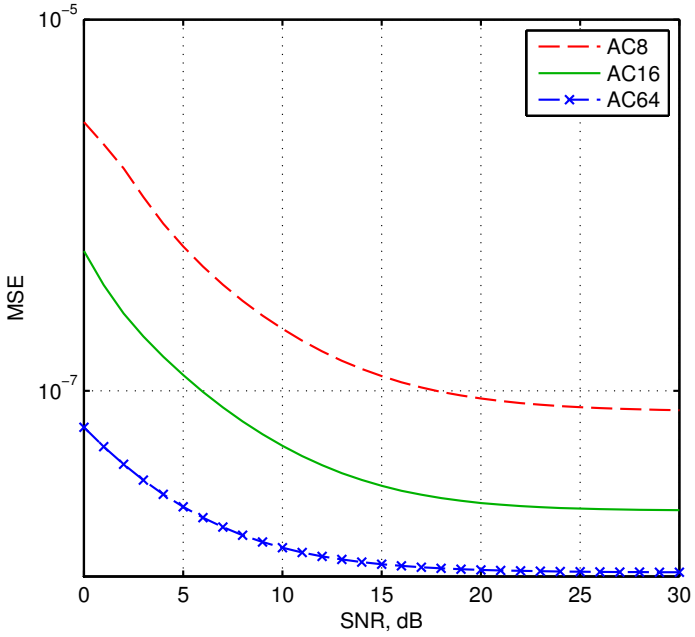

Figure 5.9: Accuracy of the FCFO estimator based on the AC algorithm (5.15) at UW lengths 8, 16 and 64 samples in a PMC system with an AWGN channel and FCFO $\varepsilon = 0.001$

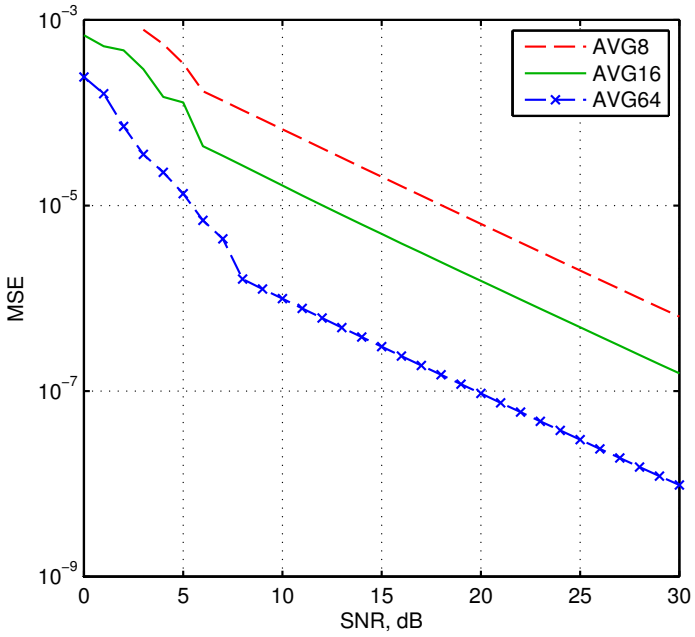

Figure 5.10: Accuracy of the FCFO estimator based on the XC algorithm with averaging (5.37) at UW lengths 8, 16 and 64 samples in a PMC system with an AWGN channel and FCFO $\varepsilon = 0.001$

The accuracy of XC-based estimator (5.37), which utilizes slope averaging, is depicted in Figure 5.10. There is a linear dependence of MSE on SNR.

The simulation results of XC-based estimator (5.40) with the least squares algorithm are

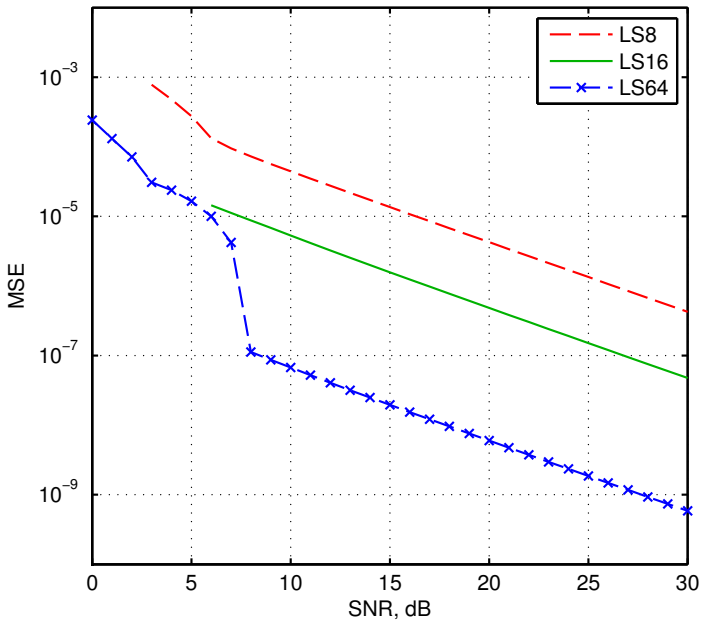

Figure 5.11: Accuracy of the CFO estimator based on the XC algorithm with least squares (5.40) at UW lengths 8, 16 and 64 samples in a PMC system with an AWGN channel and FCFO $\varepsilon = 0.001$

given in Figure 5.11. From the plot it is seen, that systems with a longer UW are more sensitive to additive noise. At low SNR, increasing the UW does not lead to accuracy improvement.

The simulation results of the XC algorithm derived for CAZAC sequences (5.41) are depicted in Figure 5.12. Similarly to the algorithm (5.37), this algorithm is immune to the noise, and the increase of UW length leads to the increase of estimator accuracy.

In the second set of the simulations a fixed number $M = 64$ of UW chips was used. Each model was tested with two different FCFOs $\varepsilon_1 = 0.001$ and $\varepsilon_2 = 0.01$. In accordance with (5.16), the estimation limits of our AC-based estimator (5.15) were set by $\varepsilon_{ACmax} = \frac{1}{2(64+64)} = 0.0039$, whereas the estimation limits of the XC-based estimators were set by $\varepsilon_{XCmax} = 0.5$.

In the first subset of simulations a signal with CFO was sent over an AWGN communication channel. MSE obtained during the simulations is depicted in Figure 5.13. The plots with legend "AC" for the AC-based estimator (5.15) are given for reference. The cross correlation-based algorithms (5.37), (5.40) and (5.41) correspond to the respective abbreviations "AVG", "LS" and "CZ".

From the simulation results it can be seen that, at small FCFO ($\varepsilon = 0.001$), the MSE of AC-based estimator is an order of magnitude smaller than that of XC-based ones. In contrast, at relatively high SNR, the accuracy of XC-based estimator (5.40) starts to surpass the accuracy of AC-based one. Among the proposed XC-based FCFO estimators, the LS-based solution (5.40) demonstrates the best results, therefore confirming the excellence of this signal processing technique.

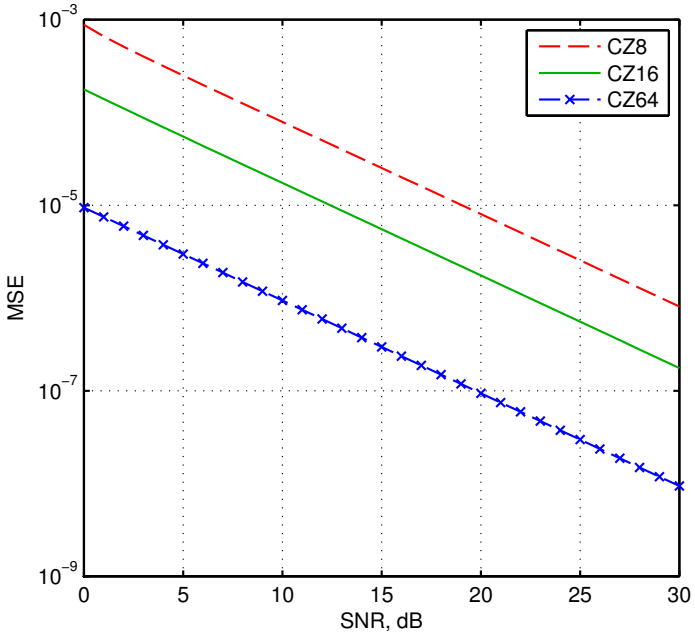

Figure 5.12: Accuracy of the FCFO estimator based on the XC algorithm for CAZAC sequences (5.41) at UW lengths 8, 16 and 64 samples in a communication system with an AWGN channel and FCFO $\varepsilon = 0.001$

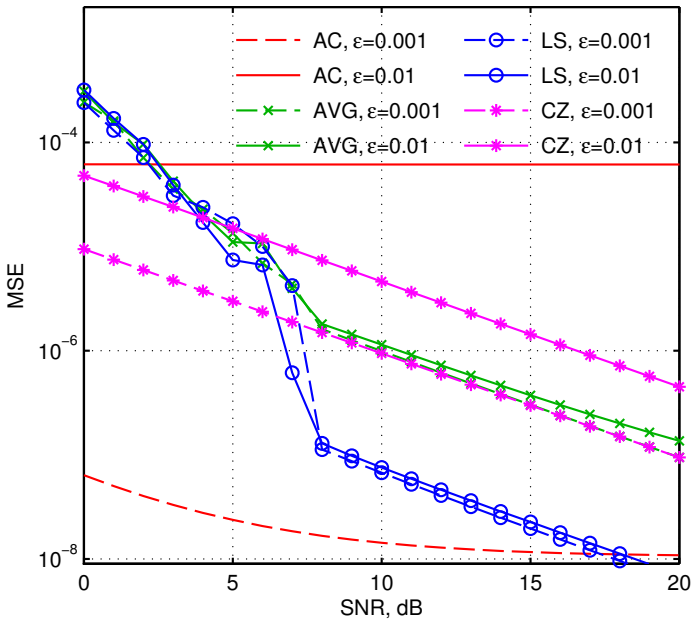

Figure 5.13: Accuracy comparison of FCFO estimators in a PMC system with an AWGN channel and the UW length of 64 samples

In the third subset of simulations, the same set of signals were sent over a dispersive channel having a 4-tap long impulse response. The simulation results are depicted in Figure 5.14. The accuracy of XC-based estimators was degraded severely, whereas the MSE of AC-based

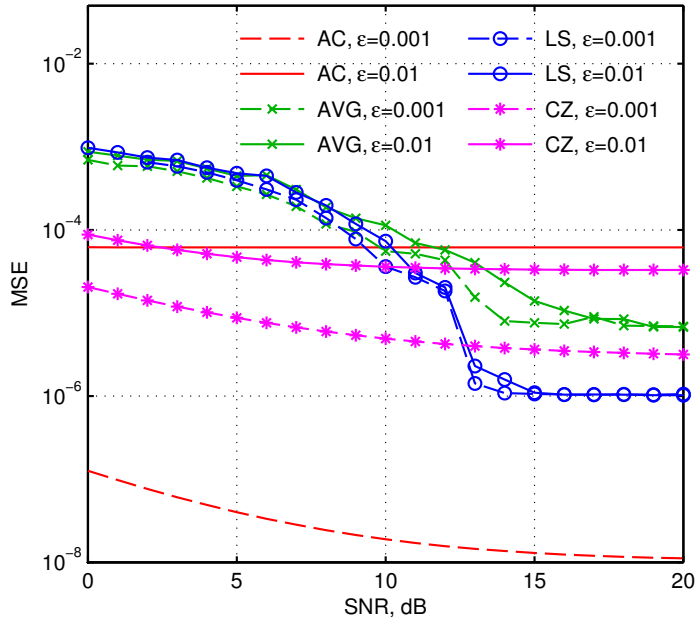

Figure 5.14: Accuracy of FCFO estimators in a communication system with a frequency selective channel and the UW length of 64 samples

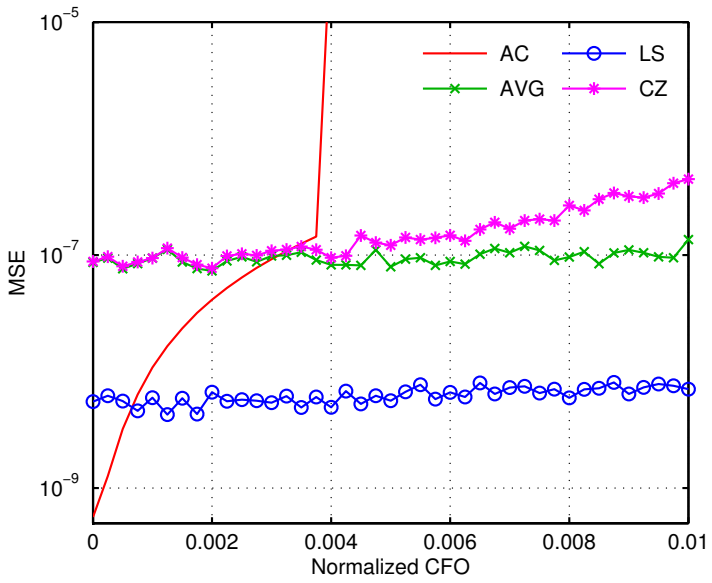

Figure 5.15: Dependence of estimator accuracy on the frequency offset

estimator remained almost unchanged. Static convolution in the communication channel affects both samples of AC-based estimator in equal manner, therefore its influence is compensated. It may be suggested, that in time-variant communication channels the AC-based estimator would perform much worse, whereas the accuracy of XC-based estimator would not change significantly.

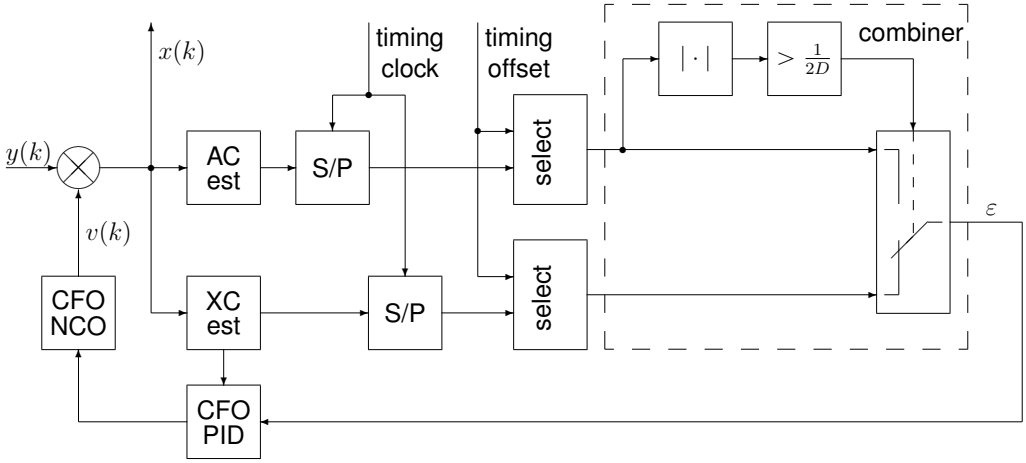

Figure 5.16: FCFO estimator combiner and control loop

In Figure 5.15 the dependence of MSE of various estimators on FCFO is depicted. Turns out that the accuracy of AC-based estimation is proportional to the frequency offset, whereas XC-based estimators have an almost constant MSE over the whole frequency offset range. Figure 5.15 confirms range limitations of AC-based estimator in the sense of frequency acquisition range.

5.4.4 Combined fractional carrier frequency offset estimator

AC- and XC-based FCFO estimators described in Sections 5.4.2.4 and 5.4.3, respectively, have different acquisition ranges and accuracies. A combination of these estimators would provide and efficient FCFO estimation solution with a wide acquisition range and high accuracy. In accordance with the graph 5.15, the accuracy of AC-based FCFO estimator is higher than the accuracy of XC-based one. However, the estimation range of AC-based estimator is highly limited.

The proposed FCFO estimation combiner is depicted in Figure 5.16. It uses the output of XC-based estimator for controlling the estimator selection for the combiner output. If FCFO, estimated by the XC-based estimator, is less than the acquisition range of AC-estimator, the output is connected to the AC-estimator. In contrast, if FCFO is outside of the AC acquisition range, the output is connected to the less accurate XC-based estimator. Therefore, the coarse fractional FCFO estimation is performed by the XC-based estimator, whereas the fine FCFO estimation is performed by the AC-based one.

5.4.5 Conclusions about fractional carrier frequency offset estimation

The simulation results have shown that the increase of the synchronization pattern length leads to the increase of the accuracy of FCFO estimator. However, the LS-based method described in Section 5.4.3.2, is more sensitive to additive noise and its accuracy at $SNR < 10dB$ does not increase with the increasing UW length.

Theoretical results and numerous simulations have confirmed that the proposed FCFO estimators provide sufficient accuracy for utilization in GUR-based PMC systems. It must be taken into account, that sufficiently large training sequences must be used in order to achieve sufficient accuracy. For example, a 64 -sample sequence provides $MSE = 10^{-8}$ at $SNR = 20dB$. Moreover, the accuracy of the proposed XC-based algorithm surpasses the accuracy of AC-based algorithms in non-dispersive communication channels with high SNR.

One of the largest advantages of XC-based methods is a large ($\varepsilon_{XCmax} = 0.5$) FCFO estimation range. On the other hand, XC-based estimators are more sensitive to the noise than AC-based ones. The accuracy of XC-based estimators can be increased by measuring the phase increment between non-adjacent sample pairs. However, the accuracy increase will occur at the cost of decreased frequency acquisition range.

Performance of the proposed algorithms in PMC systems with dispersive channels is acceptable. However, its accuracy is inferior to that of the AC-based methods.

The computational complexity of the mentioned TD FCFO estimators is compared in Table 5.1.

Estimator	Multiplications	Summations
Autocorrelation	$D \times M$	$D \times M$
Cross-correlation	$D \times M$	$D \times M$
Average phase increment	D	$3 \times D$

Table 5.1: Computational complexity of TD FCFO estimators

5.5 Residual phase offset estimation

5.5.1 Introduction

As it was said before, CFO leads to a linearly increasing phase offset of the received samples. Although the previously mentioned methods are able to estimate FCFO, the estimation of *residual phase* offset is necessary.

In telecommunications, phase detectors play a significant role as part of phase locked loop (PLL) for timing and frequency synchronization [82]. Since for a infinitely long sinusoid the phase offset is the same as a shift in time, for relatively narrowband signals the phase offset can be interchanged with the delay. In digital communications, the phase offset can be viewed as the signal delay by a fraction of chip sampling clock.

5.5.2 Phase offset estimation for GUR-based PMC systems

The cross-correlator used for timing estimation (see Section 4.3.2.2) and the ones used for FCFO estimation (see Section 5.4.3) perform multiplication of a known reference signal and the received waveform. This operation resembles the mixing in classic phase detectors and allows to find the phase offset of the signal. Indeed, if we replace y in Equation (5.33) with $xe^{j\alpha}$, where α is the phase offset, then we obtain:

$$x(k)e^{j\alpha}x(k)^* = |x(k)|^2 e^{j\alpha}, \tag{5.43}$$

from where the phase offset can be expressed directly:

$$\alpha = \angle[x(k)e^{j\alpha}x(k)^*] \tag{5.44}$$

In other words, it is sufficient to take the phase of the cross-correlation result. However, if an uncorrected CFO is present, a correct phase offset will be given for the first sample only, since the phase offset increases due to CFO. Therefore, the phase offset estimation unit must be directed by the timing offset estimator in order to obtain a correct phase offset. In Figure 5.8 it is shown how to obtain phase estimates (outputs 'phase1' and 'phase2') from a ZC sequence-based FCFO estimator. It is possible to modify other estimators shown in Figures 5.6 and 5.7 to obtain a phase offset estimate as well.

5.6 Carrier frequency offset and phase correction

5.6.1 Introduction

Most of the known FCFO correction methods [83] are based on the multiplication of the received signal by a complex exponent having a frequency, which has opposite sign compared to the FCFO. If we have the received signal (5.4) with FCFO denoted as ε, then multiplication of this signal by FCFO compensation signal $v(k) = e^{-j2\pi\varepsilon k}$ leads to the received signal without CFO:

$$y(k)v(k) = x(k)e^{j2\pi\varepsilon k}e^{-j2\pi\varepsilon k} = x(k) \tag{5.45}$$

There are two approaches how to provide interaction between the FCFO estimator and FCFO correction devices: open -loop synchronizer and feedback (closed -loop) synchronizer. In accordance with [84], open -loop synchronizers are faster than feedback ones, since synchronization must be established in one step without iterations.

5.6.2 Use of FD equalization

Since the frequency offset applies as a linear operation (multiplication with a complex exponent $e^{-j\omega_d t}$), its impact can be successfully corrected after transformation. An especially beneficial situation occurs after signal transformation to the FD using DFT, where FCFO appears as an increasing phase spectrum shift. It allows to correct FCFOs by means of FD equalizer (see Section 6.6). It must be taken into account, that FD channel *estimator* (see Section 6.5.3) is unable to detect FCFO.

5.6.3 Tracking loop

A complex exponent signal for FCFO compensation (see Section 5.6.1) can be produced by numerically controlled oscillator (NCO). NCO, in turn, can be controlled by the automatic control system, whose input signal is FCFO measured by the estimator. The resulting structure of the control loop is depicted in Figure 5.16. The design of fast, accurate, computationally efficient and stable FCFO tracking loop is one of the big challenges in communication receiver design.

5.6.4 Phase offset correction

As it was mentioned before, for an infinitely long sinusoid the phase offset by angle α is the same as a time shift of the sinusoid by $\Delta t = \alpha/\omega$, where ω is the angular frequency of the sinusoid. If the signal is not sinusoidal and has a wider spectrum, different frequencies must have a different α in order to maintain a constant time shift Δt. However, for relatively narrowband signals, the carrier phase shift can be approximated by the time shift and vice verse.

In most of the cases, for carrier phase correction, multiplication with the phase rotator $e^{-j\alpha}$ is sufficient. However, modern OFDM systems employ a Farrow variable delay filter [85], which allows to achieve better results. This is because, besides the residual phase offset, there is a fractional delay of the signal, which cannot be compensated by relatively coarse timing offset correction (see Section 4.3).

5.7 Fractional carrier frequency offset synchronization in GUR-based PMC system

A simplified PMC system model containing frequency synchronization control loop in the receiver has been created and simulated. Perfect timing synchronization was used. Since an AWGN communication channel was used, no equalization was necessary. A TD signal sample block consisted of 16 samples long ZC UW prefix, used for FCFO estimation, and 64 samples of data.

The structure of the frequency synchronization subsystem is depicted in Figure 5.16. Frequency compensation is performed by NCO, which is driven by the automatic control system based on proportional integral (PI) controller. The AC part of the FCFO estimator is shared with the timing offset estimator from Section 5.4.2.4, whereas the XC-based estimator was implemented using the design from Section 5.4.3.3. In order to measure FCFO at correct time positions (the beginnings of UW), FCFO estimators take into account the current timing offset using a selector. Switching between the estimates is provided by means of the combiner described in Section 5.4.4.

Phase adjustments are done by adding the estimated phase offset (see Section 5.5) to the input of CFO PID controller. Since the phase offset range is small, the phase offset impact on FCFO adjustment is neglectable. On the other hand, when CFO measured by the estimator becomes 0, the phase offset starts to drive "CFO PID" and "CFO NCO" until this adjustment finally allows to eliminate the residual phase offset.

For the evaluation of the PMC system performance an AWGN communication channel has been chosen. The simulation results are depicted in Figure 5.17. BER was measured after stable frequency synchronization was established. From the simulation results we can observe that the performance of a PMC system with an AWGN channel does not depend on CFO. One of the reasons for such constant behavior is that the accuracy of XC-based FCFO estimators is independent of CFO (see Section 5.4.3.4).

5.7.1 FCFO synchronization dynamics in a GUR-based PMC system

5.7.1.1 Fractional carrier frequency offset acquisition

When the receiver is just switched on, the FCFO synchronization process starts. Since the difference between the estimated FCFO and the real FCFO in the beginning could be large, the receiver starts in the acquisition mode. In this mode the synchronizer has to have a wide acquisition range. A simulation of FCFO estimator, built in accordance with the diagram 5.16, has been done for 'hopping' FCFO, which may represent the acquisition mode. The simulation

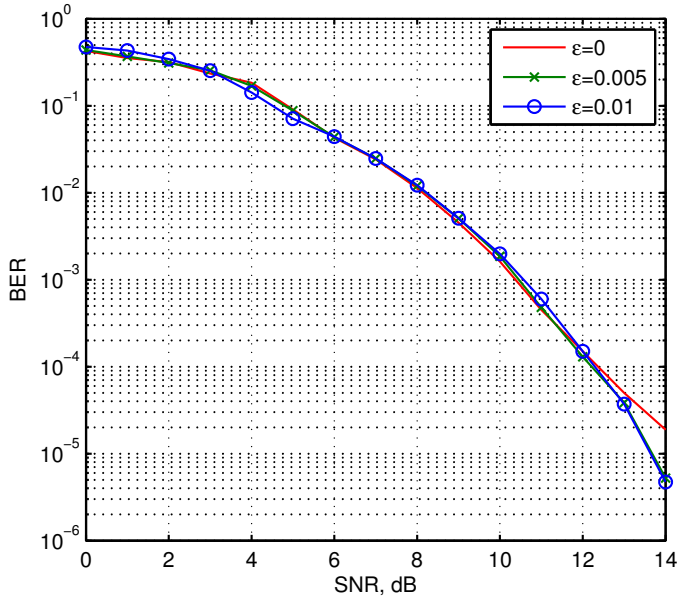

Figure 5.17: Performance of the simulated PMC system at various frequency offsets

results are given in Figure 5.18. We can notice, that the XC-based estimator detects the offset correctly, whereas the AC-based one fails. This is due to a much wider acquisition range of XC-based estimators compared to the AC-based ones (see Section 5.4.3). However, it is noticeable, that the XC-based estimator is more sensitive to the noise component of the incoming signal. Due to relatively large hops by $\Delta\varepsilon = 0.02$ and proportional integral derivative (PID) oscillations, synchronization takes more than one second. However, the reduction of PID overshoot and oscillations leads to a reduced acquisition range.

5.7.1.2 Fractional CFO tracking

When synchronization is established, the receiver switches to the tracking mode. In this mode it is assumed that CFO changes are slow enough in order to provide a precise FCFO estimation. A simulation of the FCFO synchronizer based on the diagram 5.16 in the tracking mode has been performed. The simulation graphs in Figure 5.19 demonstrate stable FCFO tracking in a wide frequency offset range. In open -loop mode (upper graph in Figure 5.19) we can observe the 'overflow' of AC-based estimator at $|\varepsilon| > 0.07$. The overshoot in the PID controller is very small, since the error signal at the input of the PID controller changes gradually.

5.8 Conclusions

- In order to provide a BER less than 10^{-3} in a CCRAOT-based MC PMC system with 64 subcarriers, FCFO must be less than 0.001, i.e. 1000 ppm.

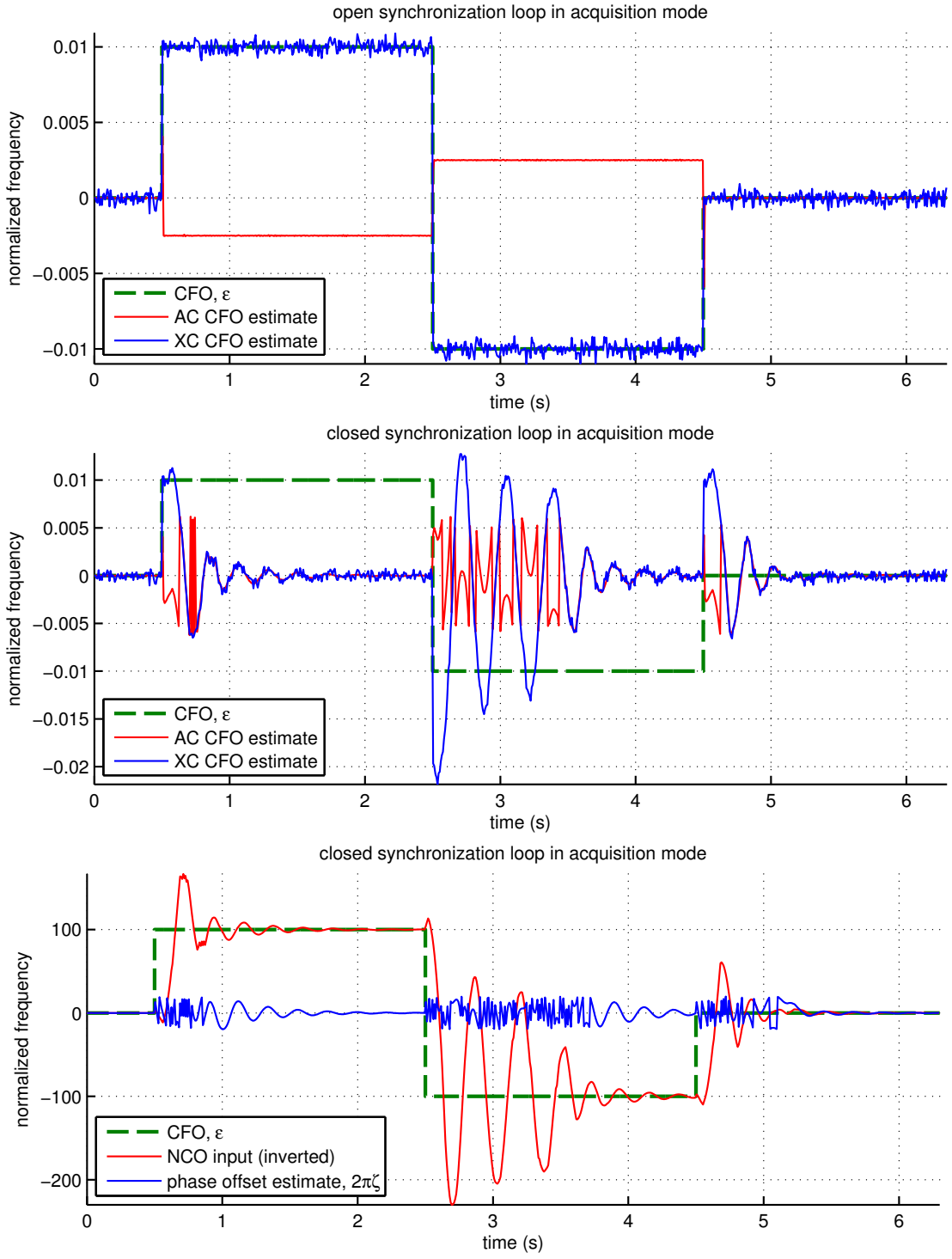

Figure 5.18: FCFO estimation in acquisition mode, SNR=30dB

- AC-based FCFO estimator provides high-accuracy estimates, but its estimation range is strongly limited.
- UW XC-based FCFO estimator provides a suitable estimation range at a moderate estima-

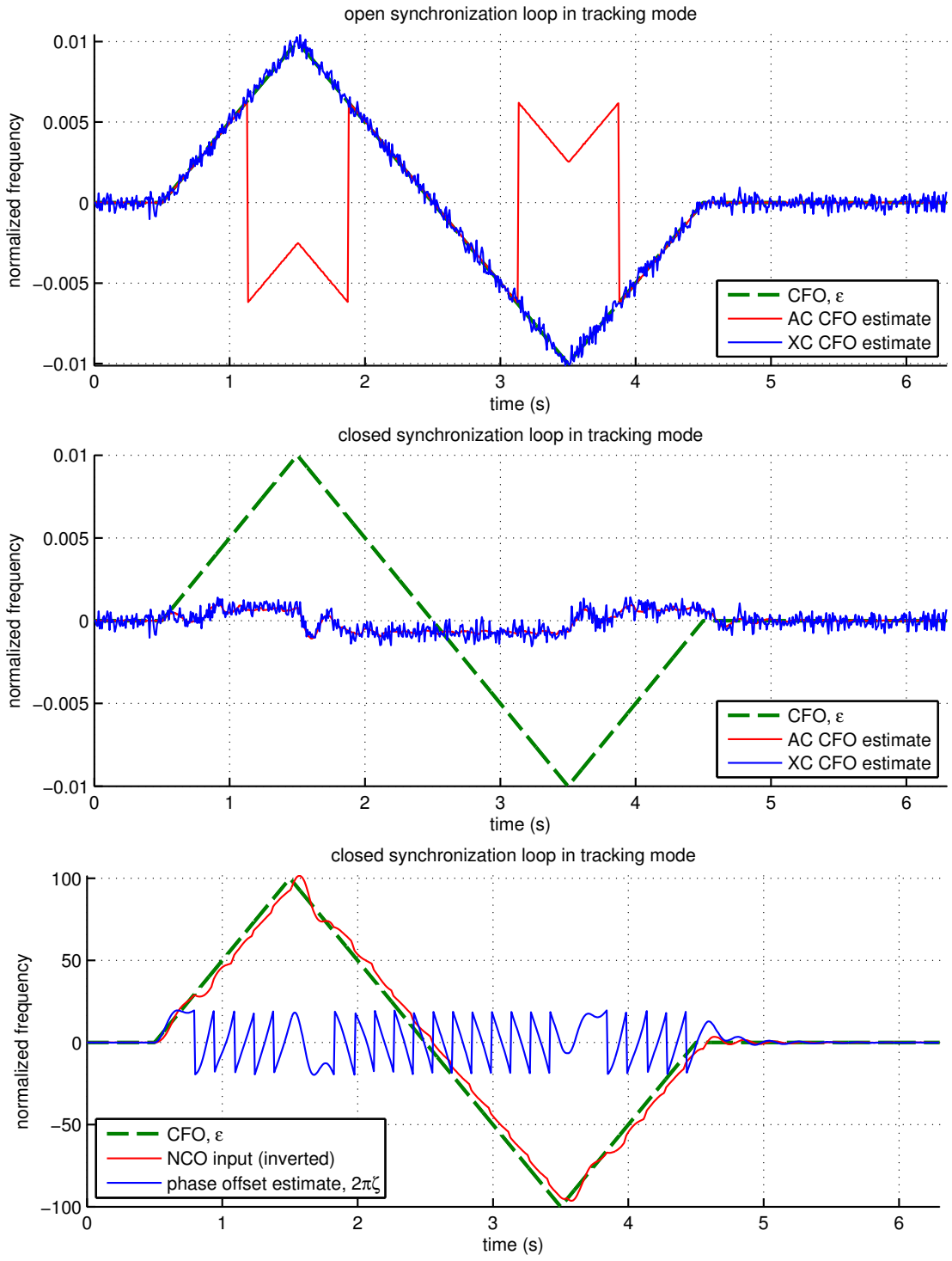

Figure 5.19: FCFO estimation in the tracking mode, SNR=30dB

tion accuracy. However, in PMC systems with frequency-selective channels, the accuracy of XC-based CFO estimator is insufficient.

- Combination of AC-based and XC-based FCFO estimators can provide a sufficient FCFO

estimation accuracy and a wide estimation range.

- Simulated feedback FCFO synchronizer provides stable synchronization in FCFO range -0.01 – +0.01.

5.9 Summary of the contributions

The following contributions in the area of frequency synchronization for GUR-based PMC systems have been done:

- Impact of CFO and SFO in a particular type of GUR-based PMC system has been experimentally evaluated (Section 5.3.4).
- AC-based FCFO estimator has been implemented and evaluated (Section 5.4.2.4).
- Derived ML AC-based FCFO estimator for normally distributed UW(Section 5.4.2.2).
- Three XC-based FCFO estimators with the following configurations have been proposed, evaluated and compared:
  1. using increment averaging (Section 5.4.3.1);
  2. using linear regression (Section 5.4.3.2);
  3. optimized for CAZAC sequences (Section 5.4.3.3).
- FCFO estimate combining algorithm has been proposed and evaluated (Section 5.4.4).
- Simple residual phase offset estimator has been implemented and evaluated (Section 5.5.2).
- Feedback FCFO and phase synchronizer for GUR-based PMC systems has been proposed and evaluated (Section 5.7).
- Proposed FCFO synchronization dynamics have been experimentally verified in acquisition and tracking modes (Section 5.7.1).

6 Channel estimation and equalization

6.1 Formulation of the problem

6.1.1 Objective

This chapter is aimed to solve the problem of equalization in Generalized Unitary Rotation (GUR)-based parametric multicarrier (PMC) systems. The ultimate goal is to develop a GUR domain (GD) equalizer.

6.1.2 Tasks

In order to meet the objective the following tasks have to be fulfilled:

- Review of time domain (TD) signal disturbances caused by the communication channel;
- Review of known *channel estimation* methods;
- Development of a GD channel estimation method;
- Review of known *equalization* methods;
- Trial of known equalization methods in the GUR domain;
- Development of a GD equalization method;
- Performance comparison for equalizers working in different domains.

6.2 Introduction

In a real communication system, due to dispersion, reflection and multipath propagation in the communication channel, several distorted and shifted copies of the same signal are received. Moreover, impact of channel can vary in time. There are two approaches for providing correct demodulation of digitally modulated signal transmitted over dispersive media.

- To to overcome dispersion, it is possible to use differential modulation, for instance, differential quadrature amplitude modulation (DQAM) or differential phase shift keying (DPSK), and measure relative variations of the adjacent samples. This technique makes it possible to transmit information without the equalization but, at the same time, results in a reduced capacity of the communication channel.

- The second approach is to use coherent detection. In such a case, the information on the current impact of the communication channel to subcarriers can be obtained through the channel estimation. Channel estimates can be used for reversing the changes inferred by the communication channel, i.e. equalization (see Section 6.6).

6.3 System model

In a PMC system where transmitter baseband TD output signal $x(t)$, is being transferred via baseband equivalent of the communication channel with impulse response $h(t)$, the receiver input signal $y(t)$ can be described as follows:

$$y(t) = x(t) * h(t) + w(t), \tag{6.1}$$

where $w(t)$ is additive noise. If transmitted signal is sampled with the sample time T_s and grouped into blocks (vectors) $\boldsymbol{x}$, and there is no inter-block interference (IBI), then baseband communication can be described by the following matrix equation:

$$\boldsymbol{y} = \boldsymbol{H}\boldsymbol{x} + \boldsymbol{w}, \tag{6.2}$$

where $\boldsymbol{H}$ is the channel matrix and $\boldsymbol{w}$ is the additive noise vector. If time-dispersive channel is static and linear, then linear influence of the communication channel in the TD, known as convolution, can be described by a subset of Toeplitz matrices [23] called *convolution matrix* :

$$\boldsymbol{H} = \begin{bmatrix} h_0 & 0 & \dots & 0 & 0 \\ h_1 & h_0 & \dots & \vdots & \vdots \\ h_2 & h_1 & \dots & 0 & 0 \\ \vdots & h_2 & \dots & h_0 & 0 \\ h_{L-2} & \vdots & \dots & h_1 & h_0 \\ h_{L-1} & h_{L-2} & \vdots & \vdots & h_1 \\ 0 & h_{L-1} & \dots & h_{L-3} & \vdots \\ 0 & 0 & \dots & h_{L-2} & h_{L-3} \\ \vdots & \vdots & \vdots & h_{L-1} & h_{L-2} \\ 0 & 0 & 0 & \dots & h_{L-1} \end{bmatrix}, \tag{6.3}$$

where h_i are the samples of the channel impulse response with length L. Due to the channel influence, the received vector $\boldsymbol{y}$ differs from the transmitted vector $\boldsymbol{x}$.

In order to recover the transmitted information, the receiver must reverse the changes inferred by the communication channel by means of an equalizer. Thus, the function of the channel equalizer is to invert the channel matrix $\boldsymbol{H}$, which describes the relationship between channel input and output samples:

$$\boldsymbol{x} = \boldsymbol{H}^{-1}(\boldsymbol{y} - \boldsymbol{w}) \tag{6.4}$$

However, the inversion of convolution matrix $\boldsymbol{H}$ can not performed easily [23]. Moreover, before equalization this matrix must be acquired by the receiver using means of *channel estimation*. Many TD equalizers (see Section 6.6.1) use the least mean squares (LMS)-based algorithm, which iteratively adjusts $\boldsymbol{H}^{-1}$ filter taps to minimize the difference between transmitted and received training samples.

In an multicarrier (MC) communication system, each sample of the information vector modulates a different basis function of the transform $\boldsymbol{\Phi}$:

$$\boldsymbol{x} = \boldsymbol{\Phi}^{-1}\boldsymbol{X} \tag{6.5}$$

Multipath propagation, reflection and noise in the communication channel causes distortion of transmitted samples. A TD signal at the receiving end of the channel can be described as follows:

$$\boldsymbol{y} = \boldsymbol{H}\boldsymbol{\Phi}^{-1}\boldsymbol{X} + \boldsymbol{w}, \tag{6.6}$$

where $\boldsymbol{X}$ is the transform domain input vector i.e. quadrature amplitude modulation (QAM) samples, $\boldsymbol{\Phi}^{-1}$ is the inverse of the unitary transform matrix. The received vector is transformed back into the transform domain, equalized and passed to the QAM detector. Receiver operation can be described as follows:

$$\hat{\boldsymbol{X}} = \boldsymbol{A}^{-1}\boldsymbol{\Phi}\boldsymbol{y}, \tag{6.7}$$

where $\boldsymbol{A}^{-1}$ is the equalizer matrix, which can be obtained by inverting the transform domain channel matrix:

$$\boldsymbol{A} = \boldsymbol{\Phi}\boldsymbol{H}\boldsymbol{\Phi}^{-1} \tag{6.8}$$

6.4 Disturbances caused by the communication channel

6.4.1 Introduction

Due to various effects in the communication channel as well as in the transmit (see Section 2.5) and receive filters, there is mutual interference between the transmitted *transform domain* samples. In MC communication systems, this interference is divided into two types:

- Disturbance from neighboring symbols of the same subcarrier - inter-symbol interference (ISI);

- Disturbance from neighboring subcarriers within one block - inter-carrier interference (ICI);

In order to provide maximum throughput of the MC communication system, both types of the interference must be eliminated. Inter-carrier interference (ICI) and inter-symbol interference (ISI) cancellation can be provided by means of channel estimation and equalization.

6.4.2 Inter-symbol interference

In order to avoid ISI, the *first Nyquist criterion* [86] must be fulfilled:

$$h^{\mu\mu}(k) = \varphi_t(\mu, k) * h(k) * \varphi_r(\mu, k) \tag{6.9}$$

$$h^{\mu\mu}(k) = \delta(k) \begin{cases} 1 & \text{if } k = 0 \\ 0 & \text{if } k \neq 0 \end{cases} \tag{6.10}$$

where $\varphi_t(\mu, k)$ is the transmitter basis function (BF) at the subcarrier $n = \mu$ and $h(k)$ is the channel impulse response, and $\varphi_r(\mu, k)$ is the receiver BF at the subcarrier $n = \mu$. If this condition is fulfilled, there is no interference between subsequent *transform domain* samples on a certain subcarrier.

ISI is strongly related to the IBI, since the interfering symbols are located in the neighboring blocks, which, for example, in case of filter bank multicarrier (FBMC) [87] significantly overlap with each other.

6.4.3 Inter-carrier interference

ICI shows the amount of interference between the subcarriers within a block:

$$h^{\mu\eta}(k) = \varphi_t(\mu, k) * h(k) * \varphi_r(\eta, k) \tag{6.11}$$

$$h^{\mu\eta}(k) = 0 \quad \forall k \tag{6.12}$$

where $\varphi_t(\mu, k)$ is the transmitter BF at the subcarrier $n = \mu$ and $\varphi_r(\eta, k)$ is the receiver BF at the subcarrier $n = \eta$. If this condition is fulfilled, there is no interference between *transform domain* samples belonging to the same block.

6.4.4 Double orthogonality condition

If zero interference conditions (6.10) **and** (6.12) **hold, it is said that the *double orthogonality condition* is fulfilled.** In this case the transform domain channel matrix $\boldsymbol{A}$ in Equation (6.8) becomes diagonal.

6.5 Channel estimation

In order to provide equalization, information about the communication channel characteristics, i.e. channel state information (CSI) is necessary. If characteristics of the communication channel do not vary, one can measure it beforehand and then assume that CSI is known. Otherwise, dynamic measurement of CSI, i.e. channel estimation is necessary.

Channel estimation can be performed by analyzing the properties of the received signal. In this case it is said that *blind* channel estimation and equalization is performed. On the other hand, the method of channel estimation using special training (pilot) signals is widely used. In this case it is said that pilot signal assisted modulation (PSAM) is used and channel is estimated by comparing received training sequences with transmitted ones.

6.5.1 Time domain channel estimation

There is a big variety of TD channel estimation methods. TD channel estimation and equalization methods are being developed since 1860 [88]. Since in GUR-based PMC system signal processing at the receiver side starts in TD, most of TD channel estimation and equalization methods are suitable to GUR-based PMC systems. On other hand, it must be noticed, since TD is a specific case of the more general GD, therefore, all GD channel estimation methods must work in the TD too.

6.5.1.1 Trivial methods for TD channel estimation

Both methods, mentioned below, are strictly theoretical and requires transmission of many zeros. Noise immunity of such estimators are very low.

6.5.1.1.1 Delta function method

Method is based on the transmission of a discrete analogue of Dirac delta function - one non-zero sample followed by many zeroes. At the receiving side channel impulse response $h(k)$ can be obtained directly.

6.5.1.1.2 Identity matrix method

In this method channel estimate can be obtained by transmitting an identity matrix (3.1)-based training sequence. In this case, the TD channel matrix estimate $\hat{\boldsymbol{H}}$ appears at the output of the serial to parallel (S/P) converter of the receiver each time when the training sequence is transmitted.

6.5.1.2 Back-substitution method

The rhombus-like structure of the *convolution matrix* (6.3) allows to use *back-substitution* in order to provide channel estimation. It is similar to solving the system of linear equations using the Gauss-Seidel method (method of successive displacement) [89].

Rewriting (6.2) into the following form:

$$\begin{cases} y_0 = h_0 x_0 + w_0 \\ y_1 = h_1 x_0 + h_0 x_1 + w_1 \\ \dots \\ y_{N-1} = h_{N-1} x_0 + ... + h_0 x_{N-1} + w_{N-1} \end{cases} \tag{6.13}$$

allows to obtain the coefficients of the channel impulse response $\boldsymbol{h}$ in an iterative way:

$$\begin{cases} h_0 = \frac{y_0 - w_0}{x_0} \\ h_1 = \frac{y_1 - h_0 x_1 - w_1}{x_0} \\ \dots \\ h_{N-1} = \frac{y_{N-1} - h_0 x_{N-1} ... - w_{N-1}}{x_0} \end{cases} \tag{6.14}$$

The drawback of the given method is that it accumulates the error, caused by the unknown noise component w, which is present in the received vector $\boldsymbol{y}$. Therefore, the last samples of the channel impulse response $\boldsymbol{h}$, which are obtained in the last iterations, are most imprecise.

6.5.1.3 LMS system identification method

The channel impulse response can be obtained by means of adaptive LMS filter [90] (see additional details in Section 6.6.1.1) in system identification mode. Unlike equalization mode, the filter takes the actual receiver input as a target, whereas training blocks are treated as (non-equalized) input. In other words, system identification mode can be obtained by just swapping inputs of LMS filter in equalization mode. Then the TD channel matrix $\hat{\boldsymbol{H}}$ can be constructed like in the previous method.

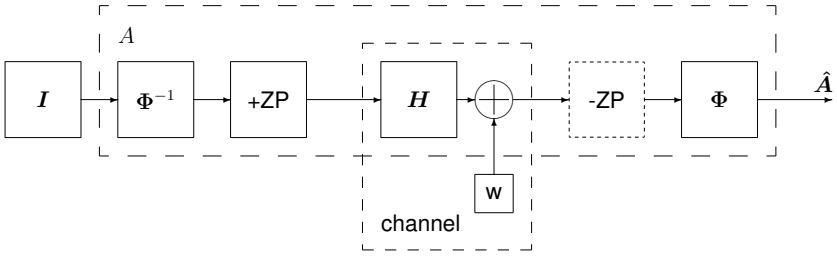

Figure 6.1: GD channel estimation based on the Identity matrix

LMS system identification can provide means for very accurate channel estimation. The unique word (UW) (see Section 2.3.4.3) padding for blocks of useful samples, which is used for timing offset estimation (see Section 4.3.2) and for carrier frequency offset (CFO) estimation (see Section 5.4), can be reused for channel estimation using LMS. One of the most suitable for channel estimation UW sequences are Zadoff-Chu (ZC) sequences (see Section 2.4.3.1), since they have a constant magnitude and a non-periodic waveform.

6.5.2 GUR domain channel estimation

GUR can produce a wide variety of transforms, including well-known ones, such as Fourier transform (see Section 3.2.2) and Identity transform (see Section 3.2.1). Moreover, a variety of transforms with specific features can be created (see classification in Section 3.2.4.2). *In GUR-based PMC system (see Section 3.5.1) flexible GD channel estimation method, which is usable in all these domains, is required.*

6.5.2.1 Identity matrix method for GD channel estimation

A simple GD channel estimation method has been reported in [16]. However, a lot of the work has to be done in this area, since the efficiency of the proposed method is low.

A GUR domain channel estimate can be obtained by transmitting an identity matrix (3.1)-based training sequence. In this case, processing at the receiver end is very simple (see Figure 6.1), since GD channel matrix estimate $\hat{\boldsymbol{A}}$ appears at the output of the GUR transform block of the receiver each time when the training sequence is transmitted. However, this kind of channel estimation is far from the optimal one, since training sequance is long and has many zeroes and, therefore, it is susceptible to the noise. Moreover, this training sequence is difficult to use for other purposes such as timing (see Chapter 4) and frequency (see Chapter 5) synchronization.

6.5.2.2 GD channel estimation using conversion from the TD

Another way, how to obtain the GD channel estimate $\hat{\boldsymbol{A}}$, is to calculate it from the TD channel estimate (see Section 6.5.1) using (6.8). In this case all classical TD channel estimation

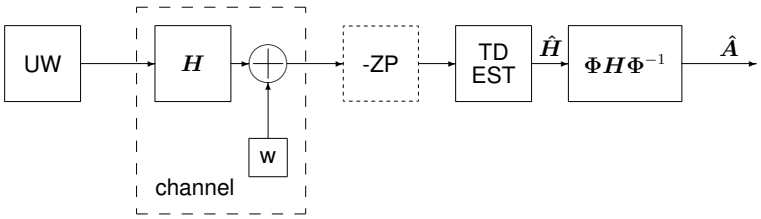

Figure 6.2: GD channel estimation using conversion from the TD

methods are applicable and it is possible to use much shorter training sequences. However, the computational complexity of the receiver increases, since additionally (6.8) must be calculated. The baseband PMC system diagram exploiting this approach is depicted in Figure 6.2.

6.5.3 Frequency domain channel estimation

Frequency domain (FD) channel estimation is widely used in orthogonal frequency division multiplexing (OFDM) communication systems due to low computational complexity and high accuracy in case of slowly-changing time-dispersive communication channel. A necessary condition for FD equalization is fulfillment of the *double orthogonality condition* (see section 6.4.4).

FD channel estimation is based on transmission of training subcarriers called *pilot tones*. There are several ways how to insert pilot symbols (tones):

- Pilot symbols can be inserted into particular subcarriers of all OFDM blocks. In this case the receiver obtains continuous estimates on some subcarriers. Interpolation on the frequency axis is necessary.

- Selected OFDM blocks (pilot blocks) with all their subcarriers occupied by pilot signals are used. After the attainment of the frame synchronization (see Section 4.4), the OFDM receiver periodically obtains a full channel estimate. Interpolation on the time axis is necessary.

- Pilot symbols can be scattered, i.e., appear in particular subcarriers of particular blocks, according to a specified law. In such a case, the unit for the estimation of the channel parameters needs to perform two-dimensional interpolation with respect to the frequency and time simultaneously. Such an approach based on the use of finite impulse response Wiener filters is discussed in article [67].

A discrete signal transmitted with the aid of N subcarriers is described by Equation (2.1). The *frequency response* of the channel, which is equal to the discrete Fourier transform (DFT) of the discrete channel impulse response $h(k)$, is represented as:

$$\boldsymbol{\Lambda} = \boldsymbol{F}\boldsymbol{h} \tag{6.15}$$

If received TD samples $\boldsymbol{y}$ are *circular convolution* between the transmitted TD samples $\boldsymbol{x}$ and channel impulse response $\boldsymbol{h}$, then received FD samples are obtained by *element-wise multiplication* between transmitted FD samples $\boldsymbol{X}$ and channel frequency response $\boldsymbol{\Lambda}$ i.e.:

$$\text{if} \quad \boldsymbol{y} = \boldsymbol{x} \circledast \boldsymbol{h} \quad \text{then} \quad \boldsymbol{Y} = \boldsymbol{X}\,\mathrm{diag}(\boldsymbol{\Lambda}), \tag{6.16}$$

The circular convolution can be obtained by use of the cyclic prefix (CP) (see Section 2.3.4.1) or repeating UW (see Section 2.3.4.3). Moreover UW prefix can replace pilot tones for the FD channel estimation [28], [91]. However, in this case the largest challenge is requirement that UW must be generated and added in the FD. In paper [92] it is proposed to use both UW prefix and suffix to improve channel estimation even more.

Let's mark known pilot subcarriers sent by the transmitter as $X_p(n)$ and received pilot subcarriers as $Y_p(n)$. The simplest method how to obtain channel estimates, is to use the *zero forcing algorithm* [93]. In this case an FD channel estimate can be found using the expression:

$$\hat{\Lambda}(n) = \frac{Y_p(n)}{X_p(n)} \tag{6.17}$$

Formula (6.17) shows that all complex channel gains $\hat{\Lambda}(n)$ can be obtained by element-wise division of the received pilot samples, which are obtained from pilot symbols by means of DFT, by the sent ones. The largest drawback of the zero-forcing algorithm is the amplification of noise on the subcarriers, where the magnitude of the channel frequency response is small (spectral nulls).

Different strategies can be employed to minimize the error in the estimation of the channel parameters. An algorithm for finding the optimum estimate in terms of the minimum mean squared error (MMSE), i.e., for the minimization of $E \parallel \hat{\boldsymbol{\Lambda}} - \boldsymbol{\Lambda} \parallel^2$, is given in article [94]. The described method also uses singular value decomposition (SVD), along with the theory of optimal rank reduction. The method in question is of purely theoretical significance, since its practical implementation is extremely complicated. Simplified (and more suitable for practical implementation) approaches based on the method described above are given in study [95].

It is significant that the number of pilot subcarriers is to be chosen in accordance with the widely known Nyquist criterion, which asserts that the interval between the samples of a signal is to be smaller than the reciprocal width of the signals duplex frequency band. Thus, when computing the timing interval between pilot symbols, one needs to allow for the scattering of the Doppler frequency shift B_d so that $T_t < 1/B_d$. On the other hand, when computing the frequency interval between pilot subcarriers, it is necessary to take into account the scattering

of the signal delay B_τ so that $T_f < 1/B_\tau$. As one example, in wireless networks [68], pilot signals are transmitted continuously on four of 52 subcarriers at 4.375 MHz intervals. For the given scheme of pilot signals, the maximum admissible scattering of the signal delay is 228 ns, while the scattering of the Doppler effect is unlimited.

Paper [96] is dedicated to a comparative mathematical analysis of diverse schemes for the allocation of pilot signals. For a communication system with the impulse response of length L and the number of subcarriers N, the following implications hold:

- In the absence of noise, any L of N pilot signals would suffice to restore the channel parameters completely.

- If the channel parameters are time independent, then the scheme with periodic pilot blocks and the scheme with continuous pilot subcarriers are equivalent.

- In a channel with time variant parameters, the scheme with continuous pilot subcarriers is superior to the scheme with periodic pilot blocks.

Unfortunately FD channel estimation can not be used in PMC systems, which employ basic (see table 3.1) GUR transforms, because convolution in the communication channel and filters causes ICI, which forbids use of aforementioned algorithm. However, in the future (see Chapter 8) it is planned to develop such parametric unitary transforms, which do not cause transform domain ICI. In this case FD channel estimation and frequency domain equalizer (FDE) methods will be usable in these communication systems.

6.6 Channel equalization

6.6.1 Time domain equalization

TD equalization is usually based on the classic adaptive algorithms, such as LMS and recursive least squares (RLS). These algorithms iteratively adjust the coefficients of the finite impulse response (FIR) filter in order to minimize the difference between the desired signal and the filter output. In the following sections only a brief introduction will be given. More details about these algorithms can be found in the book [90], written by one of the inventors of the LMS algorithm. TD equalization can be used with both inserted and super-imposed (see Section 2.4.2) training signals. As it was mentioned before, TD equalization can be successfully used within parametric GUR-based PMC systems.

6.6.1.1 LMS algorithm

One of the most popular TD equalization methods is LMS. It is based on the stochastic gradient descent method, which minimizes the objective function, which is the sum of functions related to different observations Q_i:

$$Q(w) = \sum_{i=1}^{n} Q_i(w) \tag{6.18}$$

Besides direct TD equalization the LMS filter can be used in system identification mode (more details see in Section 6.5.1.3).

6.6.1.2 RLS algorithm

The RLS algorithm provides an advanced method for finding the coefficients of an unknown FIR filter. In contrast to the LMS method (see Section 6.6.1.1), it tries to minimize a weighted linear least squares cost function relating to the input signal.

6.6.1.3 Equalization using super-imposed training signals

In accordance with the review paper [97] devoted to the PSAM, periodic super-imposed (SI) TD training signals (see Section 2.4.2.2) can lead to TD channel estimation solutions based on LMS (see Section 6.6.1.1) or RLS (see Section 6.6.1.2) with a relatively low complexity. Moreover, in accordance with the same paper, SI training allows to track variations of the communication channel faster. In paper [48] the authors describe an OFDM communication system which uses periodic super-imposed training.

6.6.2 Frequency domain equalization

During the last two decades a modulation technique known as OFDM has become popular due to its high spectral efficiency and ease of equalization. In OFDM it is assumed that the original transmit block (vector) $\boldsymbol{X}$ is located in the FD and represents complex amplitudes of N sinusoidal subcarriers. Before transmission over the communication channel, samples from the QAM mapper are transformed into the TD by means of inverse discrete Fourier transform (IDFT). Thus the transform $\boldsymbol{\Phi}$ in Equation (6.6) becomes the Fourier transform $\boldsymbol{F}$, based on complex exponents.

It is interesting, that if the TD channel matrix $\boldsymbol{H}$ is a *circulant* matrix [23], then the transform domain channel matrix $\boldsymbol{A}$ is *diagonal*, because from (6.8) follows the *eigendecomposition* of the matrix $\boldsymbol{H}$:

$$\boldsymbol{A} = \boldsymbol{F}\boldsymbol{H}\boldsymbol{F}^{-1} \tag{6.19}$$

In turn, the matrix $\boldsymbol{H}$ becomes circulant, if blocks with a CP (see Section 2.3.4.1) are used. Therefore, the combination of CP and DFT enables a simultaneous fulfillment of the conditions (6.10) and (6.12).

Due to the absence of ICI (see Section 6.4.3) between OFDM subcarriers, their frequency responses can be considered flat. This significantly simplifies the estimation and correction of the channel parameters, because the problem concerning the estimation of the channel parameters is reduced to finding the complex scalar attenuations of the subcarriers.

Although channel estimation can be performed using any method described in Section 6.5, in most of the cases FD equalization is used in conjunction with FD estimation (see Section 6.5.3). In this case, if we have estimated channel gains $\hat{\Lambda}(n)$ for all n, they can be applied directly to the received samples. The sent samples $\boldsymbol{X}$ can be restored using the formula:

$$X(n) = \frac{Y(n)}{\hat{\Lambda}(n)} = \frac{\hat{\Lambda}(n)^*}{|\hat{\Lambda}(n)|^2} Y(n), \tag{6.20}$$

where $\hat{\boldsymbol{\Lambda}}$ is the estimated frequency response and $\boldsymbol{Y}$ is the received FD sample block.

Unfortunately FDE technique can not compatible with PMC systems, who employ ordinary (see table 3.1) GUR transforms. However, as it was already mentioned in Section 6.5.3, if PMC system, where transform domain ICI is eliminated, will be developed, it will be possible to use FDE.

6.6.3 GUR domain equalization

Performance of modern transform domain equalizers, such as FDE, allows to achieve better performance and reduced computational complexity compared to TD equalizers. In OFDM the FD channel matrix $\boldsymbol{A}$ is diagonal, and its inversion is straightforward (see Section 6.6.2 about FD equalization). Therefore, in OFDM the orthogonality conditions of zero ISI (6.10) and zero ICI (6.12) in case of a linear communication channel with convolution are automatically fulfilled.

It is possible to build an MC communication system, where non-sinusoidal subcarriers are used [8], [12]. In this case Equations (6.4)-(6.8) are still valid. The main problem, though, is that the matrix $\boldsymbol{A}$ most likely is *non diagonal* anymore (it is diagonal if subcarriers are channel eigenfunctions) and double orthogonality condition (see Section 6.4.3) is not fulfilled. The inversion of non-diagonal GD channel matrix $\boldsymbol{A}$ requires an additional effort. The problem of GD equalization is explained in Figure 6.3.

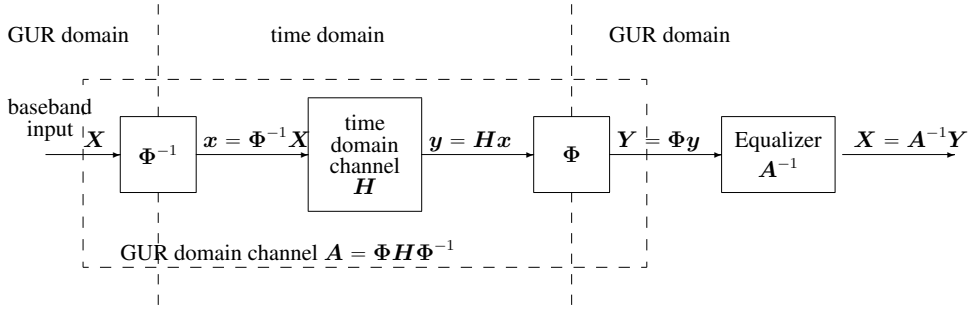

Figure 6.3: GD channel equalization problem

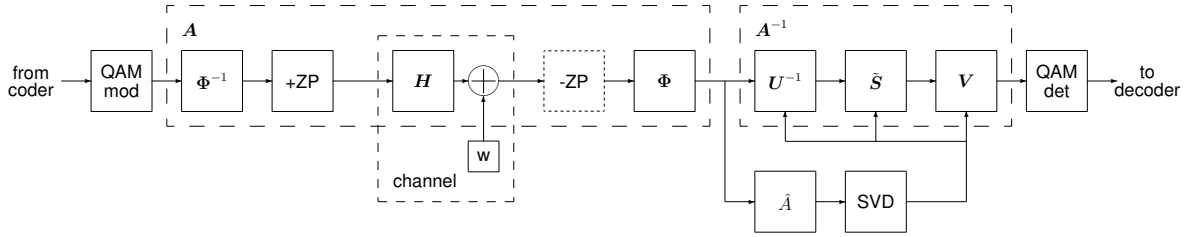

Figure 6.4: Communication system baseband with SVD equalization and transform domain channel estimation

6.6.3.1 SVD-based equalization

As it was mentioned before in this section, the purpose of the equalizer is the inversion of transform domain channel matrix $\boldsymbol{A}$. One of the great methods to perform matrix inversion is SVD [98]. SVD decomposes a given rectangular matrix into two unitary square matrices $\boldsymbol{U}$and $\boldsymbol{V}$, which share common eigenvalues, and a diagonal matrix $\boldsymbol{S}$ with singular values sorted in descending order:

$$\boldsymbol{A} = \boldsymbol{U}\boldsymbol{S}\boldsymbol{V}^{-1} \tag{6.21}$$

The pseudo-inverse of this non-square matrix:

$$\boldsymbol{A}^{-1} = \boldsymbol{V}\tilde{\boldsymbol{S}}\boldsymbol{U}^{-1} \tag{6.22}$$

now can be found easily, since for unitary matrices $\boldsymbol{V}^{-1} = \boldsymbol{V}^*$ and $\boldsymbol{U}^{-1} = \boldsymbol{U}^*$ i.e. matrix inverse is obtained using conjugate transpose. The elements of the diagonal rectangular matrix $\tilde{\boldsymbol{S}}$, which is the pseudo-inverse of (non square) $\boldsymbol{S}$, can be found using the relation:

$$\tilde{\boldsymbol{S}}_{k,k} = \frac{1}{S_{k,k}} \quad k \in 0, N \tag{6.23}$$

Examples of PMC system basebands with transform domain channel estimation (Section 6.5.2) and TD channel estimation (Section 6.5.1) are shown in Figures 6.4 and 6.5, respectively.

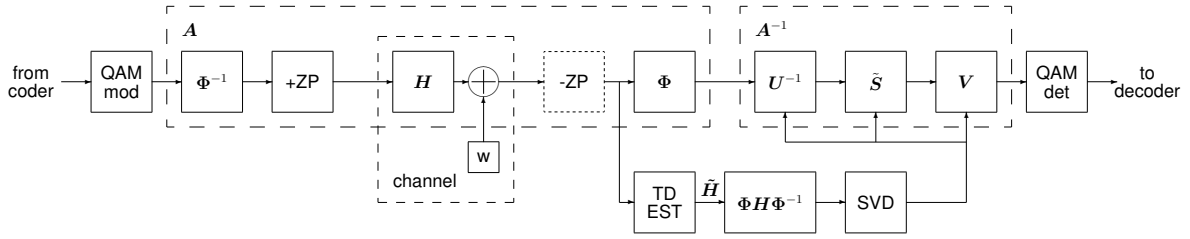

Figure 6.5: PMC system baseband with SVD equalization and TD channel estimation

Estimation method	**Complexity, flops**
Unity (Section 6.5.2.1)	0
Delta function, mean (M blocks)	$M(N+1)$
LMS (K updates) + mean (M blocks)	$N(K+M)+M$

Table 6.1: Computational complexity of the channel estimation

SVD-based equalization is a known method, described, for example, in [94], [99], [100]. However, due to large computational complexity it is not popular. Still, SVD is a perfect choice for the PMC systems, because this equalization will continue to work after the change of unitary transformation.

Computational complexity of the researched channel estimation methods is given in Table 6.1. The total computational complexity of Jacobi SVD for a square matrix with N rows, in accordance with [101], is $3N^3$. The transform $\mathbf{\Phi}$ generally requires $2N^2$operations and equalization (6.22) requires $4N^2+N$ flops. Therefore, the total complexity of SVD-based equalizer, LMS-based TD estimator with converter to GD having M training blocks and K LMS updates per block would achieve$3N^3+6N^2+N(1+K+M)+M$. The most computationally expensive operation is SVD.

6.7 Simulation results of equalization

Here is given some simulation results from [16]. A baseband PMC system with perfect timing and frequency synchronization was built for the simulations. Complex constant rotation angle OT (CCRAOT) (see Section 3.2.4.2.1) with $\phi=\frac{\pi}{6}$, $\psi=0$, $\gamma=\frac{\pi}{2}$ in (6.5) was used in the role of GUR transform $\mathbf{\Phi}$. Transmission was carried out in frames consisting of 64 training blocks and 20 payload blocks. Zero padding (ZP) blocks consisting of 64 payload samples and 16 padding samples were used in all simulations. Adaptive LMS filters for both equalization and system identification (estimation) were 8 taps long. Seven different communication systems were simulated and compared. The simulation results in the form of bit error ratio (BER) plots

of PMC systems are depicted in Figure 6.6.

The first PMC system (Figure 6.6, **graph A**) utilized GD channel estimation and GD equalization. Channel estimation was performed using an Identity matrix-based training signal structure (see Section 6.5.2.1). This setup requires the smallest amount of computational resources.

In the second experiment (Figure 6.6, **graph B**) estimation was moved into the TD, but the estimation algorithm was leaved unchanged. From the BER graphs in Figure 6.6 it is visible that the change of estimation domain almost does not affect PMC system performance.

The third PMC system (Figure 6.6, **graph C**) exploited a different channel estimation algorithm. Unlike previous ones, it did not sample the channel matrix directly, but used an averaged TD impulse response for the construction of this matrix. A 2dB improvement over the previous experiments is achieved due to noise suppression in impulse response averaging process.

The fourth model (Figure 6.6, **graph D**) employed even more advanced channel estimation process based on LMS system identification. This model gives very serious improvement of PMC system performance. This PMC system achieves BER 10^{-2} at signal to noise ratio 7dB.

In order to identify the impact of the channel estimation on the performance of communication system, the fifth model (Figure 6.6, **graph E**) was created. In this model the channel impulse response and, hence, the channel matrices (6.3) and (6.8) were perfectly known to the receiver.

A Simulation result of PMC system with the well-known TD equalization using LMS algorithm is shown in Figure 6.6, **graph F**. This simulation was done in order to compare the performance of SVD with popular equalization algorithm. We can see that TD LMS estimation with GD equalization using SVD works better than pure TD LMS equalization.

And finally, in Figure 6.6, **graph G** simulation result of pure OFDM system with FDE, having the same number (64) of training blocks and same number of subcarriers, is shown.**We can observe, that performance of FDE is slightly worse than performance of SVD-based equalizer**.

6.8 Comparison of channel estimation and equalization methods

The goal of this section is to describe the results of an experiment [15], where different combinations of unitary transforms and equalizers were tried. The objective of those simulations was to examine the following questions:

- Impact of the choice of unitary transform on BER of MC system;
- Impact of transform on the efficiency of equalization;
- Impact of equalization method on BER of MC system;

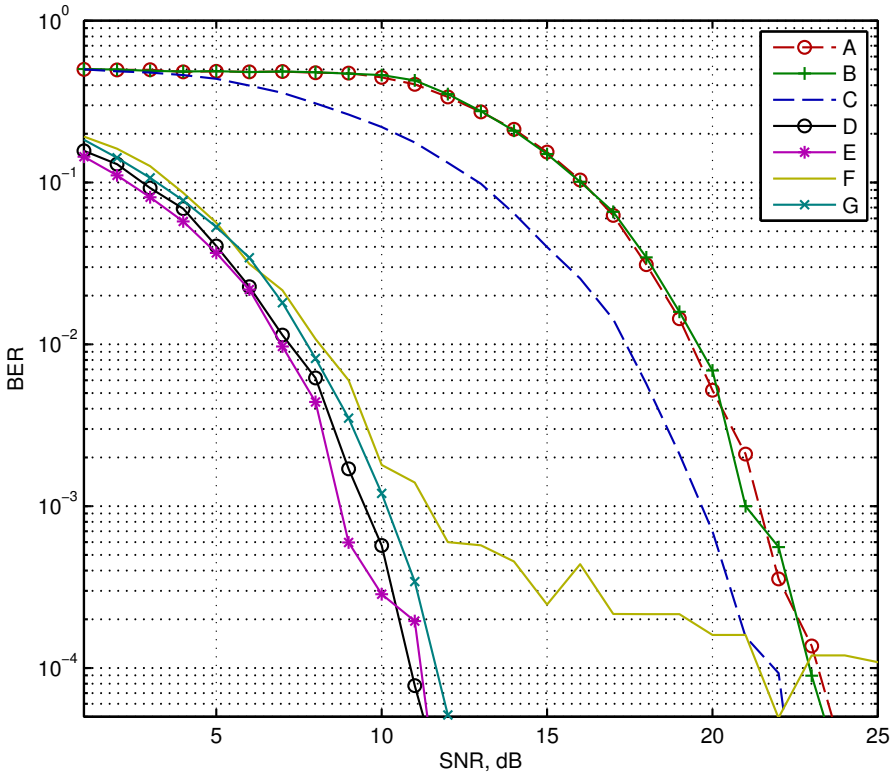

Figure 6.6: Performance comparison of various estimators and equalizers. See the explanation of the plot in the text of Section 6.7

.

- Compatibility between unitary transforms and equalization methods;
- Impact of peak-to-average power ratio (PAPR) of the transmitted signal on BER of communication system having a nonlinear channel.

The results of these simulations allow better understand the impact and importance of the orthogonal transformations in MC systems and outline interesting topics in the MC system design. Communication systems with four different orthogonal transformations have been modeled:

- Identity transform (see Section 3.2.1);
- Discrete Fourier transform (see Section 3.2.2);
- Complex Hadamard transform (see Section 3.2.3);
- CCRAOT 30° transform (see Section 3.2.4.2.1).

If the communication channel is frequency-selective, i.e. time-dispersive, an equalizer is required in order to achieve a viable BER. Theoretically, each transform requires its own transformdomain equalization method. In identity transform (see Section 3.2.1)-based communication systems, i.e. pure QAM, an adaptive LMS algorithm-based TD equalizer is usually utilized. This equalizer performs deconvolution between the estimated channel impulse response and the transmitted samples. In the case of DFT-based OFDM, equalization is usually based on the

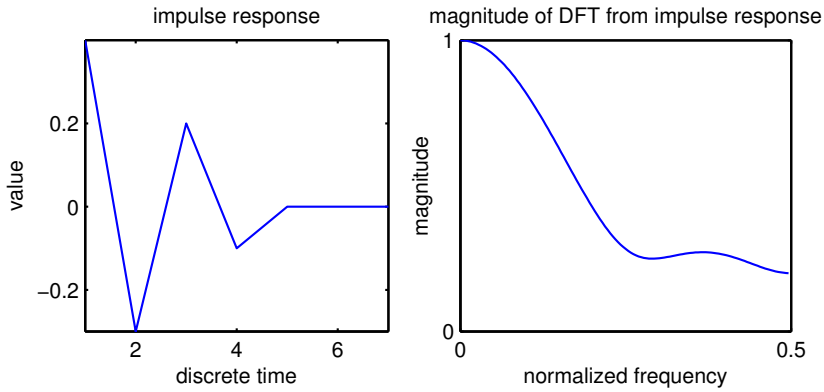

Figure 6.7: Characteristics of time-dispersive channel used in simulations

relatively simple FD channel estimation and equalization (see Section 6.6.2).

One of the major disadvantages of DFT-based OFDM modulation scheme is a large PAPR (see Section 3.4), since a TD signal is a sum of sinusoids with different frequencies. The impact of nonlinear channel on the mentioned transforms was examined.

6.8.1 Simulation of different equalizers

MC communication system models were built using the Mathworks Simulink environment. Synchronization mechanisms in the models were simplified to minimize the impact of the synchronization issues on the performance of the models. The transmitter and receiver clocks were the same and both units were launched simultaneously. Therefore, frequency, block timing and frame synchronization were ideal. Impulse response and frequency response of the baseband communication channel, used un the simulations, are shown in Figure 6.7

An MC TD signal consisted of frames (see Section 2.3.3). Each frame consisted of four training blocks at the beginning of the frame and 20 payload blocks. Each block (including training blocks) consisted of 64 4QAM samples, which yields 64 subcarriers in the FD, and 16 CP samples.

To measure the impact of various communication channel impairments, each transform was tested with four different channels:

- Additive white Gaussian noise (AWGN) channel;
- Channel with clipping at 0.5 of the peak magnitude and AWGN;
- Frequency selective channel with AWGN. Impulse and frequency responses of this channel are given in Figure 6.7.

In all experiments the variance of the additive noise to achieve required signal-to-noise ratio (SNR) of the received signal was adjusted.

The simulation results for AWGN, frequency-selective and nonlinear channels are depicted

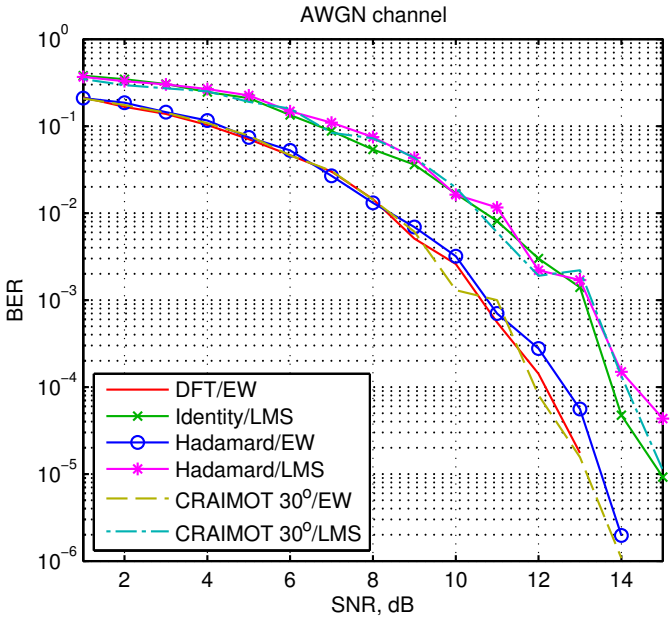

Figure 6.8: MC system performance in the AWGN channel

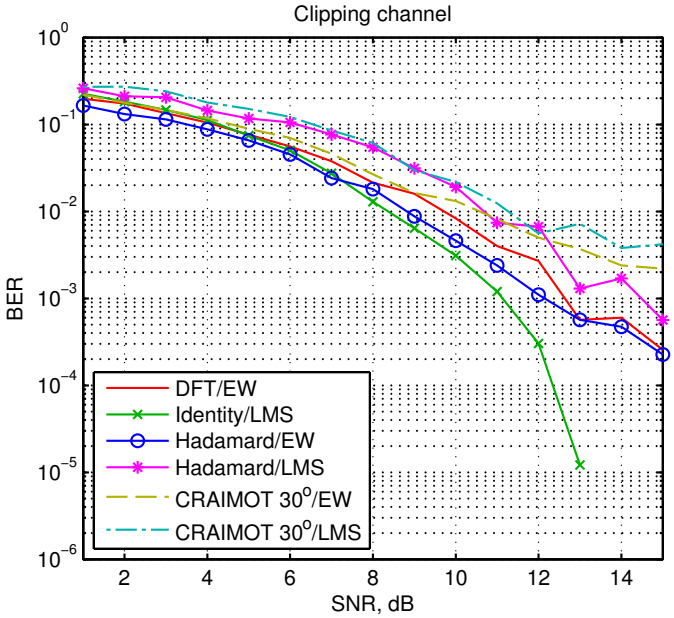

Figure 6.9: MC system performance in the clipping channel

respectively in Figure 6.8, Figure 6.9 and Figure 6.10. In the legend, "LMS" means the use of LMS equalizer (see Section 6.6.1.1), whereas "EW" stands for "element-wise division", i.e. the algorithm used in FDE (see Section 6.6.2). In other words, two different approaches - deconvolution and multiplication have been tested.

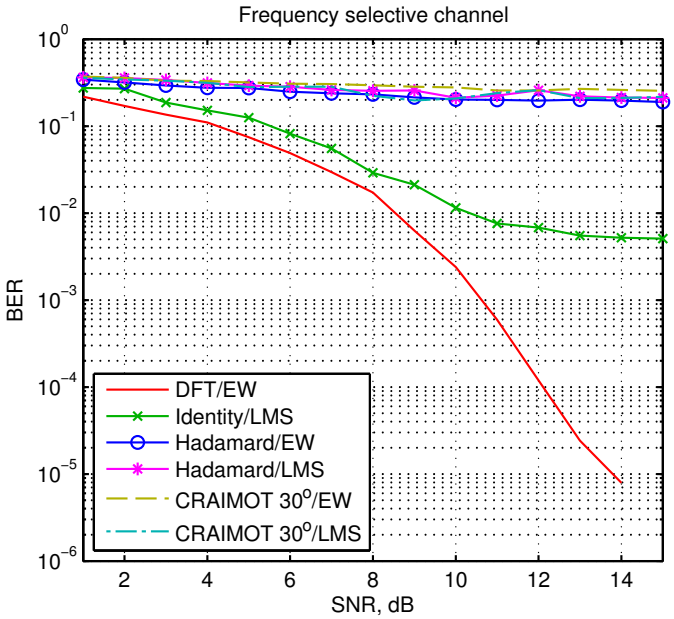

Figure 6.10: MC system performance in the frequency selective channel

6.9 Conclusions

- In a PMC system with an AWGN channel the performance of all transforms is the same.
- LMS is applicable to TD equalization only.
- FD channel estimation and equalization techniques are not applicable to CCRAOT domain.
- SVD provides a precise method for GD equalization.
- SVD-based equalizer can be used in PMC systems with a variable transform.
- Highest PMC system performance can be achieved using an LMS-based TD channel estimator in conjunction with an SVD-based GD equalizer.

6.10 Summary of the contributions

The following contributions related to channel estimation and equalization have been done in this thesis:

- Simple GD channel estimation method based on the identity matrix is proposed (Section 6.5.2).
- GD channel estimation method based on the conversion from TD is proposed (Section 6.5.2.2).
- TD channel estimation method based on the system identification has been evaluated

(Section 6.5.1.3).

- SVD-based GD equalization method has been proposed (Section 6.6.3.1).
- Applicability of two equalization methods to the communication systems with four different transforms has been explored (Section 6.8).

7 Design of parametric multicarrier modulation system

7.1 Formulation of the problem

7.1.1 Objective

The purpose of the given chapter is to prove the viability of the proposed synchronization and equalization methods and verify their mutual consistency.

7.1.2 Tasks

In order to meet the objective the following tasks have to be fulfilled:

- Proposal of a design for the Generalized Unitary Rotation (GUR)-based parametric multicarrier (PMC) system transmitter;
- Proposal of a design for the GUR-based PMC system receiver;
- Measurement of the performance of the developed PMC system model.

7.2 Introduction

This chapter describes a complete example of one particular GUR-based PMC system baseband, using a selection of the previously described methods. Although proven methods are selected to obtain maximum performance (in terms of bit error ratio (BER)) of the PMC system, the proposed design can be considered as initial implementation. All elements of the PMC system are based on the solutions presented in the previous chapters.

7.3 Structure of the parametric multicarrier modulation system

The physical layer of a PMC system is described in detail in Section 2.2. The particular PMC system described in this chapter follows the structure depicted in Figure 2.1. However, this PMC system does not include an radio frequency (RF) parts and channel encoder/decoder. The structure of the described *baseband* PMC system is depicted in Figure 7.1. A baseband signal from the transmitter baseband propagates via the baseband equivalent of RF communication channel and after that enters the baseband of the communication system receiver. Detailed information on parameters of modeled PMC system is given in Appendix 8.

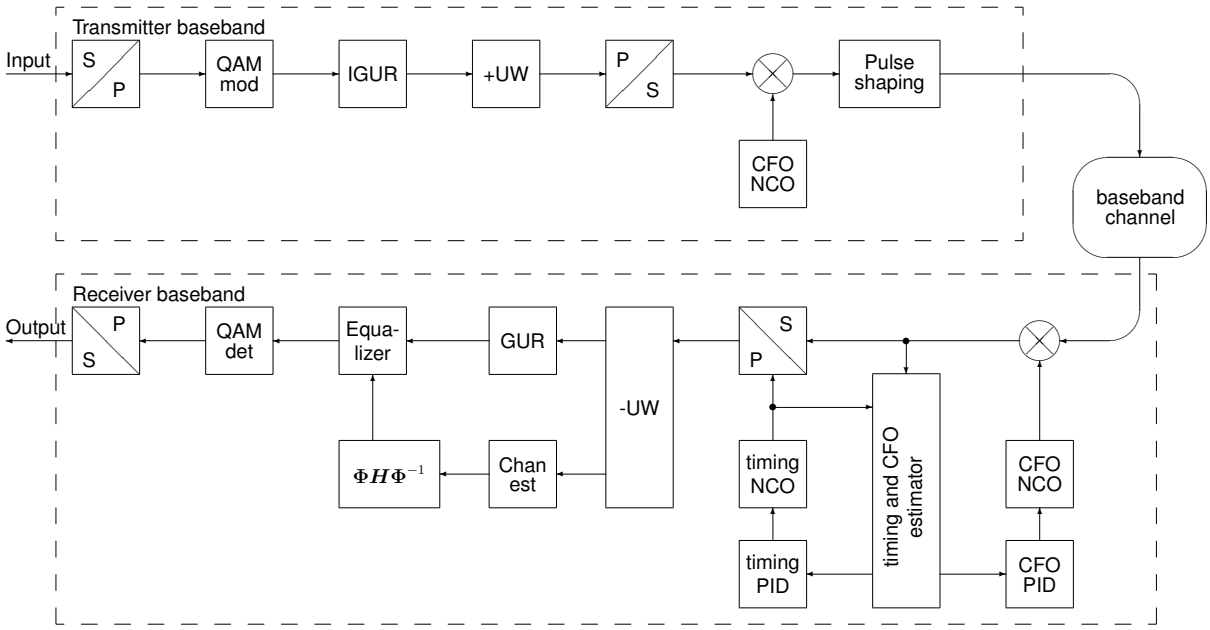

Figure 7.1: Block diagram of the modeled PMC system

7.3.1 Transmitter

The detailed transmitter operation is described in Section 2.2.2. The most important operation within the transmitter is GUR-based multicarrier (MC) modulator (see details in Section 3.2). This initial implementation contains the most basic structure of the unitary transform unit – matrix-type transform unit (see Section 3.3.1). The test configuration is based on a 64-dimensional complex constant rotation angle OT (CCRAOT) (see Section 3.2.4.2), which is the most basic type of GUR.

For timing and frequency synchronization as well as for channel estimation the unique word (UW) padding (see Section 2.3.4.3) is used. Zadoff-Chu (ZC) sequences (see Section 2.4.3.1) are selected as the most appropriate type of UW sequences in terms of correlation and envelope properties.

Taking into account considerations about transformation and the necessity for channel estimation and synchronization, a simplified frameless structure for a PMC system, shown in Figure 7.2, has been used. The overhead, consumed by the training and synchronization, is reduced by the use of the same sequences for both tasks simultaneously.

For investigation of the impact of carrier frequency offset (CFO), an appropriate local oscillator (unit 'CFO NCO') is added to the transmitter .

Before output to the communication channel, 4x upsampling and pulse shaping (see Section 2.5), based on classic root-raised-cosine (RRC) finite impulse response (FIR) filter with 65

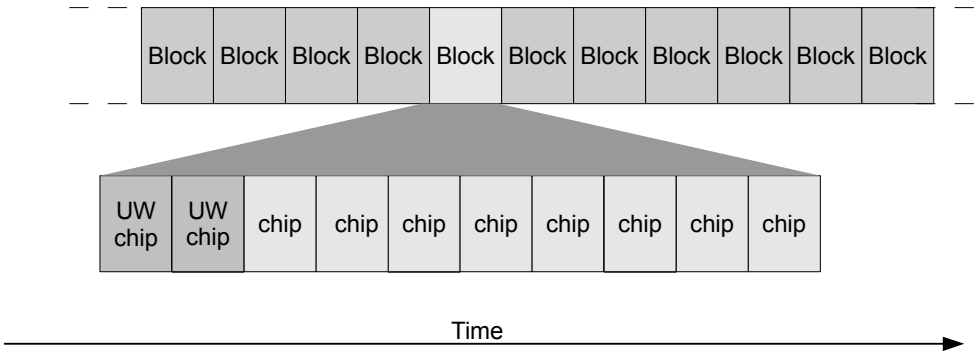

Figure 7.2: Proposed structure of a TD signal

coefficients, is performed.

7.3.2 Receiver

The receiver of the modeled PMC system incorporates a timing synchronization circuitry (see Chapter 4), frequency synchronization units (see Chapter 5), GUR-based MC demodulator (see Chapter 3) and an equalizer (see Chapter 6). The structure of the proposed receiver corresponds to the general structure proposed in Section 2.2.3.

7.3.2.1 Timing and frequency synchronization

The receiver complexity depends mostly on the complexity of the synchronization circuits. Unitary transformation and channel estimation will work correctly only if timing and frequency synchronization is established.

All timing and frequency offset estimation is performed by processing of the received UW prefixes, generated at the transmitter . A UW prefix is added to each data block and is 16 samples long. Block timing offset (BTO) and CFO estimation is performed by the means of combined estimator, shown in Figure 7.3. It consists of autocorrelation (AC) and cross-correlation (XC) estimators.

Estimator, shown in Figure 7.4 is based on AC. For BTO estimation it uses the algorithm described in Section 4.3.2.1, whereas for CFO estimation the algorithm from Section 5.4.2.1.

The second estimator, shown in Figure 7.5, is based on the XC of the received samples with the UW pattern stored in the receiver. In other words, the second estimator works as *matched filter* . The operation of BTO estimator is described in detail in Section 4.3.2.2, whereas CFO estimation is performed by means of the algorithm described in Section 5.4.3. Besides timing and CFO estimation, the combined XC estimator performs residual phase offset estimation (see Section 5.5).

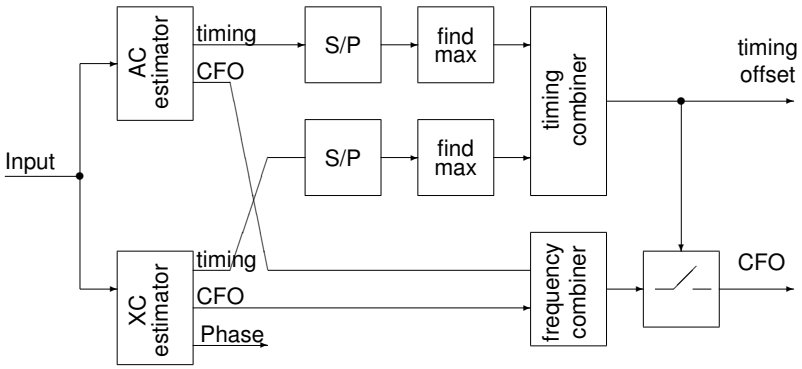

Figure 7.3: Combined BTO and CFO estimator

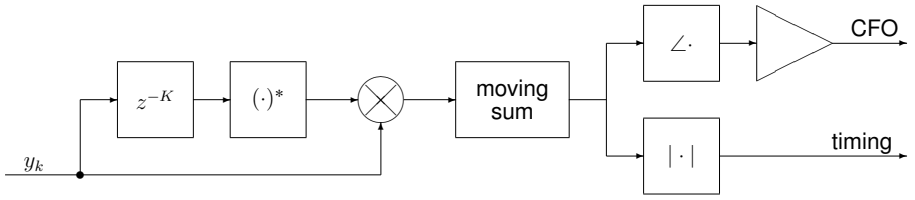

Figure 7.4: Combined AC-based BTO and CFO estimator

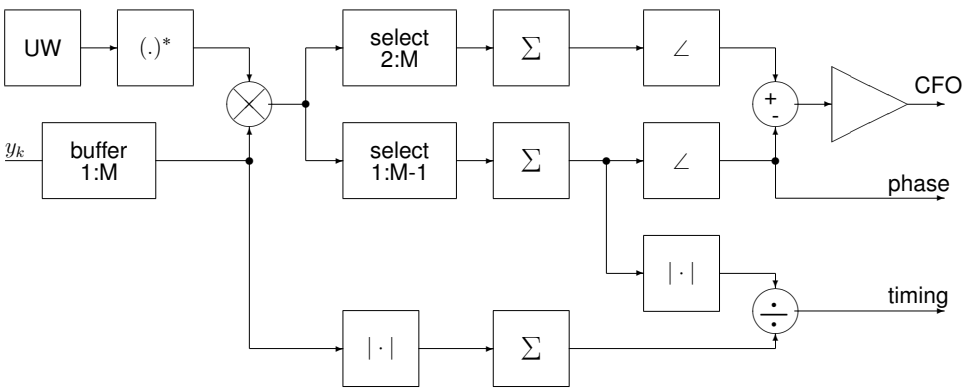

Figure 7.5: Combined XC-based BTO and CFO estimator

The combining of estimator results is performed by the unit shown in Figure 7.3. This unit incorporates both previously mentioned estimators and contains the logic for switching between the estimators. The BTO estimate combiner used here is based on the algorithm described in Section 4.3.3, whereas CFO estimate combiner employs the algorithm described in 5.4.4.

For BTO correction the *feedback* or *closed loop* synchronizer (see Section 4.3.3) is used. The value of the estimated timing offset enters the timing proportional integral derivative (PID) controller (timing PID in Figure 7.1), which is necessary to generate the driving signal for the timing numerically controlled oscillator (NCO) and to stabilize the automatic control loop, responsible for the timing. In this particular implementation of a PMC system, block timing adjustment is done by inserting or deleting samples in the clock signal, which drives the serial to parallel (S/P) converter at the (oversampled) input of the receiver.

CFO is corrected using another feedback type synchronizer. For the CFO compensation, multiplication with a complex exponent signal, having the frequency opposite to CFO, is used (see Section 5.6). For this purpose the estimated values of CFO and phase offset are passed from the combined timing and CFO estimator to the CFO PID controller. This controller generates a signal that drives NCO, responsible for CFO compensation.

7.3.2.2 Channel estimation

In order to provide equalization, the channel must be estimated first. In model of a PMC system a TD estimator, based on least mean squares (LMS) filter in system identification mode is used (see Section 6.5.1.3). In accordance with simulation results, provided in Section 6.7, LMS provides the most accurate estimate of the communication channel. The number of coefficients of the LMS estimator must be larger than the length of channel impulse response (a model uses 8 coefficients).

7.3.2.3 Equalization

The model of the PMC system contains a singular value decomposition (SVD)-based equalizer (see Section 6.6.3.1), since this is currently the only method that provides equalization in the GUR domain (GD). Figure 7.6 depicts the structure of the SVD-based equalizer unit.

7.3.3 Baseband communication channel

There are many advanced channel types described in literature [102]. They take into account many complex environmental effects (e.g. scattering, Doppler). However, since the given doctoral thesis is one of the first attempts to describe synchronization and estimation algorithms for GUR-based PMC systems, the work is limited to the basic channel model including two major

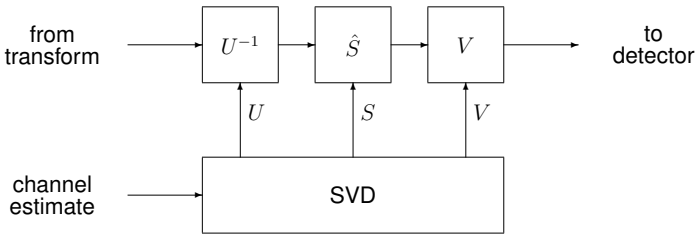

Figure 7.6: Contents of the equalizer unit

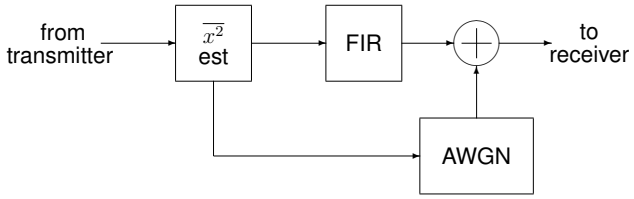

Figure 7.7: Communication channel model ("baseband channel" unit)

effects: time-dispersion (frequency-selectivity) and additive noise. Moreover, since RF part is not included into the model, a *baseband equivalent* communication channel is modeled. This baseband equivalent channel is obtained by "downconversion" of passband channel properties into baseband. Taking into account that only the basic properties of communication channel – dispersion and noise are modeled, this conversion is straightforward.

The experimental model of GUR-based PMC system has been built using communication channel models containing the superposition of FIR filter and additive white Gaussian noise (AWGN) source. The structure of the communication channel model used in all simulations is shown in Figure 7.7.

The additional unit '$\overline{x^2}$ est', which appears in Figure 7.7, is necessary for transmitted baseband signal power calculation, because signal-to-noise ratio (SNR) at the receiver input depends on the mean power of this signal:

$$SNR_{dB} = 10\log_{10}\frac{P_{signal}}{P_{noise}} = 10\log_{10}\frac{\overline{x^2}}{\sigma^2} \tag{7.1}$$

Therefore, the variance σ^2 of the AWGN source must be adjusted in accordance with the formula:

$$\sigma^2 = \frac{\overline{x^2}}{10^{\frac{SNR_{dB}}{10}}} \tag{7.2}$$

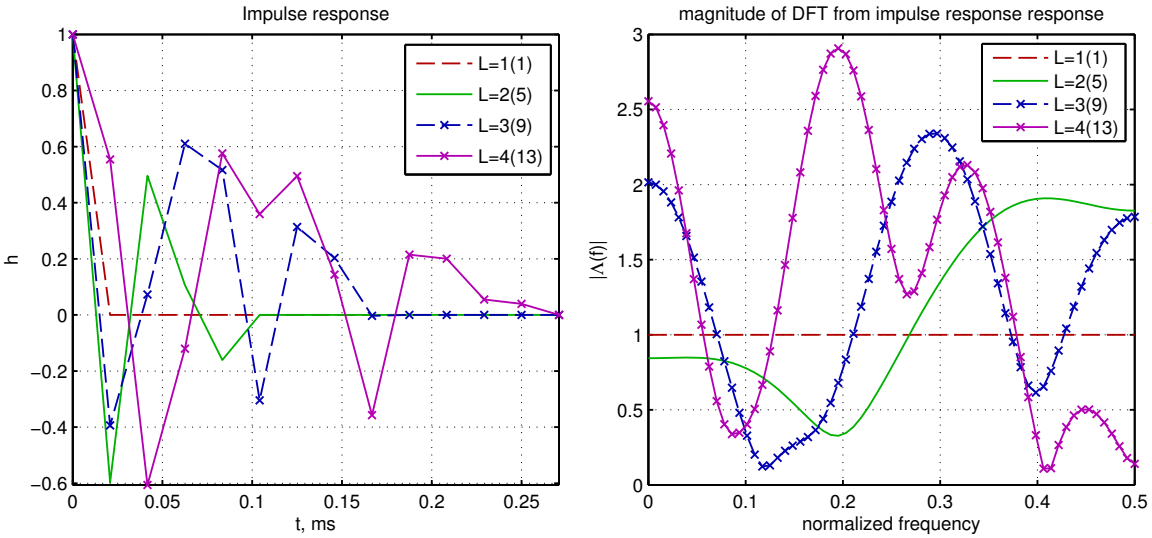

Figure 7.8: Characteristics of the tested communication channels. L designates the length of decimated impulse response. The actual length of channel impulse response is shown in brackets.

7.4 Simulation results of the model

The performance of the created PMC system model has been tested with various channel parameters. SNR of the receiver input signal has been changed in a range from 0 dB to 30 dB. The length of channel impulse response has been varied from 1 tap to 15 taps. Channel impulse responses and the corresponding frequency response are shown in Figure 7.8. Since the transmitter and the receiver uses 4x oversampling of the signal in order to provide respectively pulse shaping (see Section 2.5) and timing synchronization (see Chapter 4), an efficient length of channel impulse response has to be four times smaller than the order of the FIR filter (shown in brackets) of the channel model. However, it is prolonged due to transmitter filter impact (see Section 2.5).

The performance of the PMC system at various lengths of communication channel impulse response is shown in Figure 7.9. From this figure it is seen, that the increase of the length of channel impulse response leads to the degradation of communication system throughput. This is caused by several factors:

- LMS estimation of a longer channel impulse response is less precise;
- UW cross-correlation peaks get ‘washed’ by the convolution in the communication channel, and therefore, leads to increased BTO (see Section 4.3.2.2) estimation errors;
- Phase distortions of UW sequences, caused by the convolution in the communication channel, increase the error of cross-correlation -based CFO estimator (see Section 5.4.3).

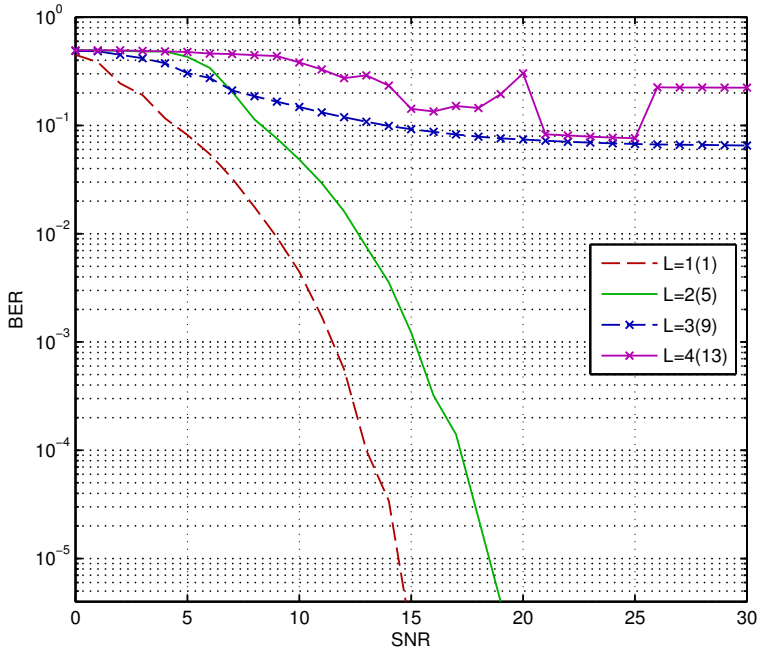

Figure 7.9: Performance of the PMC system at different lengths of impulse response of the communication channel

The parameters of the simulated PMC system are summarized in Table 1 of Appendix B. In the same appendix the *computational complexity* of the most resources-consuming algorithms is summarized in Table 2 .

7.5 Conclusions

- GUR can be successfully used for building of PMC systems.
- ZC sequence-based UWs, that are inserted at the beginning of useful sample blocks, are reusable for simultaneous timing synchronization, frequency synchronization and channel estimation.
- Simulations have demonstrated that the proposed design of the PMC system is sufficiently stable to be used as a reference for hardware prototype.
- Complexity of the proposed solution is suitable for the implementation into software-defined radio (SDR) platform based on general purpose central processing unit (CPU) or field-programmable gate array (FPGA) chip.

7.6 Summary of the contributions

In this doctoral thesis the following contributions related to the design of a PMC system are made:

- Complete structure of a GUR-based PMC system has been proposed for the first time (Section 7.3).
- Receiver structure, that utilizes the same Zadoff-Chu UW prefix for timing offset estimation, CFO estimation and channel estimation, has been proposed (Section 7.3.2).
- Complete GUR-based PMC system has been simulated and satisfactory results have been obtained (Section 7.4).

8 Utilization of the obtained results for future research

This chapter aims to give the reader an overview of the research directions that the author considers are important after completing this doctoral work.

Shift-invariant Generalized Unitary Rotation (GUR)-based transforms

A complex constant rotation angle OT (CCRAOT)-based parametric multicarrier (PMC) system is extremely sensitive to timing offset (see Section 4.3.1). Since a shift of the input vector by one sample causes cardinal changes in spectrum coefficients, a GUR-based PMC system requires block timing error tolerance less than one chip. The development of GUR-based *shift-invariant* transforms [103], [104] would allow to create robust PMC systems.

Inter-carrier interference free transmission

In research [9] it is shown, that *eigenfunctions* of the communication channel depend on its stationarity. Transmission using eigenfunctions would allow to eliminate inter-carrier interference (ICI) in PMC systems with doubly-selective channels and use low-complexity frequency domain (FD)-like channel estimation and equalization schemes (see Section 6.6.2). Since singular value decomposition (SVD) can be employed for searching the eigenfunctions, a work on GUR-based SVD algorithm is necessary. Excellent analysis and useful guidelines for the SVD-based equalization in systems with doubly-selective channels can be found in [105].

Multiple-input multiple-output

Due to the fact that unitary transforms and SVD is widely used in multiple-input multiple-output (MIMO) systems [106], a GUR-based MIMO precoder would pave a way to new possibilities. Use of GUR-based multicarrier (MC) modulation [107] in such systems would increase their flexibility even more.

Final conclusions

In this doctoral thesis parametric multicarrier (PMC) systems based on Generalized Unitary Rotation (GUR) has been proposed and analyzed. Design of whole PMC system allowed to verify viability and efficiency of the proposed designs. After completing of all theoretical analysis and practical experiments it can be concluded, that GUR-based PMC systems is a *viable concept*, which has a real perspective of practical use.

For creation of highly-efficient GUR-based PMC systems following considerations must be taken into account:

- For synchronization and channel estimation purposes both super-imposed (SI) (see Section 2.4.2.2) and inserted (see Section 2.4.2.2) sequences can be used. For communication channels with high signal-to-noise ratio (SNR) ($> 5dB$) use of SI sequences provides a way for increasing of system throughput compared to inserted sequence mode.

- Increase of length of synchronization sequence always improves block timing offset (BTO) and fractional carrier frequency offset (FCFO) synchronization. Therefore, increase of length of synchronization sequence always leads to improved bit error ratio (BER), at a cost of system throughput.

- In order to decrease computational complexity of multicarrier (MC) modulator and demodulator tree-like structures (see Section 3.3.2) can be used. These structures provide a great level of flexibility for modulator and demodulator. However, additional attention to order of serial to parallel (S/P) conversions must be paid.

- Singular value decomposition (SVD) is most appropriate tool for equalization in PMC systems. However, it is sensitive to channel estimation errors, therefore a special attention must be paid to time domain (TD) system identification algorithms, such as least mean squares (LMS).

- For communication channels with large nonlinearities complex constant rotation angle OT (CCRAOT) transform with $\phi < 30^{\circ}$, which creates low peak-to-average power ratio (PAPR) time domain signal, can be used.

By taking into account that this work is one of the first attempts to describe PMC systems, obtained results can be characterized as good and research can be considered as *successful*.

Although there are numerous limitations of algorithms proposed in this work, they provide a solid basis for rapid development of PMC systems. Moreover, many of described algorithms can be used in other MC communication systems, such as orthogonal frequency division multiplexing (OFDM). On other hand, many possible extensions (see Chapter 8) of the presented ideas can lead to even more innovative designs of communication systems.

Appendix A

The source code of MATLAB M-S function, performing complex constant rotation angle OT (CCRAOT).

```
function phi_trans(block)
  setup(block);
%endfunction

function setup(block)
  %% Register a single dialog parameter
  block.NumDialogPrms  = 2; %phi,%inv

  %% Register number of input and output ports
  block.NumInputPorts  = 1; %x
  block.NumOutputPorts = 1; %y

  %% Setup functional port properties to dynamically
  %% inherited.
  block.SetPreCompInpPortInfoToDynamic;
  block.SetPreCompOutPortInfoToDynamic;

  % Override input port properties
  block.InputPort(1).Complexity  = 'Complex';

  % Override output port properties
  block.OutputPort(1).Complexity  = 'Complex';

  %% Set block sample time to inherited
  block.SampleTimes = [-1 0];

  %% Run accelerator on TLC
  block.SetAccelRunOnTLC(true);

  %% Register methods
  block.RegBlockMethod('PostPropagationSetup', @DoPostPropSetup);
  block.RegBlockMethod('SetInputPortSamplingMode',@SetInputPortSamplingMode);
  block.RegBlockMethod('Outputs', @Output);
  block.RegBlockMethod('Start', @Start);
%endfunction

function SetInputPortSamplingMode(block, idx, fd)
block.InputPort(idx).SamplingMode = fd;
block.OutputPort(1).SamplingMode = fd;
%endfunction

function DoPostPropSetup(block)

% Initialize the Dwork vector
block.NumDworks = 1;

N=evalin('base','trans_per_block');

%% Dwork(1) stores the value of the next pulse width
block.Dwork(1).Name            = 'T';
block.Dwork(1).Dimensions      = N^2;
block.Dwork(1).DatatypeID      = 0;
```

```
53 block.Dwork(1).Complexity      = 'Complex';
54 block.Dwork(1).UsedAsDiscState = false;
55 %endfunction
56
57 function Start(block)
58 phi = block.DialogPrm(1).Data;
59 inv = block.DialogPrm(2).Data;
60 N=evalin('base','trans_per_block');
61
62 s = sin(phi);
63 c = cos(phi);
64 R = [s j*c; -j*c -s];
65 B = complex(zeros(N,N));
66 B(1:2*N+1:N*N) = R(1,1) * ones(1,N/2);
67 B(N+1:2*N+1:N*N) = R(1,2)*ones(1,N/2);
68 B(N/2+1:2*N+1:N*N) = R(2,1)*ones(1,N/2);
69 B(N*1.5+1:2*N+1:N*N) = R(2,2)*ones(1,N/2);
70 T=B^(log2(N));
71 if(inv)
72         T=T';
73 end
74 block.Dwork(1).Data = reshape(T,1,N^2);
75
76 %endfunction
77
78 function Output(block)
79 N=evalin('base','trans_per_block');
80 x = block.InputPort(1).Data;
81 T = reshape(block.Dwork(1).Data,N,N);
82 y=T*x;
83 block.OutputPort(1).Data = y;
84 %endfunction
```

Appendix B

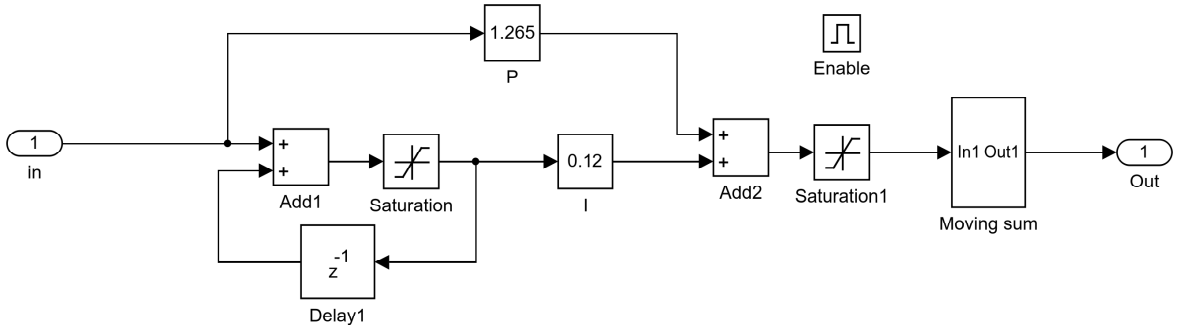

Figure 1: Simulink diagram PID controller from FCFO synchronization loop

Parameter	Value
Sample rate in channel	48kHz
Number of subcarriers, N	64
length of unique word (UW), L	16
type of transformation	CCRAOT
CCRAOT angle ϕ	30°
CCRAOT angle γ	$\pi/2$
CCRAOT angle ψ	0
UW sequence $\boldsymbol{u}$	Zadoff-Chu (ZC), $M = 3, Q = 16$
absolute carrier frequency offset (CFO), ϵ	0
least mean squares (LMS) filter length in channel estimator	8 taps
chip time, τ	$20.8\mu s$

Table 1: Parameters of the reference GUR-based PMC system described in Chapter 7

Algorithm	**Complexity**
Combined block timing offset (BTO) and CFO estimator	18432
Unitary transformation	12288
Equalizer	786432

Table 2: Computational complexity of the algorithms used in Chapter 7

References

[1] Weinstein S. and Ebert P. Data Transmission by Frequency-Division Multiplexing Using the Discrete Fourier Transform. //Communication Technology, IEEE Transactions on. 1971. vol. 19, no. 5, pp. 628–634.

[2] Bingham J.A.C. Multicarrier modulation for data transmission: an idea whose time has come. //IEEE Communications Magazine. 1990. vol. 28, no. 5, pp. 5–14.

[3] Lindsey A. and Dill J. Wavelet packet modulation: a generalized method for orthogonally multiplexed communications. //Proceedings of the Twenty-Seventh Southeastern Symposium on System Theory. 1995, pp. 392–396.

[4] Farhang-Boroujeny B. OFDM Versus Filter Bank Multicarrier. //Signal Processing Magazine, IEEE. 2011. vol. 28, no. 3, pp. 92–112.

[5] Mattera D. and Tanda M. Data-aided synchronization for OFDM/OQAM systems. //Signal Processing. 2012. vol. 92, no. 9, pp. 2284–2292.

[6] Lopez-Salcedo J.A., Gutierrez E., Seco-Granados G., and Swindlehurst A.L. Unified Framework for the Synchronization of Flexible Multicarrier Communication Signals. //Signal Processing, IEEE Transactions on. 2013. vol. 61, no. 4, pp. 828–842.

[7] Misans P. and Torkelson M. Preliminary Simulation of Multicarrier Modulation Data Transmission System. // Nordic MATLAB Conference. Stockholm, p. 4.

[8] Tsai S.H.S. Multicode transmission using Walsh Hadamard transform. 2011.

[9] Kozek W. Matched Weyl-Heisenberg expansions of nonstationary environments. Ph.D. thesis, Vienna University of Technology. 1997.

[10] Martone M. A multicarrier system based on the fractional Fourier transform for time-frequency-selective channels. //Communications, IEEE Transactions on. 2001. vol. 49, no. 6, pp. 1011–1020.

[11] Oka I. and Fossorier M. A General Orthogonal Modulation Model for Soft-ware Rados. //IEEE Transactions on Communications. 2006. vol. 54, no. 1, pp. 7–12.

[12] Misans P. and Valters G. Initial FPGA design for generalized Orthogonal Nonsinusoidal Division Multiplexing. //2009 Norchip. 2009, pp. 1–5.

[13] Forouzan A.R. and Garth L. Orthogonal Code Design for Spectrally Encoded CDMA Systems. // GLOBECOM'07. pp. 4434–4439.

[14] Misans P., Terauds M., Aboltins A., and Valters G. MATLAB/SIMULINK Implementation of Phi-Transforms–A New Toolbox Only or the Rival of Wavelet Toolbox for the Next Decade? // Nordic MATLAB User Conference. pp. 1–8.

[15] Aboltins A. Comparison of Orthogonal Transforms for OFDM Communication System. //Electronics and Electrical Engineering. 2011. vol. 111, no. 5, pp. 77–80.

[16] Aboltins A. and Misans P. Singular Value Decomposition Based Phi Domain Equalization For Multi-Carrier Communication System. //Electronics and Electrical Engineering. 2012. vol. 18, no. 9, pp. 71–74.

[17] Aboltins A. Block synchronization using unique word for Generalized Unitary rotation based communication system. // Baltic Electronics Conference - BEC2012. Tallinn, pp. 71–74.

[18] Aboltins A. Carrier Frequency Offset Estimator Based on Unique Word Cross-correlation. // 20th Telecommunications Forum - TELFOR2012. Belgrade, pp. 486–489.

[19] Aboltins A. and Misans P. Removal of Super-Imposed Synchronization Sequence Using Matched Filter. // Microwave and Radio Electronics Week, MAREW2013. Pardubice, pp. 86–90.

[20] Misans P., Valters G., Terauds M., and Aboltins A. Initial Implementation of Generalized Haar-Like Orthonormal Transforms into FPGA-Based Devices-Part I: Signal Spectrum Analyzer-Synthesizer Module. //TELECOMMUNICATIONS AND ELECTRONICS. 2008. vol. 8, pp. 16–21.

[21] Aboltins A. and Klavins D. Synchronization and correction of channel parameters for an OFDM-based communication system. //Automatic Control and Computer Sciences. 2010. vol. 44, no. 3, pp. 160–170.

[22] Wei L., Kennedy R., and Lamahewa T. An optimal basis of band-limited functions for signal analysis and design. //Signal Processing, IEEE Transactions on. 2010. vol. 58, no. 11, pp. 5744–5755.

[23] Gray R.M. Toeplitz and Circulant Matrices: A Review. //Foundations and Trends® in Communications and Information Theory. 2005. vol. 2, no. 3, pp. 155–239.

[24] Peled A. and Ruiz A. Frequency domain data transmission using reduced computationally complexity algorithms. // Acoustics, Speech, and Signal Processing, IEEE International Conference on ICASSP'80. IEEE, vol. 5, pp. 964–967.

[25] Wang N. and Blostein S. Comparison of CP-Based Single Carrier and OFDM With Power Allocation. //IEEE Transactions on Communications. 2005. vol. 53, no. 3, pp. 391–394.

[26] Muquet B., Giannakis G., de Courville M., and Duhamel P. Cyclic prefixing or zero padding for wireless multicarrier transmissions? //IEEE Transactions on Communications. 2002. vol. 50, no. 12, pp. 2136–2148.

[27] Witschnig H., Mayer T., Springer A., Koppler A., Maurer L., Huemer M., and Weigel R. A different look on cyclic prefix for SC/FDE. //The 13th IEEE International Symposium on Personal, Indoor and Mobile Radio Communications. 2002, pp. 824–828.

[28] Huemer M., Hofbauer C., and Huber J. Non-Systematic Complex Number RS Coded OFDM by Unique Word Prefix. //Signal Processing, IEEE Transactions on. 2012. vol. 60, no. 1, pp. 285–299.

[29] Hu W.W. and Li C.P. Super-Imposed Training Scheme for Timing and Frequency Synchronization in OFDM Systems. //2007 IEEE 65th Vehicular Technology Conference - VTC2007-Spring. 2007, pp. 1718–1722.

[30] van de Beek J.J., Sandell M., and Borjesson P.O. ML estimation of time and frequency offset in OFDM systems. //IEEE Transactions on Signal Processing. 1997. vol. 45, no. 7, pp. 1800–1805.

[31] Sarwate D.V. and Pursley M.B. Crosscorrelation properties of pseudorandom and related sequences. // Proceedings of the IEEE. vol. 68, pp. 593–619.

[32] Chu. Polyphase codes with good periodic correlation properties. //IEEE Transactions on Information Theory. 1972. , no. 6, pp. 531–532.

[33] Frank R. and Zadoff S. Phase shift pulse codes with good periodic correlation properties. //Information Theory, IRE Transactions on. 1961. vol. 7, no. 4, pp. 254–257.

[34] Lopez-Martinez F.J., del Castillo-Sánchez E., Martos-Naya E., and Entrambasaguas J.T. Performance evaluation of preamble detectors for 3GPP-LTE physical random access channel. //Digital Signal Processing. 2012. vol. 22, no. 3, pp. 526–534.

[35] Lopez-Martınez F.J., Martos-Naya E., and Entrambasaguas J.T. Low complexity cell search scheme for LTE and LTE-advanced mobile technologies. //Computers & Electrical Engineering. 2012. vol. 38, no. 6, pp. 1502–1512.

[36] Schmidl T. and Cox D. Robust frequency and timing synchronization for OFDM. //IEEE Transactions on Communications. 1997. vol. 45, no. 12, pp. 1613–1621.

[37] Johnson S. and Frigo M. A modified split-radix FFT with fewer arithmetic operations. //Signal Processing, IEEE Transactions .... 2007. vol. 55, no. 1, pp. 111–119.

[38] Rahardja S. and Falkowski B. Family of unified complex Hadamard transforms. //Circuits and Systems II: Analog and Digital Signal Processing, IEEE Transactions on. 1999. vol. 46, no. 8, pp. 1094–1100.

[39] FINO B.J. and Algazi V. Unified Matrix Treatment of the Fast Walsh-Hadamard Transform. //Computers, IEEE Transactions on. 1976. vol. C-25, no. 11, pp. 1142–1146.

[40] Valters G. and Misans P. FPGA implementation of Elementary Generalized Unitary Rotation. //2009 Norchip. 2009. , no. 2, pp. 1–4.

[41] Misans P. and Terauds M. Introduction into the fast orthogonal transforms based on rotation angles: A New Methodical approach only or a gateway to novel DSP algorithms? // ECS. Bratislava, pp. 85–94.

[42] Dita P. Factorization of Unitary Matrices. //Journal de Physique (main title). 2001. vol. A 36, p. 12.

[43] Aguilera A. and Pérez-Aguila R. General n-dimensional rotations. //Proc. WSCG SHORT Commun. Papers. 2004.

[44] Terauds M. A new kind of disrete orthogonal transform and errors in the corresponding signal processing applications. Ph.D. thesis, Riga Technical University. 2009.

[45] Berenguer I. Filtered multitone (FMT) modulation for broadband fixed wireless systems. //October. 2002. , no. August.

[46] Vatterli. Perfect transmultiplexers. //ICASSP '86. IEEE International Conference on Acoustics, Speech, and Signal Processing. 1986, pp. 2567–2570.

[47] Zelenkov A.V. and Litvinenko A. OFDM PAPR reduction by pre-scrambling and clipping 2 PAPR influence on the efficiency of the OFDM communication system. // BEC'2012. pp. 141–144.

[48] Chen N. and Zhou G.T. Superimposed training for OFDM: a peak-to-average power ratio analysis. 2006.

[49] Kasami T. Weight Distribution Formula for Some Class of Cyclic Codes, Tech. Report No. R-285. Tech. rep., University of Illinois. 1966.

[50] Soni R.K., Jain A., and Saxena R. Design of M-Band NPR Cosine-Modulated Filterbank Using IFIR Technique. //Journal of Signal and Information Processing. 2010. vol. 01, no. 01, pp. 35–43.

[51] Cruz-Roldán F. and Blanco-Velasco M. Joint use of DFT filter banks and modulated transmultiplexers for multicarrier communications. //Signal Processing. 2011. vol. 91, no. 7, pp. 1622–1635.

[52] Love D.J., Heath R.W., Lau V.K.N., Gesbert D., Rao B.D., and Andrews M. An overview of limited feedback in wireless communication systems. 2008.

[53] Hyvärinen A., Karhunen J., and Oja E. Independent Component Analysis, vol. 21 of Adaptive and learning systems for signal processing, communications, and control. Wiley-Interscience. 2001.

[54] Meyr H., Moeneclaey M., and Fechtel S.A. Digital Communication Receivers: Synchronization, Channel Estimation, and Signal Processing. Wiley series in telecommunications and signal processing. Wiley. 1998.

[55] Chen M., Chua K.C., and Ding Q.L. A fast algorithm for choosing frame synchronization unique word. // Global Telecommunications Conference, 1998. GLOBECOM 98. The Bridge to Global Integration. IEEE. vol. 6, pp. 3437–3442 vol.6.

[56] Tourtier P.J., Monnier R., and Lopez P. Multicarrier modem for digital HDTV terrestrial broadcasting. //Signal processing. Image communication. 1993. vol. 5, no. 5-6, pp. 379–403.

[57] Sandell M., van de Beek J.J., and Borjesson P.O. Timing and Frequency Synchronization in OFDM Systems Using the Cyclic Prefix. // Proc. Int. Symp. Synchronization. Citeseer, pp. 16–19.

[58] Sandell M., van de Beek J.J., and Borjesson P.O. ML Estimation of Timing and Frequency Offset in Multicarrier. Tech. Rep. April. 1996.

[59] Massey J. Optimum Frame Synchronization. //Communications, IEEE Transactions on. 1972. vol. 20, no. 2, pp. 115–119.

[60] Scholtz R. Frame Synchronization Techniques. //Communications, IEEE Transactions on. 1980. vol. 28, no. 8, pp. 1204–1213.

[61] Lui G. and Tan H. Frame Synchronization for Gaussian Channels. //Communications, IEEE Transactions on. 1987. vol. 35, no. 8, pp. 818–829.

[62] Moon B.H. and Soliman S.S. ML frame synchronization for the Gaussian channel with ISI. // Communications, 1991. ICC '91, Conference Record. IEEE International Conference on. pp. 1698–1702 vol.3.

[63] Robertson P. Maximum likelihood frame synchronization for flat fading channels. // Communications, 1992. ICC '92, Conference record, SUPERCOMM/ICC '92, Discovering a New World of Communications., IEEE International Conference on. pp. 1426–1430 vol.3.

[64] Fechtel S.A. and Meyr H. Improved frame synchronization for spontaneous packet transmission over frequency-selective radio channels. //Personal, Indoor and Mobile Radio. 1994.

[65] Canet M.J., Almenar V., Flores S., and Valls J. Improvement of a time synchronization algorithm for IEEE 802.11a/g WLAN standard. // Eurasipco. 2, pp. 560–564.

[66] Geetha Priya C. and Suganthi M. Two symbol timing estimation methods using Barker and Kasami sequence as preamble for OFDM-based WLAN systems. //Signal Processing. 2010. vol. 90, no. 7, pp. 2177–2189.

[67] Yang B., Letaief K., Cheng R.S., and Cao Z. Burst frame synchronization for OFDM transmission in multipath fading links. // IEEE VTS 50th Vehicular Technology Conference. Ieee, vol. 1, pp. 300–304.

[68] ISO. ANSI/IEEE Std 802.11. Tech. rep. 1999.

[69] Pan X., Zhou Y., Ma S., and Ng T.S. An Improved Derivative Method for Symbol Synchronization in OFDM Systems. //2007 IEEE Wireless Communications and Networking Conference. 2007. vol. 1, no. 1, pp. 2463–2467.

[70] Coulson A.J. Maximum likelihood synchronization for OFDM using a pilot symbol: algorithms. //Selected Areas in Communications, IEEE Journal on. 2001. vol. 19, no. 12, pp. 2486–2494.

[71] Coulson A.J. Maximum likelihood synchronization for OFDM using a pilot symbol: analysis. //Selected Areas in Communications, IEEE Journal on. 2001. vol. 19, no. 12, pp. 2495–2503.

[72] Kim J. and Cheun K. An efficient two-step approach to integer frequency offset detection for OFDM systems. //Signal Processing. 2011, pp. 1–7.

[73] Pollet T., Van Bladel M., and Moeneclaey M. BER sensitivity of OFDM systems to carrier frequency offset and Wiener phase noise. //Communications, IEEE Transactions on. 1995. vol. 43, no. 234, pp. 191–193.

[74] Speth M., Fechtel S.A., Fock G., and Meyr H. Optimum receiver design for wireless broad-band systems using OFDM. I. //Communications, IEEE Transactions on. 1999. vol. 47, no. 11, pp. 1668–1677.

[75] Oh J.H., Kim J.G., and Lim J.T. Blind Carrier Frequency Offset Estimation for OFDM Systems with Constant Modulus Constellations. //Communications Letters, IEEE. 2011. vol. 15, no. 9, pp. 971–973.

[76] Chiu Y., Markovic D., and Tang H. OFDM receiver design. //EE225CFinal Report Fall. 2000.

[77] Jeon H., Kim K., and Serpedin E. An Efficient Blind Deterministic Frequency Offset Estimator for OFDM Systems. //Communications, IEEE Transactions on. 2011. vol. 59, no. 4, pp. 1133–1141.

[78] Morelli M. and Mengali U. An improved frequency offset estimator for OFDM applications. //Communications Letters, IEEE. 1999. vol. 3, no. 3, pp. 75–77.

[79] Cvetkovic Z. and Tarokh V. Frequency synchronization in OFDM. //2004 IEEE International Conference on Acoustics, Speech, and Signal Processing. 2004. , no. 2, pp. iv–373–iv–376.

[80] de Sa J.P.M. Linear regression. // Applied Statistics Using SPSS, STATISTICA, MATLAB and R, chap. 6. 2007. pp. 272–285.

[81] Tretter S. Estimating the frequency of a noisy sinusoid by linear regression (Corresp.). //Information Theory, IEEE Transactions on. 1985. vol. 31, no. 6, pp. 832–835.

[82] Messerschmitt D. Frequency Detectors for PLL Acquisition in Timing and Carrier Recovery. //Communications, IEEE Transactions on. 1979. vol. 27, no. 9, pp. 1288–1295.

[83] Dong X., Li X., and Wu D. Recursive maximum likelihood estimation of time-varying carrier frequency offset for orthogonal frequency-division multiplexing systems. //Wireless Communications and Mobile Computing. 2011.

[84] Classen F., Meyr H., and Sehier P. Maximum likelihood open loop carrier synchronizer for digital radio. // Communications, 1993. ICC 93. Geneva. Technical Program, Conference Record, IEEE International Conference on. vol. 1, pp. 493–497 vol.1.

[85] Farrow C. A continuously variable digital delay element. // Circuits and Systems, 1988., IEEE International Symposium on. IEEE, pp. 2641–2645.

[86] Proakis J.G. Digital communications. McGraw-Hill, 4th ed. 2000.

[87] Lange C. and Ahrens A. Equalization aspects in multicarrier transmission systems. // EAPEIE 2004. 2004 7th International Conference on Actual Problems of Electronic Instrument Engineering. IEEE, I, pp. 112–119.

[88] Falconer D. History of equalization 1860-1980. //Communications Magazine, IEEE. 2011. vol. 49, no. 10, pp. 42–50.

[89] Dukkipati R.V. MATLAB An introduction with applications. New Age International, New Delhi. 2010.

[90] Widrow B. and Stearns S.D. Adaptive signal processing. Prentice-Hall signal processing series. Prentice-Hall. 1985.

[91] Wang X., Wu Y., and Wu H.C. A New Adaptive OFDM System with Precoded Cyclic Prefix for Cognitive Radio. //2008 IEEE International Conference on Communications. 2008. vol. 29, no. 2, pp. 3642–3646.

[92] Hase T. Improvement on the Channel Estimation of Pilot Cyclic Prefixed Single Carrier (PCP-SC) System. //IEEE Signal Processing Letters. 2009. vol. 16, no. 8, pp. 719–722.

[93] Poor H.V. and Wornell G.W. Wireless Communications: Signal Processing Perspectives. 1998.

[94] Edfors O., Sandell M., Wilson S.K., van de Beek J.J., and Borjesson P.O. OFDM channel estimation by singular value decomposition. // Communications, IEEE Transactions on. IEEE, vol. 46, pp. 931–939.

[95] Li Y., Cimini L., and Sollenberger N. Robust channel estimation for OFDM systems with rapid dispersive fading channels. //IEEE Transactions on Communications. 1998. vol. 46, no. 7, pp. 902–915.

[96] Negi R. and Cioffi J. Pilot tone selection for channel estimation in a mobile OFDM system. //IEEE Transactions on Consumer Electronics. 1998. vol. 44, no. 3, pp. 1122–1128.

[97] Tong L., Sadler B.M., and Dong M. Pilot-assisted wireless transmissions: general model, design criteria, and signal processing. //Signal Processing Magazine, IEEE. 2004. vol. 21, no. 6, pp. 12–25.

[98] Golub and VanLoan. Matrix computations. The Johns Hopkins University Press, 3 ed. 1996.

[99] Bianchi T. and Argenti F. SVD-based equalization for zero padded multicarrier systems in time-variant fading channels. //Signal Processing. 2006. vol. 0, no. Eusipco, pp. 0–4.

[100] Ahrens A. and Lange C. Transmit power allocation in SVD equalized multicarrier systems. //AEU - International Journal of Electronics and Communications. 2007. vol. 61, no. 1, pp. 51–61.

[101] Drmac Z. and Veselic K. New fast and accurate jacobi svd algorithm: i. lapack working note 169. //Matrix. 2006. vol. 0037120, pp. 1–25.

[102] Erceg V., Hari K.V.S., Smith M.S., Baum D.S., Sheikh K.P., Tappenden C., Costa J.M., Bushue C., Sarajedini A., Schwartz R., and Branlund D. Channel Models for Fixed Wireless Applications Background. Tech. rep., IEEE 802.16 Broadband Wireless Access Working Group. 2001.

[103] Yu R. Shift-Variance Analysis of Generalized Sampling Processes. //Signal Processing, IEEE Transactions on. 2012. vol. 60, no. 6, pp. 2840–2850.

[104] Almeida L. The fractional Fourier transform and time-frequency representations. //IEEE Transactions on Signal Processing. 1994. vol. 42, no. 11, pp. 3084–3091.

[105] Marzetta T.L. and Salz J. Singular Value Decomposition of a Matrix-Valued Impulse Response. //Proceedings. (ICASSP '05). IEEE International Conference on Acoustics, Speech, and Signal Processing, 2005. 2005, pp. 913–916.

[106] Raleigh G.C. and Cioffi J.M. Spatio-temporal coding for wireless communication. 1998.

[107] Park J., Chun J., and Jeong B.J. Efficient Multi-user MIMO Precoding based on GSVD and Vector Perturbation. //Signal Processing. 2011.

Index